5.2 MICROSTRUCTURE AND ELEMENTAL DISTRIBUTION OF AMERICIUM-CONTAINING MOX FUEL UNDER THE SHORT-TERM IRRADIATION TESTS

Kosuke Tanaka[a], Takashi Hirosawa[a], Hiroshi Obayashi[a], Shin-ichi Koyama[a], Hiroshi Yoshimochi[a] and Kenya Tanaka[a]

[a] *Alpha Gamma Section, Fuels and Materials Department, Oarai Research and Development Center, Japan Atomic Energy Agency 4002 Narita-cho, Oarai-machi, Ibaraki, 311-1393, Japan*
tanaka.kosuke@jaea.go.jp

ABSTRACT

In order to investigate the effect of americium addition to MOX fuels on the irradiation behavior, the "Am-1" program is being conducted in JAEA. The Am-1 program consists of two short-term irradiation tests of 10-minute and 24-hour irradiations and a steady-state irradiation test. The short-term irradiation tests were successfully completed and the post irradiation examinations (PIEs) are in progress. The PIEs for Am-containing MOX fuels focused on the microstructural evolution and redistribution behavior of Am at the initial stage of irradiation and the results to date are reported.

INTRODUCTION

Uranium (U) and plutonium (Pu) mixed oxide (MOX) fuels containing several percents of minor actinides (MAs) and fission products are promising candidates for a closed nuclear cycle system based on a fast reactor such as the JSFR (JAEA Sodium Cooled Fast Reactor) system of FaCT (Fast Reactor Cycle Technology Development) project [1]. Although the content of MAs in the MOX fuels varies mainly according to the required mass balance for MAs, the maximum total content of MAs is considered to be 5 % [2]. Americium (Am), which is representative of MAs, should be considered important in view of its having a high generation yield in the spent fuel, a high and lasting radiotoxicity and expected impacts on various properties of MOX fuels. Am-containing MOX (Am-MOX) fuels, therefore, are being studied as a first step to promote research and development (R&D) of the MA-containing

MOX (MA-MOX) fuels. R&D of Am-MOX fuels was started in the early 1990s in the Alpha-Gamma Facility (AGF) of Japan Atomic Energy Agency (JAEA). Fabrication, characterization and post-irradiation examinations of Am-MOX fuels have been successfully carried out for the purpose of obtaining fundamental insights into further development of MA-MOX fuels and many novel and practical results about Am effects on the fuel properties have been obtained at AGF [3].

This paper reports on the results of ceramography and electron probe microanalysis (EPMA) for Am-MOX fuel pellets at the initial stage of irradiation.

Am-1 PROGRAM

In order to confirm the effect of MA addition on irradiation behavior of MOX fuel pellets, an irradiation program named "Am-1" is being conducted in JAEA. The Am-1 program consists of two short-term irradiation tests of 10-minute and 24-hour irradiations and a steady-state irradiation test. The objectives of the short-term irradiation tests are to confirm whether or not fuel melting occurs at a high linear heating rate and to evaluate the redistribution behavior of Am during the initial burn-up. The steady-state irradiation test is expected to evaluate the behavior of the fuel cladding chemical interaction (FCCI) and helium (He) release behavior up to middle or high burn-up.

Two kinds of fuels were subjected to the irradiation tests of the Am-1 program. One consisted of Am-MOX fuel pellets containing 3% or 5% Am and the other was MOX fuel pellets containing 2% Np and 2% Am (Np/Am-MOX). Am-MOX fuel pellets were fabricated using a remote handling technique in the shielded air-tight hot cell of the AGF at JAEA's Oarai Research and Development Center. Np/Am-MOX fuel pellets were fabricated in a glove box unit at Tokai Research and Development Center of JAEA. Two values of the oxygen-to-metal ratio (O/M) of the fuel pellets were used as a test parameter in the Am-1 program [4].

The two short-term irradiation tests were successfully completed and the post irradiation examinations (PIEs) have been conducted. A detailed description concerning the Am-1 program, including fuel design and irradiation conditions, can be found in the literature [4, 5].

SPECIFICATIONS AND FABRICATION PROCEDURES OF THE FUELS

Fig. 1 shows a flow sheet of the fuel pin fabrication process. Powders of UO_2 and two kinds of Am-containing PuO_2 powders were used as raw materials. Detailed characterization

of the raw powders has been reported in the literature [6]. Before the sintering step, these three powders were annealed at 873 K for 2 h in a furnace with a cantal heater to remove their absorbed moisture. After heat treatment, the powders were weighed by using an electronic balance in order to adjust the amount to the predetermined weight ratio. This was followed by mixing in a ball mill for 5 h. Zinc stearate was added as binder and the powder was further mixed for 30 min before cold-pressing on green pellets under a pressure of 3.84 t /cm^2. The green pellets were pre-sintered at 1073 K for 2.5 h in the furnace with the cantal heater to remove the binder and were sintered at 1973 K for 5 h in a furnace with a tungsten mesh heater. The pellets were then heat treated to adjust O/M ratio to the targeted values. The O/M ratio of the pellets was confirmed gravimetrically at room temperature. All of the heat treatments and sintering processes were carried out under the flowing gas atmosphere of Ar-5 % H_2 or Ar-0.05 % H_2 by adding an appropriate amount of moisture. After the sintering, fissile content, Pu enrichment, ^{235}U enrichment and Am content were determined by using alpha-spectrometry, gamma-spectrometry and mass-spectrometry. Volatile, moisture and metal impurities were also checked for the sintered pellets.

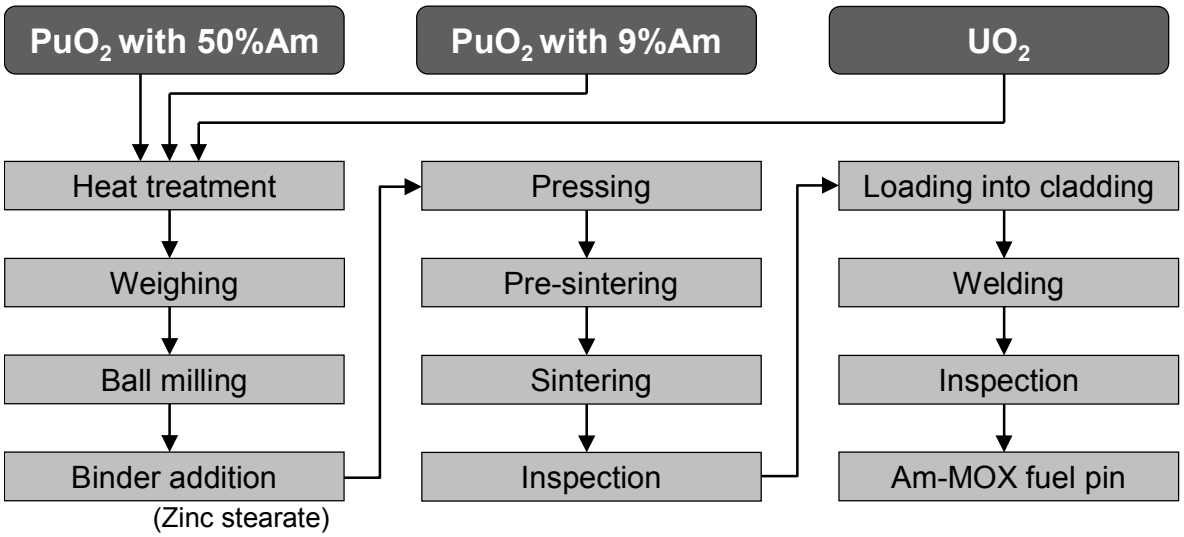

Fig. 1. Fabrication flow of Am-MOX fuel pin

The sintered and inspected Am-MOX fuel pellets were inserted into a cladding tube made of austenitic stainless steel, together with thermal insulator pellets of UO_2 and reflector components. The Am-MOX fuel pellets containing 5% Am were loaded at the middle of the fuel column and 3% Am-containing MOX fuel pellets were placed at the lower and upper ends of the fuel column. The fuel pins were sealed by TIG welding and then inspected for confirmation of their air-tightness/soundness. Fig. 2 shows a schematic drawing and main

specifications of the Am-MOX fuel pin. Manufactured fuel pins were then assembled into the fuel subassembly.

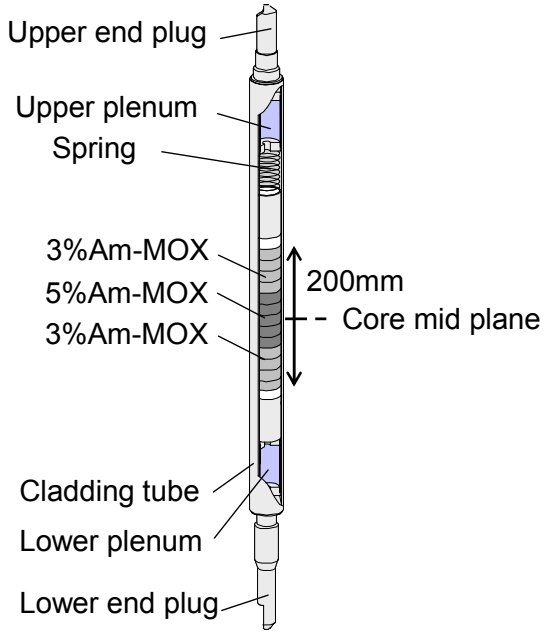

Fuel pellet

Diameter : 6.52 mm
O/M ratio : 1.95 and 1.98
Density : 93 % T.D.
Pu content : 30 wt. %
Am content : 3 and 5 wt. %

Cladding

Material : 15Cr-20Ni stainless steel
Outer diameter : 7.5 mm
Thickness : 0.4 mm

Fig. 2. Configuration and main specifications of the Am-MOX fuel pin

IRRADIATION CONDITIONS

After the reactor power was raised continuously to the targeted peak linear heating rate of 43kW/m and kept there for 10 min, the power was manually shut down. The fuel subassembly was irradiated to around 0.0057 % FIMA in the core center location [000] of the operational cycle 3-1 of the Joyo MK-III core. The burn-ups for two samples of 3 % Am-MOX and one sample of 5 % Am-MOX were determined by chemical analysis based on the isotope dilution method [7] in the AGF. Fixed linear heating rate was evaluated using fission rate derived from chemical analysis and fission energy of each nuclide [8]. The determined linear heating rate agreed well with the calculated value [5] within an experimental error of 3 %. The second irradiation test was performed at almost the same power history up to the targeted peak heating rate of 43 kW/m and hold for 24 hours.

EXPERIMENTAL PROCEDURES OF PIE

The Am-MOX fuel pins were cut at different axial positions into several segments. Several cross-sectional specimens were prepared by the following processes; each segment (about 20 mm in length) was impregnated with epoxy resin in vacuum and cut transversely into discs of about 5 mm in thickness. These disks were mounted into holders using epoxy resin, and then were ground and mirror-polished with anhydrous lubricant. The microstructure was observed with an optical microscope (TELATOM, Reichert).

EPMA of U, Pu and Am was done using the SX-100R model (Cameca) which was specially shielded with lead and tungsten to permit the analysis of irradiated nuclear fuels. Electron acceleration potential was 25 kV and beam current was 50 nA. Three wavelength dispersive spectrometers with pentaerythritol (PET) diffracting crystals were used for the analysis simultaneously. Selected characteristic X-rays were M-alpha lines for U and Am, and the M-beta line for Pu. The secondary electron image was used to obtain information about the fuel microstructure at the locations selected for analysis and to position the electron beam. Immediately prior to EPMA of the samples a thin film of carbon was applied to their surface by vacuum evaporation to avoid electron charging effects.

RESULTS AND DISCUSSION

Figs. 3 and 4 show example as-polished macroscopic ceramographs of two Am-MOX fuel pellets irradiated for 10 min and 24 h. Some cracks were observed along the radial and circumferential directions on both specimens. Plano-convex-shape lenticular pores were observed around the central void of the specimen irradiated for 10 min. Lenticular pores were also found in the vicinity of cracks which developed in this fuel pellet due to thermal stresses. Crack healings occurred in some parts of both fuel pellets after the lenticular pores moved to the fuel center along the temperature gradient. Closer inspection of the trails behind the lenticular pores (in the magnified views) showed that many of them consisted of a string of small spheres. The configuration of the lenticular pores was similar to that of conventional oxide fuels irradiated for a short time at the high linear heating rate condition [9-11]. No significant difference in the restructuring feature was observed between the 5% Am-containing and 3% Am-containing MOX fuel pellets. After the 24-h irradiation, the central void had developed to a size of about 1 mm in diameter. No lendicular pores were observed and highly dense columnar grains appeared on the specimen taken from around the axial mid position of the fuel pin. As shown in Figs. 3 and 4, fuel restructuring had started in

the Am-MOX fuel pellets even in the brief irradiation times of 10 min and 24 h.

In order to confirm whether or not the fuel melting occurred at the high linear heating rate, careful observations were carried out. It has been reported that when the fuel melted at the initial stage of irradiation, a pore-free structure was observed in the center of the fuel pellet or around the central void [12, 13]. No sign of fuel melting was found in any of the specimens taken from the Am-MOX fuel pins irradiated for 10 min and 24 h. This implied that the thermal design for this test had a sufficient safety margin.

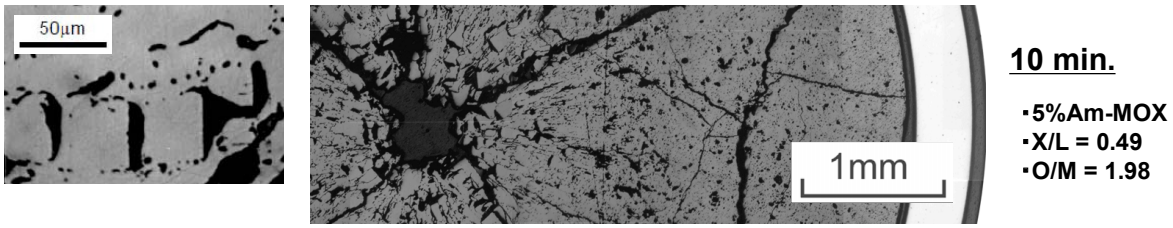

Fig. 3. Ceramographs of Am-MOX fuel irradiated for 10 min

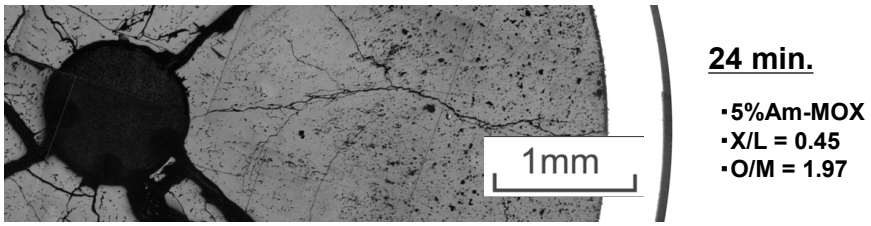

Fig. 4. Ceramograph of Am-MOX fuel irradiated for 24 h

Fig. 5 shows the radial distributions of U, Pu and Am for a specimen taken from the axial mid position of the fuel pin irradiated for 10 min. The concentration of these elements from the middle to outer part of the fuel pellets was almost the same as the chemically analyzed value for an as-fabricated pellet. In the vicinity of the central void the concentrations of Pu and Am increased whereas that of U decreased. The radial distributions of U, Pu and Am on the specimens taken from the upper and lower ends of the fuel pin were quite flat and no apparent redistribution was found. The tendency for appearance or non-appearance of redistribution agreed with the fuel restructuring behavior which could be explained by the axial distribution of linear heating rate. Fig. 6 shows the radial distributions of U, Pu and Am on the specimen taken from the axial mid position of the fuel pin irradiated for 24 h. More obvious redistributions were measured on this specimen compared to the one irradiated for 10 min. The concentrations of Pu and Am gradually increased on approaching the edge of the

central void. A slight increase in Am concentration at the center of the fuel pellet has been reported in the Am-MOX fuel in the SUPERFACT program [14].

A quick comparison between Pu and Am distribution profiles shown in Figs. 5 and 6 indicated both profiles were similar. Generally, ^{241}Am accumulates in Pu-containing fuels through the beta decay of ^{241}Pu. Therefore, careful attention should be paid to evaluating the Am concentration in MOX fuels. Calculation results obtained using the ORIGEN2 code confirmed the change in concentrations of Am and Pu was negligible during the short-term irradiation and the storage period up to the time of the EPMA. That is to say, Am behaved like Pu during the initial stage of irradiation.

It was considered that the increase in concentrations of Pu and Am in the center of the fuel pellet could be attributed to vapor transport of U during the evaporation-condensation mechanism of the pores. It is well known that the local concentration variations of Pu due to migration affect the fuel thermal properties in MOX fuel. It has been reported that the melting point temperature is decreased by the addition of a large amount of Am [15], which leads to a smaller design margin for fuel melting. The present EPMA results indicated that careful consideration must be given to the redistribution behavior of Am as well as that of Pu for evaluating the impact on the thermal performance of Am-MOX fuels.

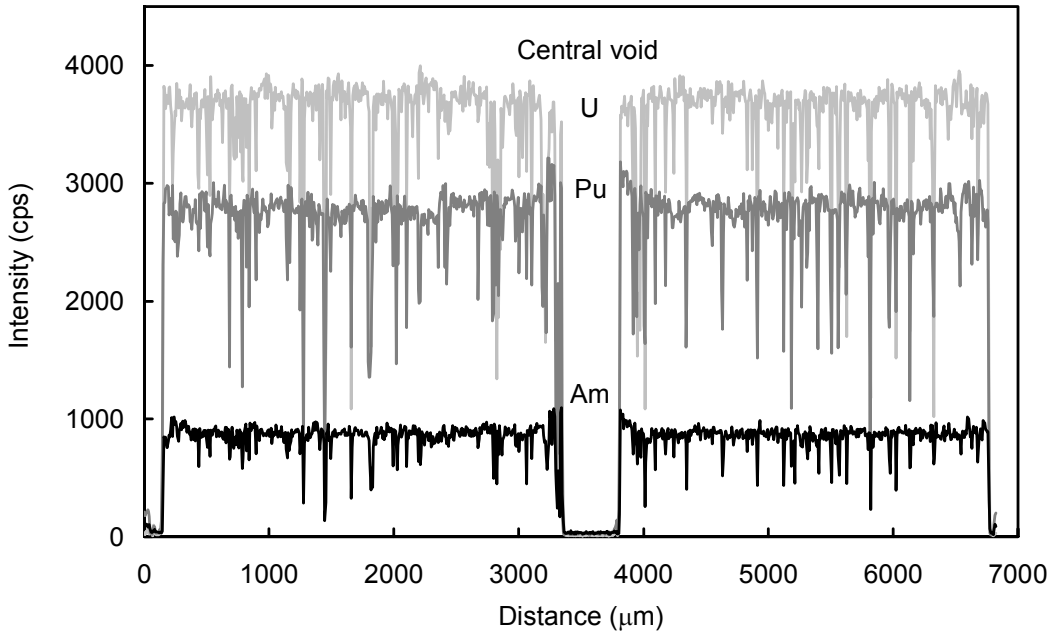

Fig. 5. EPMA results of U, Pu and Am distributions for 5% Am-MOX fuel specimen irradiated at about 43 kW/m for 10 min

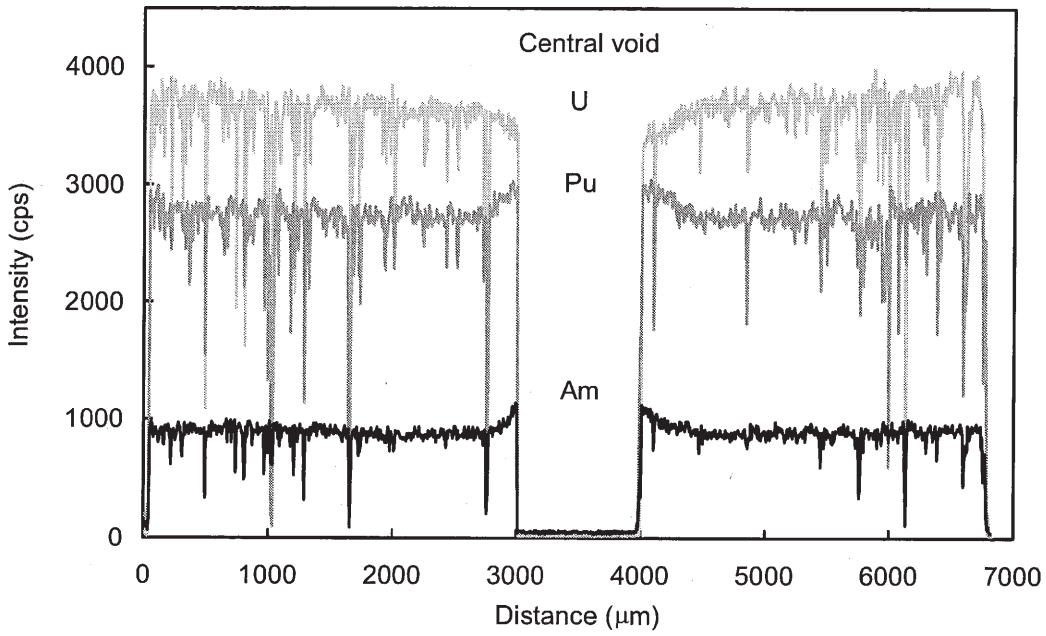

Fig. 6. EPMA results of U, Pu and Am distributions for 5% Am-MOX fuel specimen irradiated at about 43 kW/m for 24 h

SUMMARY

Short-term irradiation tests of Am-MOX fuels were conducted. The results of non-destructive PIEs showed that all of the Am-MOX fuel pins were irradiated without any failure as expected. The microstructural evolutions were observed by optical microscopy and redistribution behavior of constituent elements were determined by EPMA. The ceramography results showed that structural changes such as formation of lenticular voids and the central void occurred quickly and early within a 10-minute irradiation. The results of EPMA revealed that Am migrated to the radial center of the fuel pellet along the temperature gradient during the initial stage of irradiation. This tendency is similar to that of Pu. The irradiation behavior at the high linear heating rate obtained in the Am-1 program will be useful for the modelling and design study of Am-containing MOX fuels.

REFERENCES

[1] Y. Sagayama, Proceedings of GLOBAL 2007, Boise, Idaho, USA (2007), p. 251.

[2] T. Namekawa et al., Proceedings of GLOBAL2005, Tsukuba, Japan (2005), Paper No.424.
[3] K. Tanaka, et al., Proceedings of GLOBAL 2007, Boise, Idaho, USA (2007), p. 897.
[4] T. Soga, et al., Proceedings of ICONE 15, Nagoya, Japan (2007), paper No. 10212.
[5] T. Sekine et al, Proceedings of GLOBAL 2007, Boise, Idaho, USA (2007), p. 10.
[6] H. Yoshimochi et al., *J. Nucl. Sci. Technol.,* **41** (2004), p. 850.
[7] S. Koyama et al., *J. Nucl. Sci. Technol.*, **40** (2003), p. 998.
[8] S. Maeda et al., Trans. Int. Meeting of RRFM 2001, Aschen, Germany (2001), p. 56.
[9] P. F. Sens, *J. Nucl. Mater.*, **43** (1972), p. 293.
[10] H. Hoffmann, *J. Nucl. Mater.,* **54** (1974), p. 9.
[11] H. Kashihara et al., Trans. Am. Nucl. Soc., **60** (1989), p. 309.
[12] D. Freund, *Kerntechnik,* **55** (1990), p. 350.
[13] M. Inoue et al., *J. Nucl. Mater.,* **323** (2003), p. 108.
[14] C. T. Walker, G. Nicolaou, *J. Nucl. Mater.*, **218** (1995), p. 129.
[15] M. Kato et al., *J, Nucl. Mater.*, **373** (2008), p. 237.

5.3 MEASUREMENTS OF Xe DIFFUSION COEFFICIENT OF UN

Kwangheon Park[a], Heemoon Kim[b], Bong Goo Kim[b], Jae Won Lee[b], Ho Jin Ryu[b], Geun Il Park[b]

[a] *Dept. of Nuclear Engineering, Kyunghee University*
Seochon-1, Kiheong, Yongin, Kyunggi, 449-701, Rep. of Korea
[b] *Korea Atomic Energy Research Institute*
150 Ducjin, Yusung, Daijeon, 350-353, Rep. of Korea

Post irradiation annealing (PIA) tests were performed to obtain the Xe-133 diffusion coefficients of uranium nitride (UN). UN powder was obtained from the mixed powder of UO_2 and carbon under the H_2-N_2 gas mixture. Porous discs (45%TD) of UN were made and used for the specimens for the PIA tests. For comparison purposes, porous discs of UO_2 (47%TD) were also made. Each 300mg specimen was irradiated to a burnup of 0.1 MWd/t-U. PIA tests were performed at 1200°C, 1300°C and 1400°C for UN, and 1400°C, 1500°C and 1600°C for UO_2, continuously. The oxygen potential during the annealing tests was about 440 ± 20 kJ/mol. The disc specimens of UN and UO_2 were found to be cracked or broken in pieces after annealing tests. The xenon diffusion coefficient for the near stoichiometric UN turned out to be about 1,000 times higher than that of UO_2 at 1400°C. And, the activation energy of diffusion in UN is about 230 kJ/mol, while that of UO_2 measured to be about 393 kJ/mol.

2008 KAERI-JAEA Joint Seminar on Advanced Irradiation and PIE Technology
November 5-7, 2008, KAERI-Daejun, South Korea

Measurements of Xe Diffusion Coefficient in UN

Kwangheon PARK[1], Heemoon KIM[2], Bong Goo KIM[2], Jae Won Lee[2],
Ho Jin Ryu[2] and Geun Il Park[2]

[1] Dept. of Nuclear Engineering, Kyunghee University
Seochon-1, Kiheong, Yongin, Kyunggi, 449-701, Rep. of Korea

[2] Korea Atomic Energy Research Institute
150 Ducjin, Yusung, Daijeon, 350-353, Rep. of Korea

1

Introduction

❑ **Fission gas diffusion coefficients :**

Fundamental property essentially used for the fuel performance analysis, and a good indicator for the mobile characteristics of fission gases.

❑ **Fission gas diffusion in UN fuel :**

UN fuel is a potential candidate for the fast and thermal reactors due to its high U density and good thermal conductivity.
To estimate or analyze the fuel performance behavior of UN fuel, fission gas diffusion coefficient has to be known.

2

Experimental Procedure

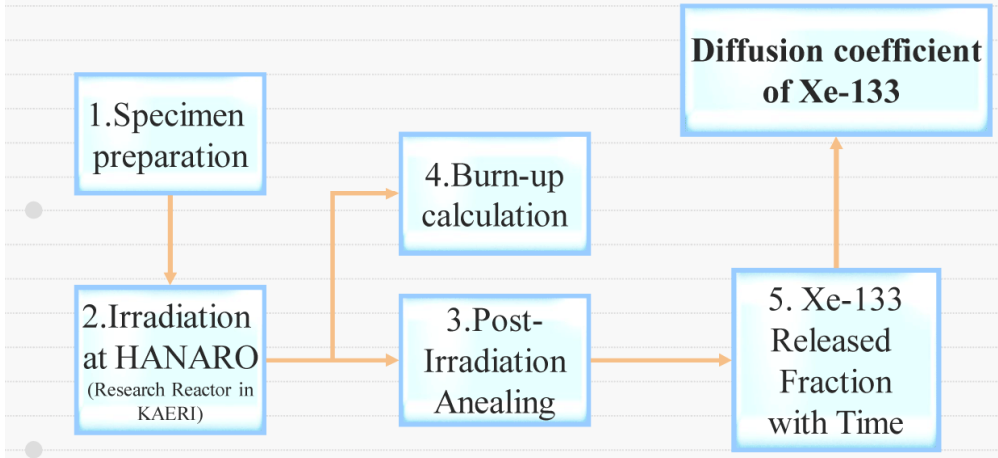

3

Experimental : 1. Specimen preparation

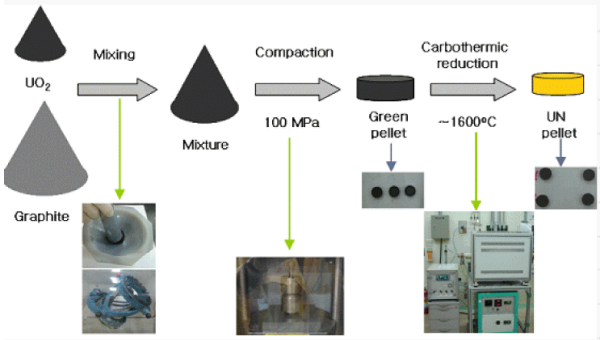

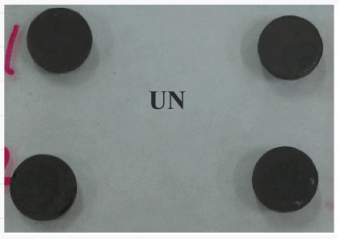

UN samples

Index	Weight(g)	Dia.(mm)	Length(mm)
SX-38	0.2290	7.078	0.900
SX-39	0.2419	7.060	0.956
SX-40	0.2462	7.087	0.965
SX-41	0.2496	7.109	0.0973

UO_2 samples

Index	Weight(g)	Dia.(mm)	Length(mm)
SX-42	0.2623	7.058	1.292
SX-43	0.2634	7.050	1.306

4

UN sample

UO_2 sample

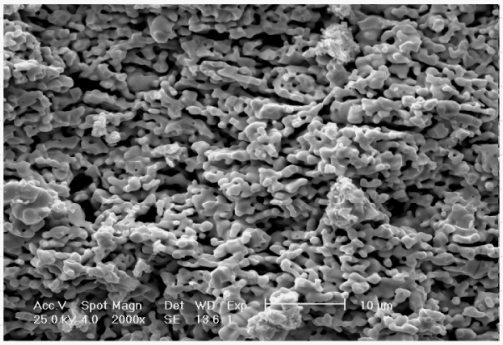

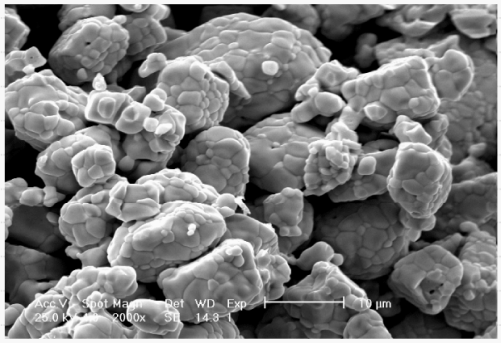

Samples	Theoretical D(%)	BET (m^2/g)
UN	45.2	0.2434±0.0036
UO_2	47.6	0.3132±0.0301(?)

5

Experimental : 2. Irradiation at HANARO (1)

Container tube

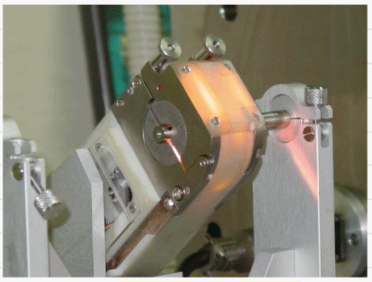

TIG welding

Irrad. capsule

6

Experimental : 2. Irradiation at HANARO (2)

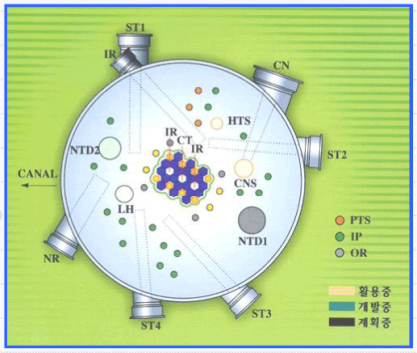

Samples	Irrad.(16 min.)	Irrad. Hole
SX-38(UN1)	08.3.11(09:40~09:56)	IP4
SX-39(UN2)	08.3.18(09:35~09:51)	IP4
SX-40(UN3)	08.3.20(09:30~09:46)	IP4
SX-41(UN4)	08.3.25(09:45~10:01)	IP4
SX-42(UO_2-1)	08.3.13(09:35~09:51)	IP4
SX-43(UO_2-2)	08.3.27(09:35~09:51)	IP4

Irradiation Hole : HTS hole (Thermal neutron flux : 8.31×10^{13} #/cm^2.s)

Total Burn-up : 0.1 MWD/t-U

7

Experimental : 3. Post-Irradiation Annealing(1)

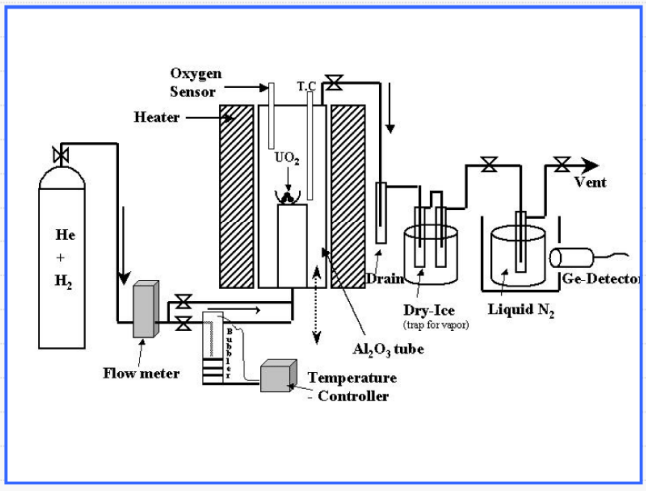

8

Experimental : 3. Post-Irradiation Annealing(2)

Capsule dismantling

Sample in cask

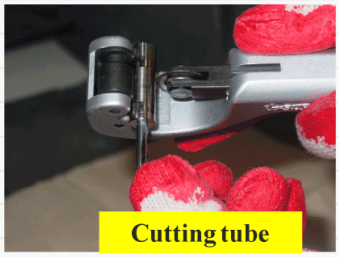

Cutting tube

Crucible and cap

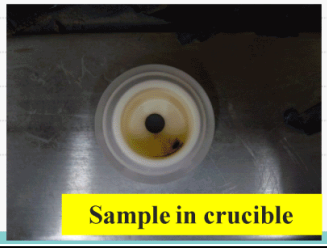

Sample in crucible

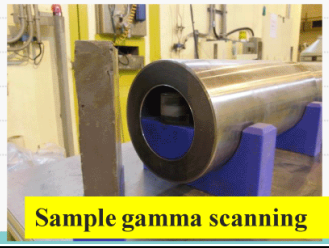

Sample gamma scanning

Experimental : 4. Burn-up Calculation

Gamma scanning (Ba-133 & sample)
→ I-131 radioactivity (364 keV)

ORIGEN-2 calculation
(Burnup calculation & Xe-133 radioactivity)

Amount of Xe-133 in sample

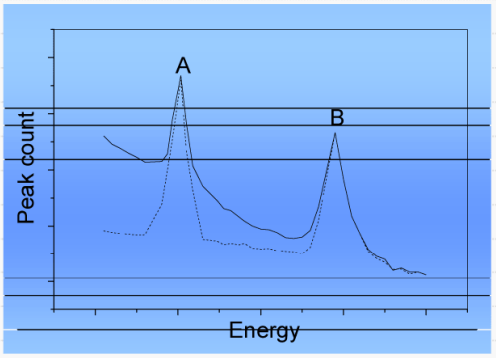

sample	Aactivity of I-131 (μCi)	Burnup (MWd/t-U)	Aactivity of Xe-133(μCi)	Remarks
SX-38(UN1)	18.73	0.0687	60.17	
SX-39(UN2)	23.858	0.0829	76.68	
SX-40(UN3)	21.91	0.0747	70.34	The efficiency of the detector for I-131(364 keV) and Ba-133(356 keV) is assumed to be the same.
SX-41(UN4)	32.64	0.11	105.2	
SX-42(UO_2-1)	29.51	0.105	94.6	
SX-43(UO_2-2)	26.2	0.0922	83.85	

Experimental : 5. Xe-133 Detection, Diffusion Coefficient

Annealing history

Sample	Detection gap (min.)	Annealing time(hour)				
		1200℃	1300℃	1400℃	1500℃	1600℃
SX-38(UN1)	30	4		3		3
SX-39(UN2)	10	1		1		1
SX-40(UN3)	10	2	1	1		
SX-41(UN4)	10	2	1.5	1.5		
SX-42(UO2-1)	30			3.5	2.5	3
SX-43(UO2-2)	30			4	2.5	2.5

Gamma detection in filtration system
(Xe-133 released from sample)

Amount of released Xe-133

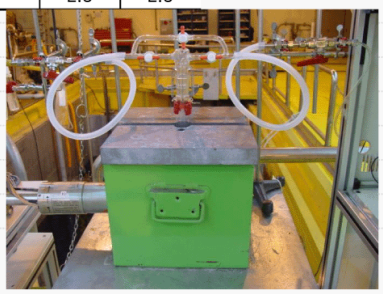

Experimental : 5. Xe-133 Detection, Diffusion Coefficient

Fractional gas release

$$f^2 = \frac{36D}{\pi a^2} t$$

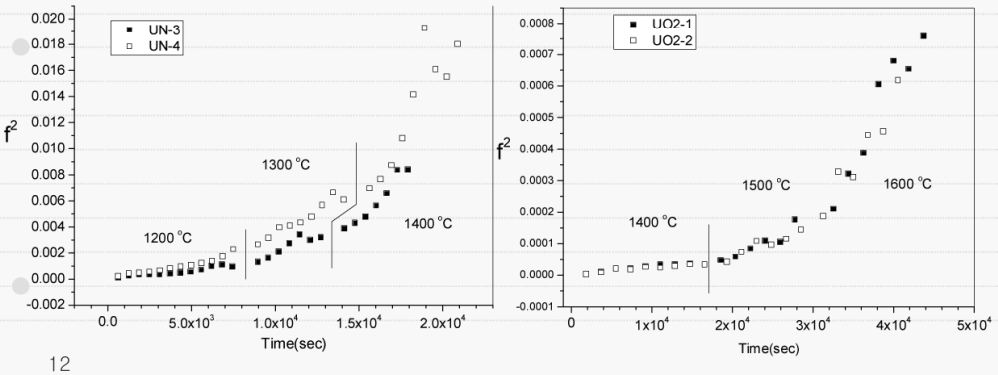

12

Results

$$S = \frac{36D}{\pi a^2} \qquad \frac{S_T}{V} = \frac{3}{a}$$

Diffusion Coefficient of Xe-133

Sample	Diffusion coefficient(mm²/s)					'a' value(mm)	
	1200℃	1300℃	1400℃	1500℃	1600℃	'a'	Avg.
UN1	1.49×10^{-12}		1.70×10^{-12}		1.62×10^{-12}	1.905×10^{-3}	1.9064×10^{-3}
UN2	3.57×10^{-13}		7.09×10^{-13}		5.03×10^{-13}	1.9068×10^{-3}	
UN3	4.24×10^{-14}	1.77×10^{-13}	4.18×10^{-13}			1.9057×10^{-3}	
UN4	8.06×10^{-14}	2.32×10^{-13}	7.30×10^{-13}			1.9071×10^{-3}	
UO_2-1			8.46×10^{-16}	4.28×10^{-15}	1.72×10^{-14}	1.988×10^{-3}	1.9857×10^{-3}
UO_2-2			6.89×10^{-16}	3.29×10^{-15}	1.42×10^{-14}	1.9834×10^{-3}	

Results

$$D(mm^2/s) = 8.756\times10^{-6}\exp\left(-\frac{230(kJ/mol)}{RT}\right)$$

$$D(mm^2/s) = 1.437\times10^{-3}\exp\left(-\frac{393(kJ/mol)}{RT}\right)$$

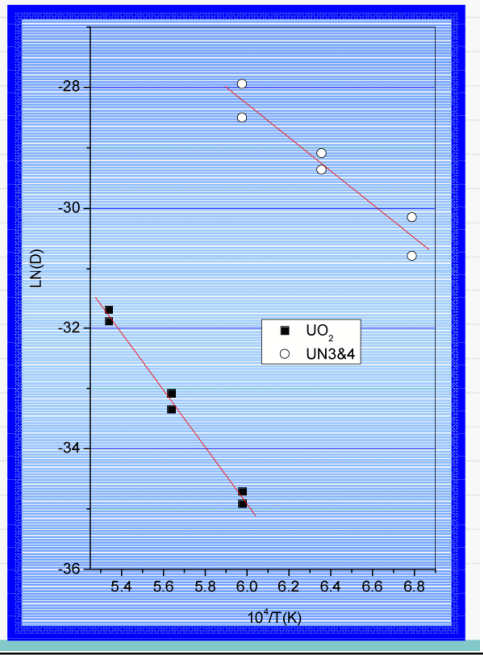

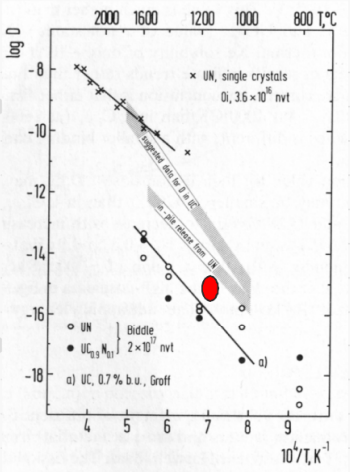

Xe diffusion in UN

Matzke

Fig. 9.22. Available data for Xe release from U(C,N) and UN measured either in post-irradiation laboratory anneals [27, 39] or in-pile [26]. The band of suggested D values for UC from fig. 9.19 is shown for comparison. The data for UN single crystals are unexpectedly high and the corresponding ΔH is unexpectedly low. All these release data as well as those of figs. 9.18 to 9.21 were obtained on specimens with very low burn-up ($\leqslant 10^{18}$ f cm^{-3}, $\leqslant$0.01 at% burn-up). The line labelled a) shows data [90] for UC irradiated to a much higher burn-up of ~0.7 at%. (D in cm^2 s^{-1})

15

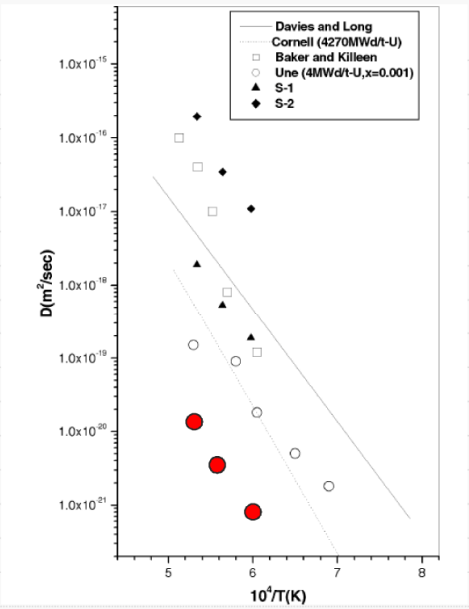

Xe diffusion in UO_2

2~3 orders lower.

BET data may be wrong. (Average radius of a grain in the SEM figure is about 5 microns.)

16

5.4 RESEARCH INFRASTRUCTURE FOR ACTINIDE SCIENCE AT IMR

Makoto WATANABE, Yoshimitsu SUZUKI,
Yoshiya HOMMA, Dai AOKI*, Y, HAGA[A], S. KAMBE[A], A. NAKAMURA[A]
Mitsuo HARA, Kenji KONASHI, and Tatsuo SHIKAMA

International Research Center for Nuclear Materials Science, IMR, Tohoku University
Narita, Oarai, Ibaraki, 311-1313 Japan
[A]Advanced Science Research Center, Japan Atomic Energy Agency
Tokai, Ibaraki 319-1195 Japan
** Present Address: INAC/SPSMS, CEA-Grenoble, Grenoble 38054 France*

ABSTRACT

The new project research on the physical properties of the transuranium compounds, which had been studied within engineered approach in Japan, was started from April 2003 under the collaboration of Institute for Materials Research of Tohoku University (IMR) and Advance Science Research Center of JAEA (ASR). Preparation of neptunium metal, crystal growth for the neptunium compounds and microscopic measurements have been performed at the laboratory for actinides experiment (LAE) of IMR by using gram order materials. Until this moment, our subject at LAE, which was designed for the transuranium materials, had been limited to the uranium and thorium compounds and the dilute solution of actinides. Computational approach has been also started to elucidate the intrinsic properties of the transuranium compounds in our laboratory.

INTRODUCTION

The Oarai-branch of Institute for Materials Research in Tohoku University has been an open facility to researchers in Japanese universities who want to utilize irradiation service in the Japan Materials Testing Reactor (JMTR) of the Oarai Research and Develop Center of Japan Atomic Energy Agency since its original foundation in 1969. To meet increasing interest in studies on actinide physics and chemistry, a new laboratory for actinides experiment (LAE) was constructed during 1987-1991. This laboratory was designed for the

solid state physics and chemistry of Th, U, Np, and Am compounds. But our subject had been limited to the uranium and thorium compounds and the dilute solution of actinides because of technical and financial problem. The new project research on the physical properties of the transuranium compounds, which had been studied within engineered approach in Japan, was started from April 2003 under the collaboration of Institute for Materials Research of Tohoku University (IMR) and Advance Science Research Center of JAEA (ASR). Preparation of neptunium metal, crystal growth for the neptunium compounds and microscopic measurements such as he Haas-van Alphen (dHvA) effect, the NMR spectrometer and the Mössbauer spectrometer have been performed at the laboratory for actinides experiment (LAE) of IMR by using macro order materials. Standard measurements for electric resistivity, specific heat and magnetization were also performed at LAE. New exotic properties originated from strong correlation of the 5f electrons was clarified for several neptunium compounds. Computational approach has been also started to elucidate the intrinsic properties of the Pu oxide in our laboratory.

In this paper, we describe process and facility for transuranium samples at LAE and also mention recent research activities.

LABORATORY FOR ACTINIDES EXPERIMENT

The LAE is three stories high with one basement and has earthquake-proof structure made of reinforced concrete. Most of the experimental equipment is settled in the first floor. Fig. 1 shows a layout of the first floor, i.e., main hole of LAE. Radiation protected area (RPA), shown in bold line, is divided into two zones, a low level zone and a high level zone. The rooms for contamination test, radiometry, physical characterization, and cell operation are in the low level zone and samples enclosed in proper vessels or capsules are treated in these rooms. Thus, these rooms are regarded as contamination free area.

In the rooms of pyrochemistry and solution chemistry, unsealed actinide samples are treated and these rooms are called as umber rooms. Handling of highly radioactive materials is performed in the hot cell and precise experiments are carried out in the rooms of solution chemistry and pyrochemistry by using glove boxes or draft hoods

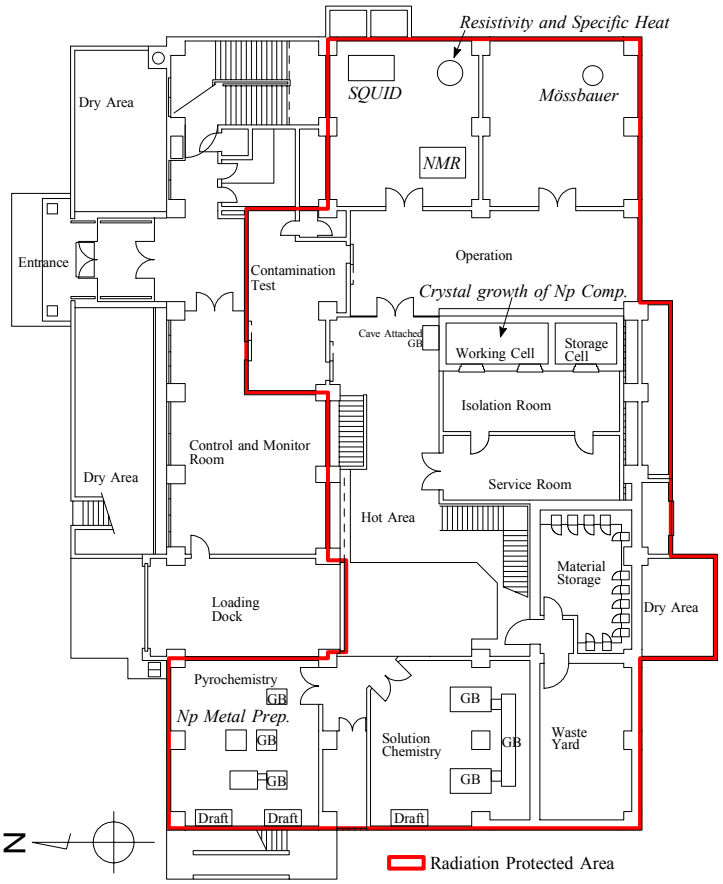

Fig.1 Layout of the Laboratory for Acitinide Elements(1F)

Mass Flow of Actinide Research

A small quantity of TRU has been produced from commercially available actinides such as U,Np,and Am by neutron irradiation in JMTR. Materials for the irradiation are also prepared in LAE. The materials are encased in a sealed sub capsule usually made of fused silica which is then encapsulated into a stainless steel clad for a short term irradiation in hydraulic rabbit or a stainless steel capsule-rig for along term irradiation. Every enclosure is examined by X-ray autoradiography before irradiation and transported to JMTR. After the irradiation, the rabbit or the rig is cooled in a water pool in JMTR to wait for the decay of short-lived induced radioactivities. Then, the sub capsule is retrieved in a hot cell in JMTR and transported to LAE by using a container applied with thick lead shield.

The container is transported into LAE through the loading dock and settled on to the transfer port, named gamma-gate, of storage cell by using a 10 tons crane. The gamma-gate has an air tight structure applied with 250 mm thick lead shield and the irradiated sub capsule can be transferred into the storage cell. The irradiated actinide containing specimen is

retrieved by using a cutter in the storage cell and then transferred to the working cell through a transfer port which consists of a pair of double-sealed and air-leak-tight doors on each side of the two cells.

The chemical separation of TRU is carried out in the working cell and the isolated TRU is transferred to the cell glove box attached on the side wall of the working cell. Then, TRU thus isolated may contain impurities of other actinides and lanthanides. The final purification to remove these impurities is carried out in the room for solution chemistry by using a glove box or a draft-hood. Sometimes, commercially obtained actinides contain impurities. The removal of these impurities is also performed by using these equipments.

Specification of Hot Cell

Fig. 2 illustrates the structure of the hot cell. The cell shield is made of 350 mm thick SS-41 steel and the inside of the shield is covered with polished lining made of 4mm thick SUS 316L plates. Each SUS 316L plate was welded together to make air-leak-tight structure of the two cells. Seven air-tight manipulators (Sargent Model-L),five lead glass windows,250 mm thick lead equivalent, and a control desk are attached in the front wall of the two cells. Major experiment in the working cell can be carried out by using four manipulators inspecting the inside condition through one of the three windows. The setting of the experimental apparatus inside the cell can be made by using a glove port attached at the rear side of SUS lining wall. Many feed-throughs are available to get easy access for electricities, gases and chemical reagents.

An isolation room is provided for the maintenance and decontamination of apparatus settled in the cells. The room also has air-tight structure and the maintenance works will be done appling a tunnel suit attached to the tunnel port. These maintenance works will be supported by supporters in service room. Air in the isolation room is taken from hot area through a gallery attached at the wall of service room and transported through one of the two over hanged HEPA filter cases. Another HEPA filter case is equipped at the rear wall of the cell shield to transport the air into the cells. Air ducts are attached to each filter case to insure the down blow of the air.

For the cleaning of the exhaust from the cell, cell filters are also equipped and the exhaust is treated finally by using a filter assembly of hot cell. The filter assembly is consisted from two ULPA filters and one charcoal filter. The ULPA filter can remove 99.999% of airborne radioactive particles of 0.0001 mm in diameter. Leak-tight automatic-valves are attached to the cell ventilation system. These assemblies can sustain a pressure difference up to 500 mmAq. The measured leak rates are less than 0.01 vol%/h and less than 0.007 vol%/h for the cells and cell glove box, respectively.

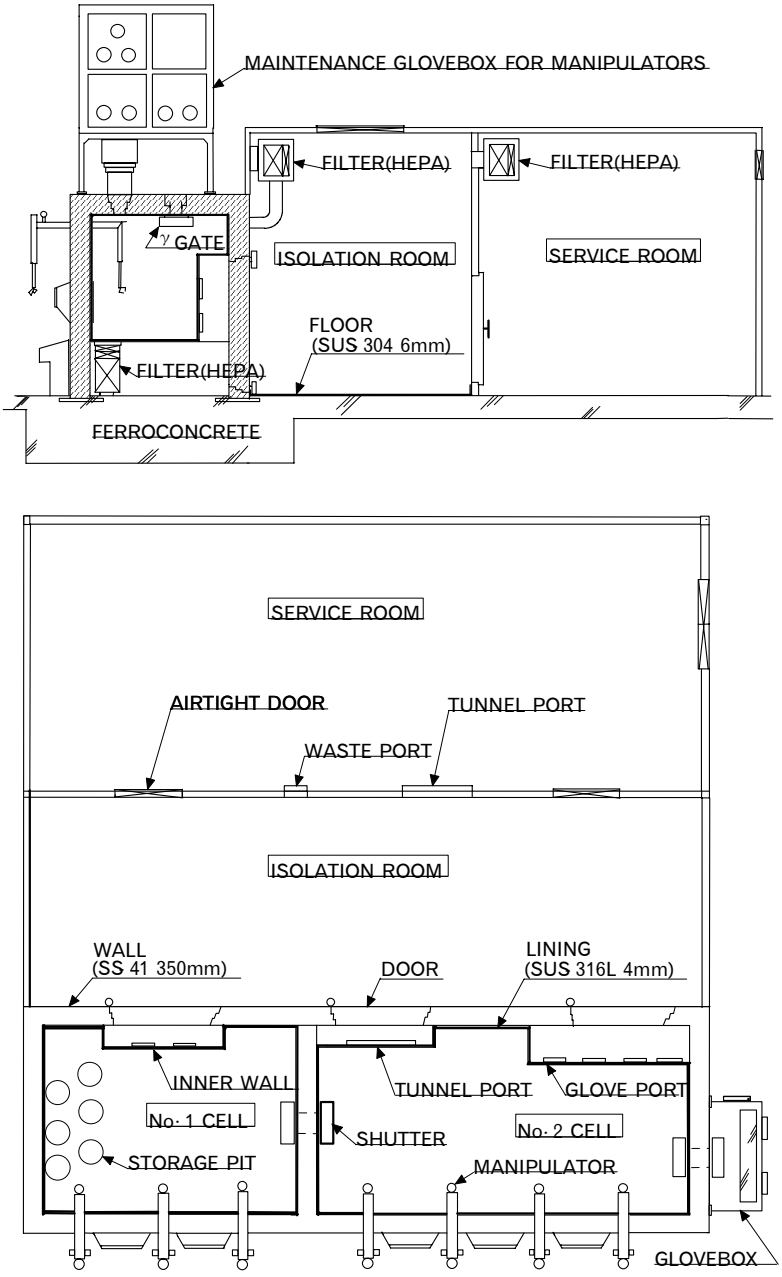

Fig.2 The structure of the hot cell

Maximum Limits of Main Actinide Nuclides for Daily Use

Table 1. shows maximum permissible amount of main actinide nuclides which can be used in LAE. To keep maximum freedom and to minimize the official inspection due to NPT, the amount of Pu is restricted to be less than 1g/y. The actinide element swhich can be used in substantial study of solid state physics and chemistry are Th, U, Np, and Am. The

conceptual design of health physical protection system and monitoring system is made to sustain the experimental use of these nuclides.

Table 1.Maximum limits of main actinide for daily use

Nuclide	In Hot Cell	In Glove Box
^{233}Ra	15 GBq	5 MBq
^{232}Th	(500 g)	(1,000 g)
Irrad. Th	250 GBq (50 g)	10 MBq (50 g)
^{231}Pa	1 GBq	15 MBq
^{233}U	(100 mg)	(40 mg)
^{238}U	(500 g)	(1,000 g)
Irrad.U	250 GBq (50 g)	10 MBq (50 g)
Conc.U(<20%)	(15 g)	(5 g)
Conc.U(>90%)	(50 mg)	(20 mg)
^{237}Np	500 MBq	200 MBq
^{238}Pu	20 GBq	20 GBq
^{239}Pu	(200 mg)	(100 mg)
^{241}Am	25 GBq	250 MBq
^{243}Am	2 GBq	250 MBq
^{242}Cm	25 GBq	250 MBq
^{243}Cm	10 GBq	25 MBq
^{244}Cm	2 GBq	100 MBq
^{248}Cm	10 MBq	500 kBq
^{251}Cf	100 MBq	5 MBq
^{252}Cf	30 MBq	1.5 MBq
^{253}Es	100 MBq	10 MBq

RECENT PROGRESS IN ACTINIDE'S RESEARCH AT IMR

Solid State Physics of Np Compounds

The new project research on the physical properties of the transuranium compounds was started from April 2003 under the collaboration of Institute for Materials Research of Tohoku University (IMR) and Advance Science Research Center of JAEA (ASR) to extend the actinide science in Japan, which had been confined mainly within the uranium compounds. We had integrated several techniques at Oarai branch of IMR; a metal preparation by hydrometallurgy, a crystal growth by flux or chemical transport method, and microscopic measurements. As shown in Fig. 3(a), we made the neptunium amalgam in aqueous solution by electrolytic process. Finally, we obtained the neptunium metals about 1 g for each compounds by thermal decomposition of the amalgam (Fig. 3(b)).

Fig.3(a) Electrolytic reduction process in aqueous solution for Np amalgam.

Fig.3(b) Np metal made by thermal decomposition.

We installed several equipments for solid state physics at Actinide Laboratory; He-3 cryostat for measuring the specific heat and the electric resistivity, dilution refrigerator for the Haas-van Alphen (dHvA) effect, the NMR spectrometer and the Mössbauer spectrometer as assigned in Fig. 1. First main research subject was the $NpTGa_5$ (T= transition metals) compounds motivated by the recent discovery of superconductivity at 18.5K in the plutonium based compound, i.e. $PuCoGa_5$. Microscopic measurement revealed a huge variety of magnetic phase transition of the $NpTGa_5$ compounds, in which a freedom of orbital in the strong correlated f electrons may play an important role. As shown in Table I, we clarify the intrinsic physical properties of several neptunium compounds, which have been studied in polycrystalline samples, by using high quality single crystals made by flux method or

chemical transport. Typical single crystals are shown in Fig. 4.

Table II. Np Compounds made at Oarai Center

Compounds	Phase Transition	Ordering Temperature
$NpFeGa_5$	AF	T_N=118K, T*=78K
$NpCoGa_5$	AF	T_N=47K
$NpNiGa_5$	F, AF	T_C=30K, T*=18K
$NpRhGa_5$	AF	T_{N1}=36K, T_{N2}=32K
$NpPtGa_5$	AF	T_N=26K
$NpGe_3$	Para	
$NpGa_3$ (Trigonal)	F	T_C=70K
$NpIn_3$	F, AF	T_C=14K, T_N=10K, T*=8K
$NpSn_3$	AF	T_N=9.5K
$NpPb_3$	AF	T_N=13K
$NpAl_4$	AF	T_N=49K
$NpSb_2$	F	T_N=47K
NpO_2	O	T_O=26K
$NpFe_4P_{12}$	F	T_C=23K
$NpCu_2Si_2$	F	T_C=37K
$NpCd_{11}$	CW	
$NpPd_5Al_2$	SC	T_c=5K

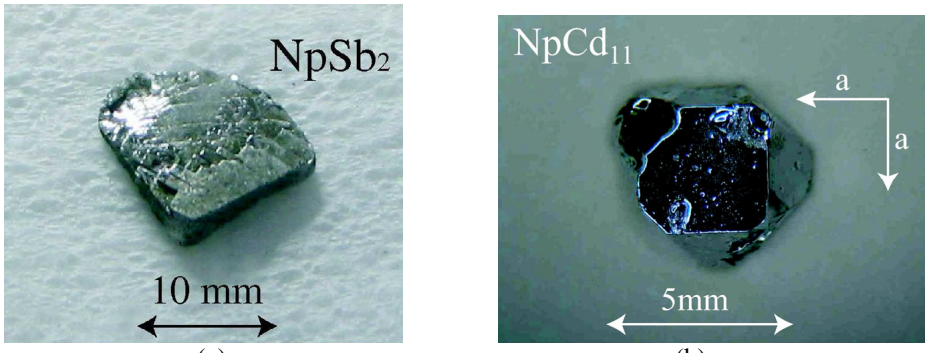

(a) (b)

Fig.4 Photograph of single crystal of (a) $NpSb_2$ and (b) $NpCd_{11}$.

Computational Science of TRU Oxide

In addition to above experimental studies, computer science studies of TRU oxides have been done. The first principles molecular dynamics simulation for TRU oxide has been carried out using the Vienna Ab Initio Simulation Package (VASP), which is a density functional theory-based code for systems with periodic boundary conditions. The total energy and the electronic structure of TRU oxide are calculated by the projector augmented wave (PAW) method within the generalized gradient approximation (GGA) for exchange-correlation density and potential, using the Perdew-Wang parameterization. The calculations are performed with the HITACHI/SR-8000 in Tohoku University.

Figure 5 shows an example of the first principles calculation results; a contour map of charge density difference near oxygen vacancy in plutonium dioxide. The difference in the charge density between the defect model and the perfect model has been calculated to make the effect of vacancy clear. The oxygen partial pressure, which controls the chemical reaction in the fuel pin, has also been studied by means of the first principles calculation. The thermophysical properties of plutonium dioxide have also been evaluated by using simulation results of the first principles calculations.

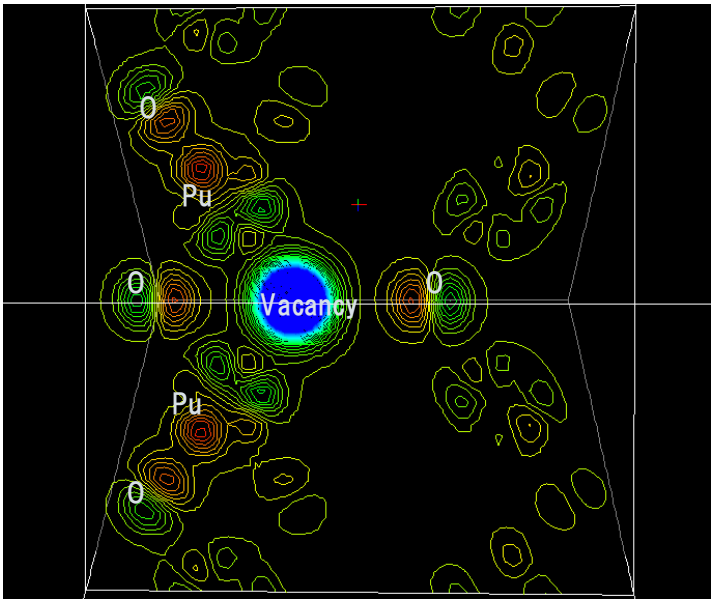

Fig.5 Charge density difference near oxygen defect in plutonium dioxide

ACKNOWLEDGEMENTS

Solid State Physics of Np compounds was performed in the frame work of IMR-JAEA collaboration. Prof. Y. Shiokawa (IMR & JAEA), Dr. D. Aoki (IMR), Dr. Y. Haga (JAEA), Dr. A. Nakamura (JAEA), Dr. E. Yamamoto (JAEA), Dr. T. Matsuda (JAEA), S. Ikeda (JAEA), Dr. S. Kambe (JAEA), Dr. Y. Tokunaga (JAEA), Dr. H. Sakai (JAEA), Dr. H. Chudo (JAEA), S. Nasu (Osaka Univ. & JAEA) and Prof. Y. Ōnuki (Osaka Univ. & JAEA) joined this program. Computational calculation studies were done under the collaboration with staff of Center for Computational Materials Science of IMR.

5.5 PIE TECHNIQUES FOR HYDRIDE REORIENTATION TEST AT NDC

Tomohiro Tsuda, Yasunari Shinohara, Yoichiro Yamaguchi

Nuclear Development Corporation,622-12, Funaishikawa ,Tokaimura,Ibaraki319-1111, Japan
tsuda@ndc.hq.mhi.co.jp, shinohara@ndc.hq.mhi.co.jp, yamaguchi@ndc.hq.mhi.co.jp

ABSTRACT

Dry storage of spent fuels in the interim storage facility is being planned in Japan. However, the gradual deterioration of the mechanical property of fuel cladding due to internal pressure and temperature during the storage term is known. Therefore, the integrity of stored fuel rods should be confirmed before the start of dry storage.

For the last several years, NDC had a lot of experiences on the hydride reorientation test. The specimen preparation techniques on the hydride reorientation test and the mechanical testing techniques after the hydride reorientation are shown in this paper.

INTRODUCTION

Spent fuel assemblies which had been used in nuclear power plants are kept in the spent fuel storage pool of the nuclear power plant till they are transported to the fuel reprocessing plants. However, as the ability for reprocessing is not enough the dry storage in the interim storage facility is expected.

To continuously keep the safety of dry storage, it is most important that the integrity of cladding tube during dry storage is maintained. One of the issues on the mechanical properties of cladding tube during interim dry storage is hydride reorientation. Therefore, the reorientation test which simulates the environment of dry storage fuel rod and the cladding mechanical test have been performed at NDC's hot cells for the commission of Japan Nuclear Energy Safety Organization (JNES). Flow chart for hydride reorientation test and mechanical property test are show in Fig.1. Temperature, hoop stress and cooling rate were considered as the simulated parameters in the hydride reorientation test.

HYDRIDE REORIENTATION TEST

1. Preparation of the hydride reorientation specimen

Fig.2 shows the schematic of specimen for the hydride reorientation test. Several short length rods were cut from spent fuel rods. To prevent the fission gas release from pellets during hydride reorientation test, pellets in the rod were removed from a short length rod with the drilling device. Fig. 3 shows the process of drilling [1]. Pellet was removed without damaging the inner surface of the cladding through four steps. The remained thin pellets layer on the inner surface of the cladding was dissolved by nitric acid. Fig.4 shows an example of the inside of claddings before and after the dissolution by the nitric acid.

After defueling, the outer oxide film of the central part of the cladding was removed to spot-weld the thermocouple at the central part of the cladding. The outer oxide film of both ends of the cladding is also removed to keep gas pressure shielded.

A piece of mandrel was put in a cladding before fixing the top plug (swagelok) and the bottom plug (swagelok) to decrease inner gas volume. It is also required to prevent the cladding from being damaged by fastening stress of end plugs. Therefore the outer diameter of mandrel was adjusted adequately corresponding to the inner diameter of cladding.

In addition to that, the torque of the end plugs was restrained low in the range in order to keep that the inner pressure. Excessive torque might cause the occurrence of cracks under the hydride orientation test.

2. Device & Method

Fig.5 shows the schematic of device for the hydride reorientation test. This device is composed of the furnace and the high-pressure gas line to supply the internal pressure. Though it can supply gas pressure enough to burst the cladding, 85-130MP was used for the hydride reorientation test. This pressure range is wider than that of the real storage condition to confirm the fundamental behaviors of hydrides.

Fig.6 shows the historical schematic of temperature and hoop stress during hydride reorientation test.

The specimens were cooled from max.340℃ to 100℃ at the cooling rate of 0.6～30 ℃/h in the furnace. Though the real cooling rate during the dry storage is at 10^{-3} ℃/h, the accelerated cooling rates were adopted as a hot cell scale test.

The orientation and length of hydrides were compared with before and after the hydride reorientation test with the optical microscope and the image analysis.

MECHANICAL PROPERTIES TEST

1. Specimen preparation

Ring compression test and tensile test were carried out to confirm the changes of mechanical characteristics before and after the hydride reorientation test. Fig.7 shows the process to manufacture the specimens.

Ring specimens with a width of 8 mm were used for compression test. In case of tensile test, the dog-bone type specimens with gage length of 33mm were made with a diamond whetstone. Fig.8 shows the grinding device used for the dog-bone type specimens. It is composed of X-Y table, circulation water pump and control system. The manufacturing accuracy of the specimen is below ±0.1mm to the gage width.

2. Device &Methods

Shimadzu AG-20 was used for compression test and tensile test. The capacity of the load cell is below 20 kN. The methods for mechanical tests are shown below.

Fig.9 shows the schematic of jigs for compression test. Two displacement transducers were attached to upper platen for the displacement measurement. The compression speed was about 2mm/min.

Fig.10 shows the schematic of jigs for tensile test. The strain rate and the test temperature for the tensile tests were approximately about 8.3×10^{-5}/s and 20℃, respectively.

RESULT

The hydride reorientation test techniques and the mechanical testing techniques had been established to confirm the integrity of spent fuels under the dry storage. These PIE techniques have been applied to the commission test of Japan Nuclear Energy Safety Organization (JNES). The results of PIE are accessible through the papers [2, 3] reported by JNES.

REFERENCES

[1] T.Tsuda, Y. Yamaguchi, Y. Shinohara, M. Sugano, Y. Kosaka, Y. Takeda , T.Kitagawa, Proceedings of 2005 JAEA-KAERI Joint Seminar on Advanced Irradiation and PIE Technolojies, P.82.

[2] Japan Nuclear Energy Safety Organization (JNES), *Investigation of storage technology of recycled fuel*, JNES fiscal report, 06-0006, JNES (2007).

[3] M. Aomi., K. Kamimura, T. Baba., T. Miyashita, Management of Spend Fuel from power Reactors, Proceedings of an international conference Vienna,19-22 June 2006

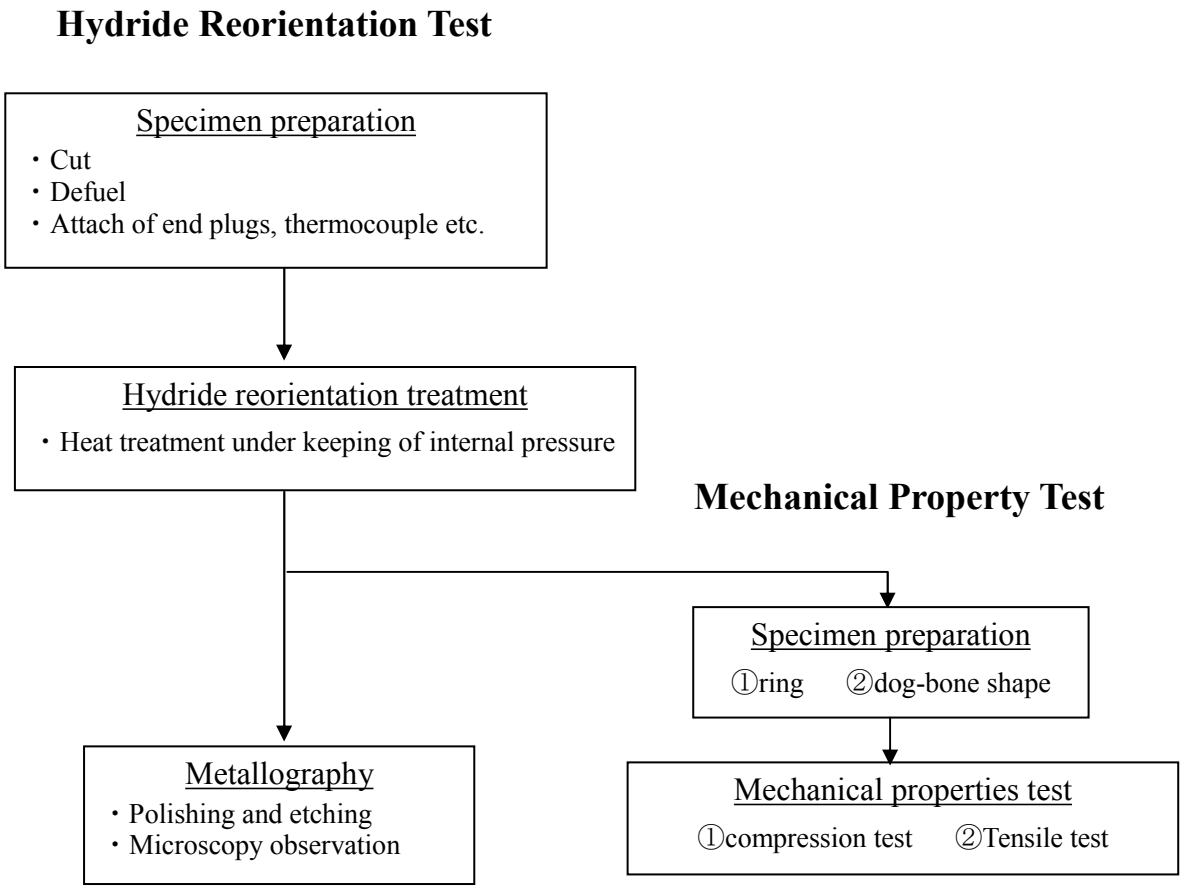

Fig.1 Flow chart for hydride reorientation test and mechanical property test

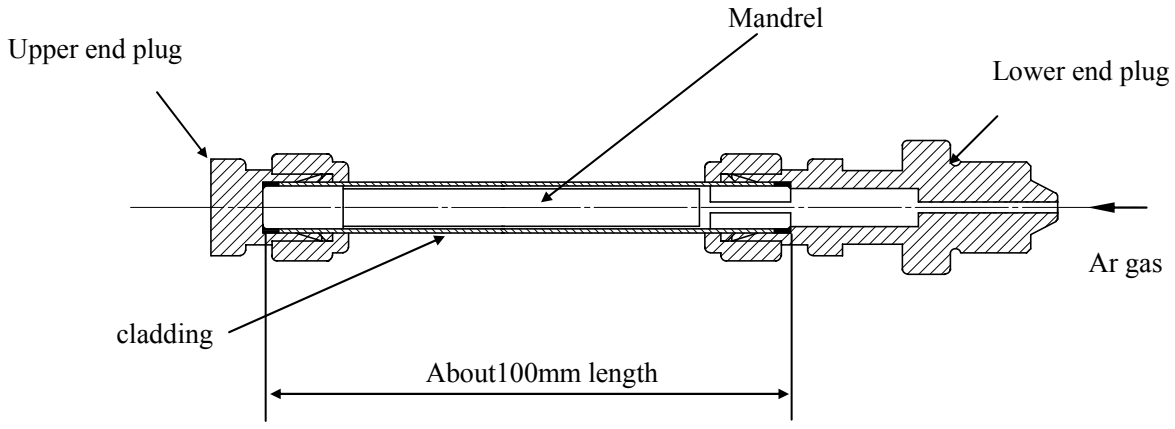

Fig.2 Schematic of specimen of hydride reorientation test

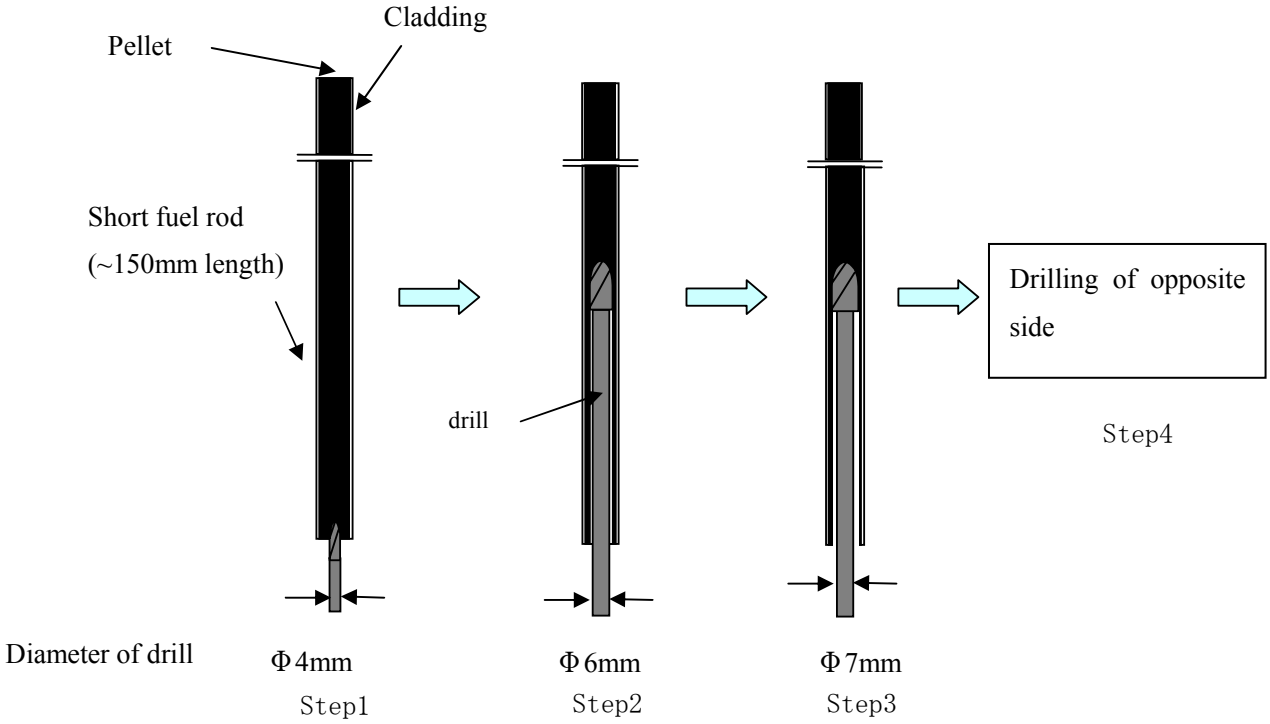

Fig.3 Process of drilling [1]

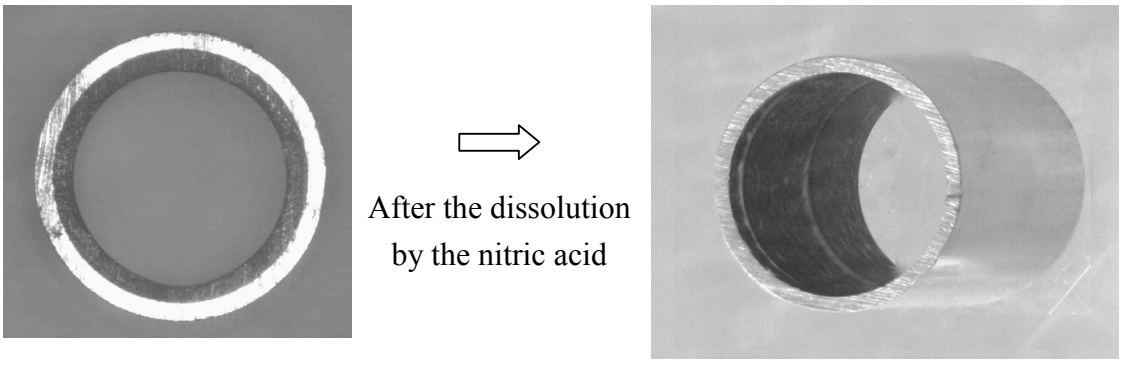

Fig.4 An example of the inside of claddings before and after the dissolution by the nitric acid

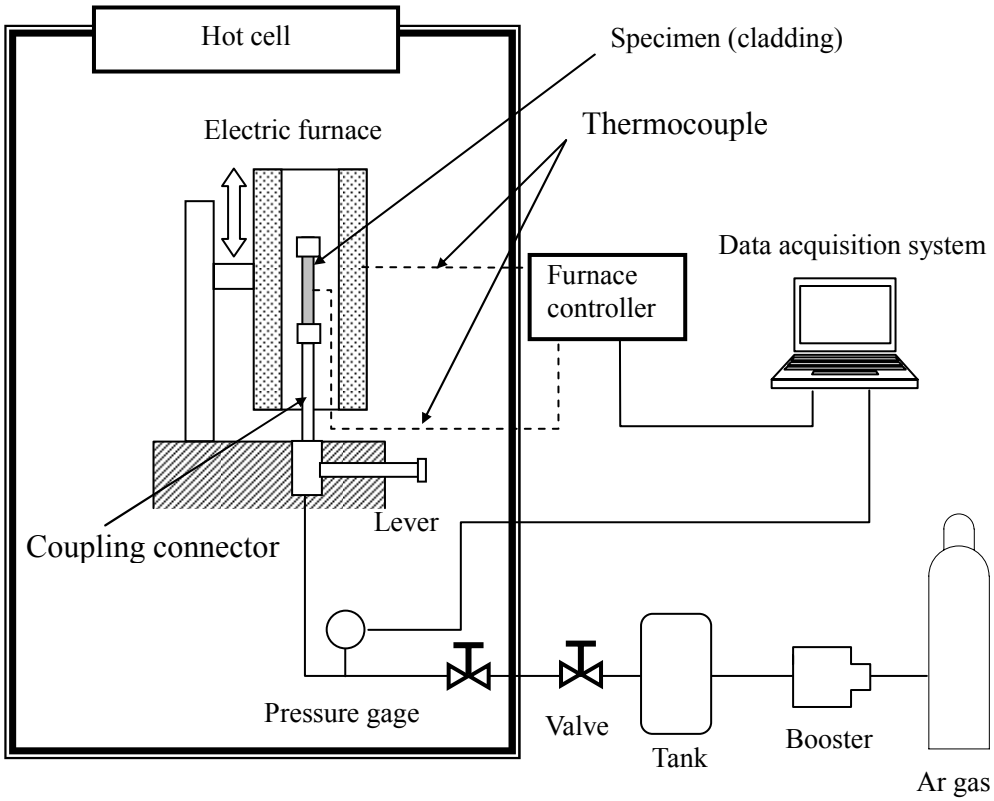

Fig.5 Schematic of device for hydride reorientation test

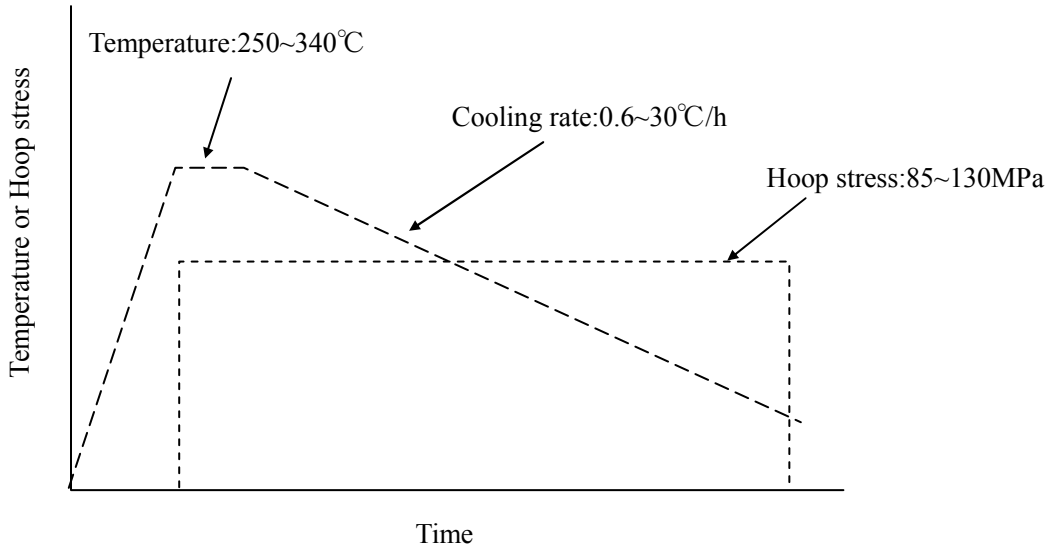

Fig.6 Historical schematic of temperature and hoop stress during hydride reorientation test

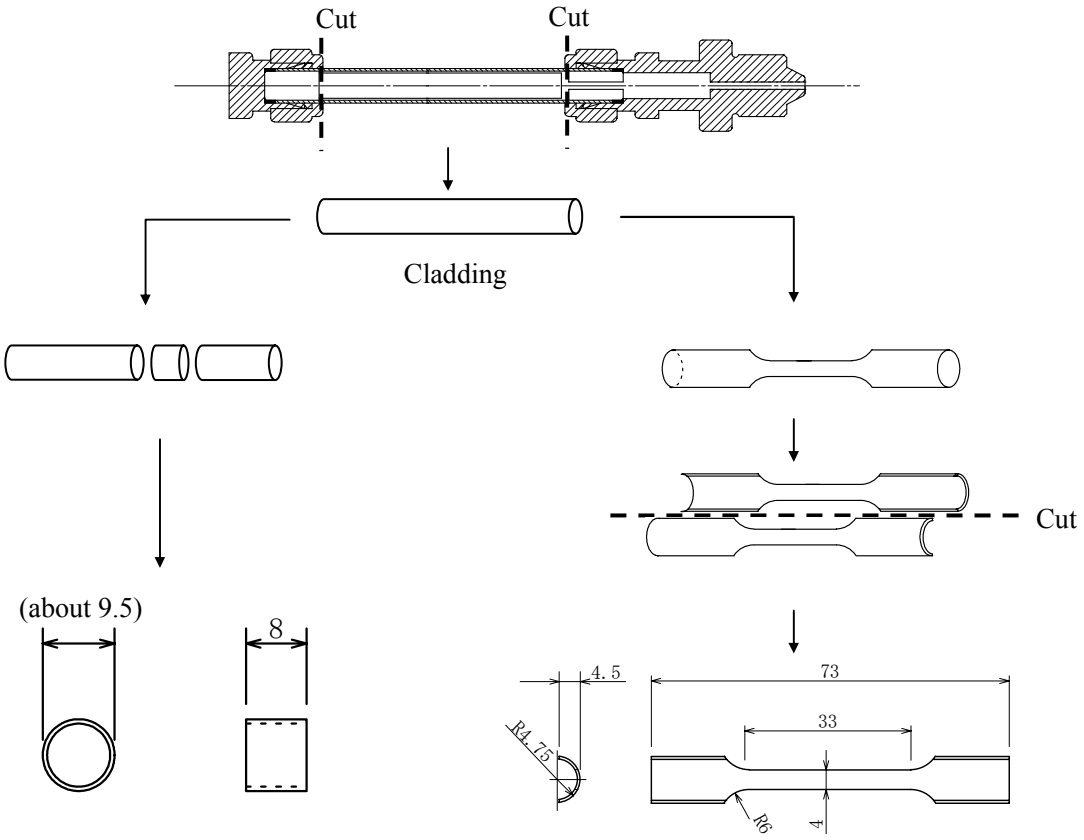

(Ring compression specimen) (Tensile specimen: dog-bone shape type)

Fig.7 Ring compression specimen and tensile specimen

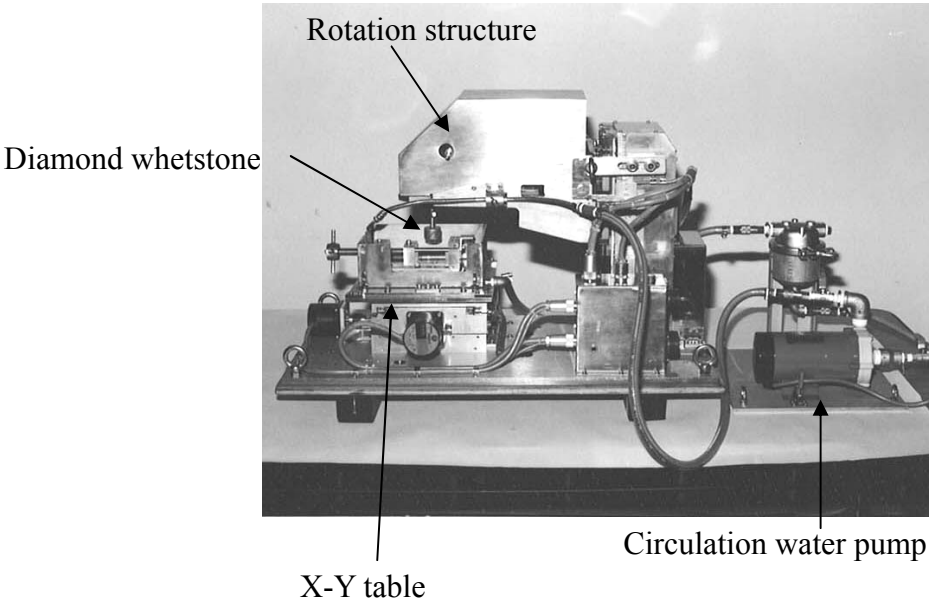

Fig.8 Photograph of the grinding device

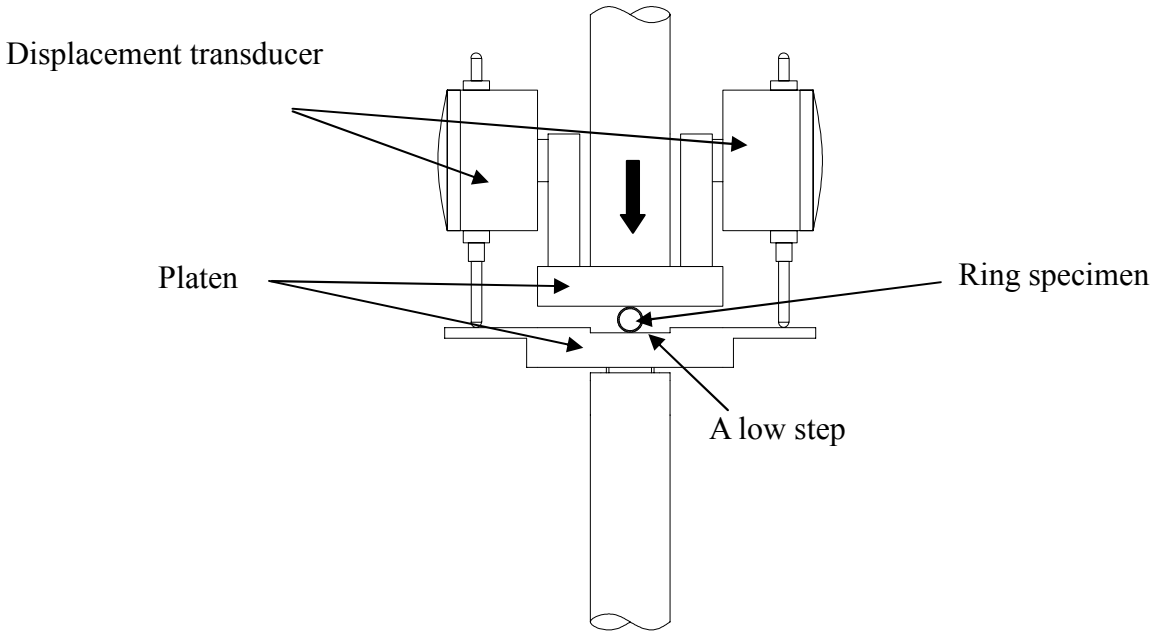

Fig.9 Schematic of ring compression test

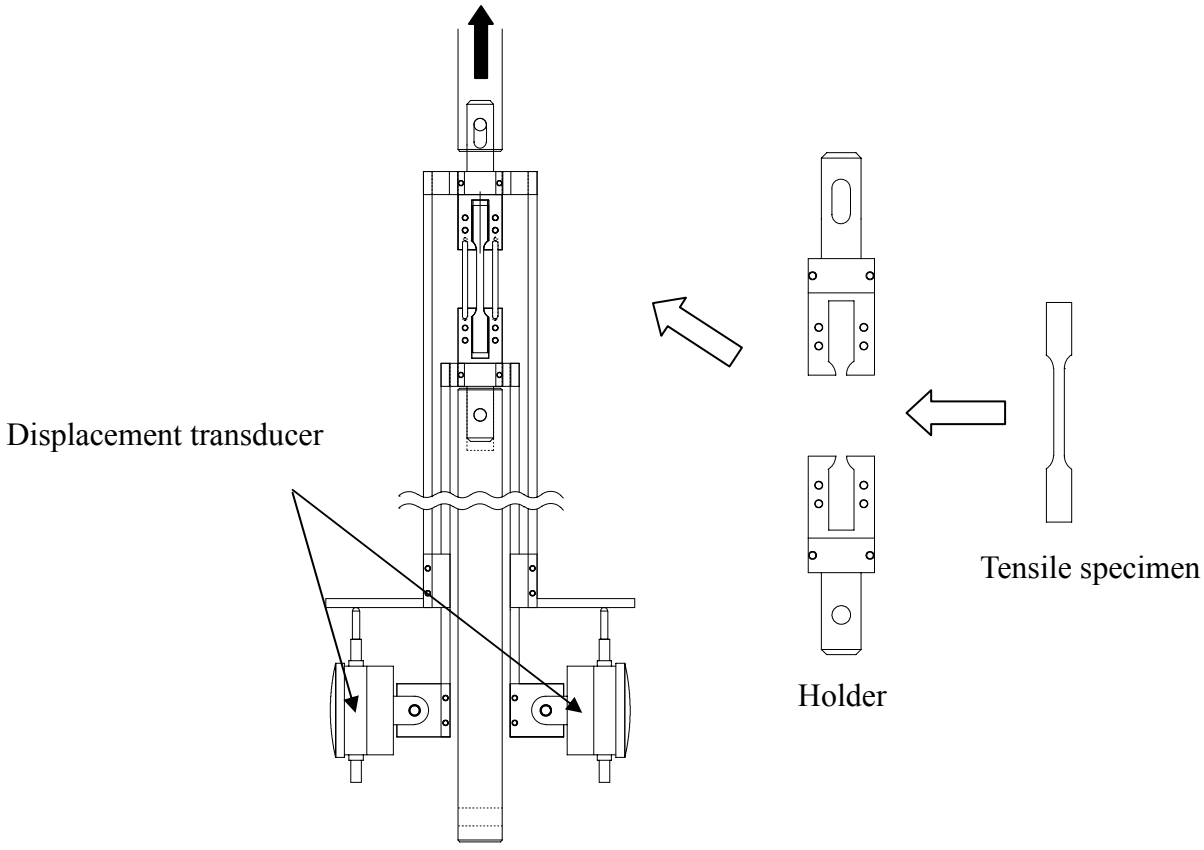

Fig.10 Schematic of tensile test

5.6 IMPROVED TECHNIQUE FOR HYDROGEN CONCENTRATION MEASUREMENT IN FUEL CLADDINGS BY BACKSCATTERED ELECTRON IMAGE ANALYSIS (II)

Atsushi Onozawa [a], Akio Harada [a], Junichi Honda [a],
Masahito Nakata [b], Hiroyuki Kanazawa [a], Tamio Sagawa [a]

[a] *Department of Hot Laboratories and Facilities, Tokai Research and Development Center,*
[b] *Safety Section, Project Promotion Sector,*
Japan Atomic Energy Agency
Tokai-mura, Naka-gun, Ibaraki pref 319-1195, Japan
onozawa.atsushi@jaea.go.jp

ABSTRACT

The measurement technique for hydrogen concentration using Backscattered Electron Image (BEI) analysis (BEI method) had been developed by Studsvik Nuclear AB. The hydride in claddings is identified using BEIs with Scanning Electron Microscope and the hydrogen concentration is calculated from the area fractions of the hydride in those BEIs. The BEI method is suitable for the measurement of local hydrogen concentration in fuel claddings.

In the Reactor Fuel Examination Facility, the sample polishing techniques and image processing procedure for BEI method were improved to measure the hydrogen concentration in the irradiated fuel claddings more precisely. In the previous confirmation tests using the un-irradiated fuel claddings, which were reported in the last seminar, the hydrogen concentrations measured by the improved BEI method gave good agreement with the results of Hot Vacuum Extraction method (HVE).

The radial and axial hydrogen concentration profiles of the irradiated fuel claddings were measured with improved BEI method. As the results of these measurements, the local hydrogen concentration could be indicated more precisely with the improved BEI method compared to the other methods for the hydrogen concentration measurement and observation.

INTRODUCTION

From the viewpoint of the effective utilization for the nuclear energy, the burn-up of the

commercial reactor fuel tends to be extended. The burn-up extension causes several physical property changes on the fuel and fuel cladding, including the hydrogen absorption increase to the cladding due to the growth of the oxide layer thickness. Once the absorbed hydrogen level that exceeds solid solubility limit, the hydride is precipitated. The hydride segregated to a local area by the temperature gradient causes the embrittlement of the fuel cladding. Therefore it is important to evaluate the hydrogen concentration at local area in the cladding, such as radial or axial profile, to confirm the safety margin of the cladding.

As previously reported in the 2005 K-J Joint Seminar[1], an improved technique for hydrogen concentration measurement by backscattered electron image analysis (improved BEI method) was developed in JAEA, based on the technique developed by Studsvik Nuclear AB[2]. This improved technique is very suitable to measure the local hydrogen concentration in the fuel cladding and the results of the confirmation test indicated superior performance of this improved technique.

THE IMPROVED BEI METHOD

The backscattered electron images (BEIs) were taken by SEM, and the hydride area fraction in the image is measured by the image analysis system. After that, the hydrogen concentration is calculated with substituting the area fraction into following formula.

$$Wt_H = Wt_\delta \cdot F \left(\frac{\rho_\delta}{\rho_{Zr}(1-F) + \rho_\delta \cdot F} \right) \quad (1)$$

Wt_H = Hydrogen concentration (wt ppm)

Wt_δ = Hydrogen concentration in δ-phase hydride (17,570 ppm)

F = Measured area fraction of hydride

ρ_δ = Density of δ-phase hydride (5.65g/cm^3)

ρ_{Zr} = Density of α-phase metal (6.54g/cm^3)

To measure the hydrogen concentration precisely with the BEI method, it is necessary to make the image of the hydride on the observation plane accurately and also to measure the hydride area fraction precisely. Therefore, the BEI method was improved on following two points, polishing technique for the sample surface and image analysis technique for the hydride area fraction measurement. Fig.1 shows a brief diagram of improvement points [3].

For the sample provided to BEI method, the observation surface should be flatter than usual metallography one to prevent the over- or under-estimation of the hydride area. To polish the

hydride and matrix uniformly, they are different in its hardness, the polishing technique is improved by a combination of the diamond abrasive polishing and the oxide abrasive polishing, and the combination polishing make the flat surface to determine the hydride area accurately. About image analysis technique, “Color Gamut Selection (CGS) method” was developed to distinguish only the hydride from other compositions such as the matrix, scratches and pits. This is an innovative technique which isn’t subject to the brightness threshold of binarization, brightness irregularity of images on the hydride and the amount of the other compositions. With this CGS method, it became possible to measure the hydride area fraction reliably and quantitatively from various image conditions.

The confirmation test with un-irradiated sample was performed to determine the reliability of the improved BEI method. The measured hydrogen concentration by improved BEI method and Hot Vacuum Extraction method indicated a good agreement from 150ppm to 700ppm and its error was lower than 10%. This result shows the improved BEI method can provide the accurate and reliable hydrogen concentration at the local area of the fuel claddings.

CONFIRMATION TEST ON IRRADIATED SAMPLE

To confirm the applicability of the improved BEI method for the irradiated samples, the combination polishing, the CGS method and also the improved method were applied to the irradiated PWR and BWR fuel cladding.

The PWR sample is taken from the UO_2 fuel rod with ZIRLO cladding which was irradiated in the Ohi Power Station Unit 4 of the Kansai Electric Power Co. Inc[4]. The local burnup at the sample position is about 58 GWd/t. The cross-section images of the metallography as etched at several circumferential directions were taken after usual polishing. After the metallographic observation, the combination polishing was performed for the same sample and BEIs were taken at the same place as the metallographic observation. The taken images at Area (1) and Area (2) are shown in Fig.2. The two areas were selected at different circumferential directions in an identical cross section. In the metallographic images, the hydride at Area (1) seems to be precipitated the same amount as that at Area (2). However, in the BEIs, the hydride at Area (1) seems to be precipitated more than that at Area (2) and this difference is remarkable at the outer peripheral area. Additionally, the hydride amount of each image was measured by the CGS method. The images are segmented into 6 radial areas, which size is 100 μm × 100 μm for each, and normalized by the hydride amount at innermost of Area (2) as shown in Fig.3. In the result of metallography, the hydride amount at each radial area of Area (1) is almost same as the Area (2), also at the outer peripheral area. However, in the BEIs, the difference of hydride amount could be seen between Area (1) and

Area (2), and it was particular at the outer peripheral area. It is suggested this difference between metallographic image and BEI is caused by the corrosive action of an etching acid in the process of metallography. During the etching procedure, the etching acid corrodes not only the hydride but also zircaloy matrix and both corroded hydride and matrix are observed as the same black area on the metallography. This phenomenon could be observed particularly at the hydride-accumulated area as the outer peripheral of cladding. Additionally, the etching condition depends on the concentration of the etching acid and etching time, therefore, the estimation of hydride concentration at the outer peripheral area is difficult by metallography.

On the other hand, the etching procedure is not needed for the hydride observation by the improved BEI method, and the attainable depth of the electron beam used in BEI observation is shallower than 5μm. Therefore, the hydride observed by the improved BEI method indicates the only hydride on the observation surface. It means the improved BEI method is more suitable one than the metallography for the local hydride observation, i.e. the measurement of local hydrogen concentration profile.

The hydrogen concentration measurements for BWR fuel cladding irradiated in the research reactor as the burnup of about 55 GWd/t were performed by the improved BEI method. BEIs of that cladding were taken at several circumferential and axial directions. The images applied CGS method and measured hydrogen concentrations are shown in Fig.4.

From the results measured by the improve BEI method, the hydride distribution is a little different in each image and there is a variety of the hydrogen concentration from 68 ppm to 105 ppm. These measurement result mean that the improve BEI method can measure the local hydrogen concentration even if the hydrogen concentration is lower than 110 ppm and the concentration difference is smaller than 40 ppm.

SUMMARY

The hydrogen concentration measurements for the irradiated PWR and BWR fuel cladding were performed with the improved BEI method that was developed in JAEA. From the confirmation test on the irradiated PWR fuel cladding, the improved BEI method has advantage to observe the high concentration area of hydride by the comparison of metallography. In the test result on the irradiated BWR fuel cladding, the local hydrogen concentration can be determined even if the low concentration and small difference. Therefore, the improved BEI method is suitably for the determination of the local hydrogen concentration in the irradiated fuel cladding.

In the future, the simplification of the polishing procedure and the time shortening for the image analysis will be carried out to improve the efficiency of the BEI method.

ACKNOWLEDGEMENTS

The measurements with PWR cladding were performed under the cooperation with Mitsubishi Heavy Industries, Ltd. The PWR fuel cladding was provided by the Kansai Electric Power Co., Inc. The BWR fuel cladding was provided by the Fuel Safety Research Group. The sample preparations and the SEM observations were supported by the Fuel Examination section. The author wishes to express their sincere thanks to all of them.

REFFERENCES

[1] A.Onozawa, “Improved Technique of Hydrogen Concentration Measurement in Fuel Cladding by Backscattered Electron Image Analysis”, Proceedings of 2005 JAEA-KAERI Joint Seminar on Advanced Irradiation and PIE Technologies, JAEA-Conf 2006-003

[2] David I. Schrire and John H. Pearce, “Scanning Electron Microscope Techniques for Studying Zircaloy Corrosion and Hydriding”, Zirconium in the Nuclear Industry: Tenth International Symposium, ASTM STP 1245

[3] A.Onozawa et al, “Hydrogen Concentration Measurement in Fuel Cladding by Backscattered Electron Image Analysis”, JAEA-Technology 2006-010

[4] T. Fuketa, T. Sugiyama, F. Nagase, et al., “Behavior of 60 to 78MWd/kgU PWR Fuels under Reactivity-Initiated Accident Conditions”, J. Nucl. Sci. Tech., **43**[9], 1080-1088 (2006).

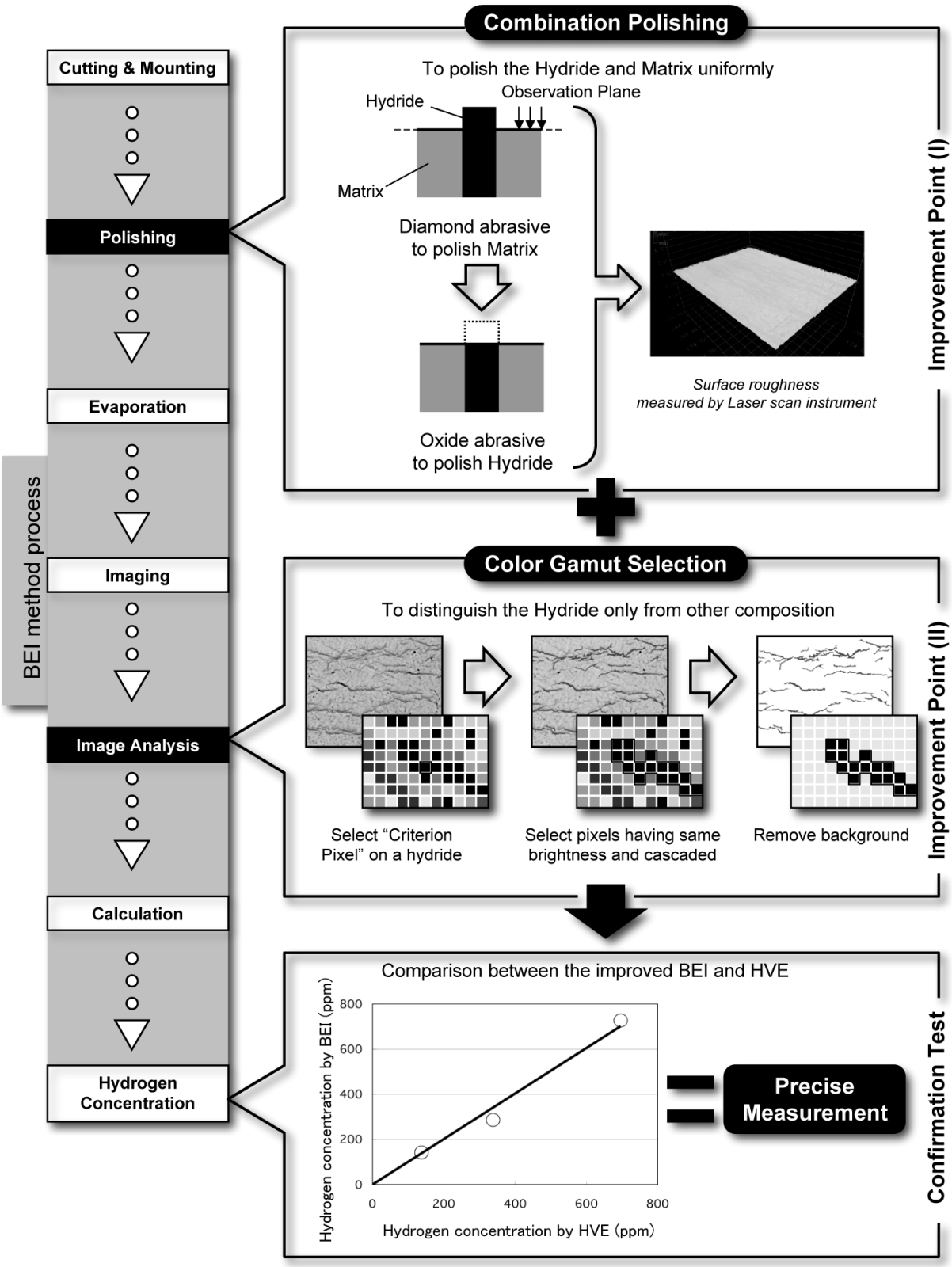

Fig.1 Brief diagram of the improved BEI method.

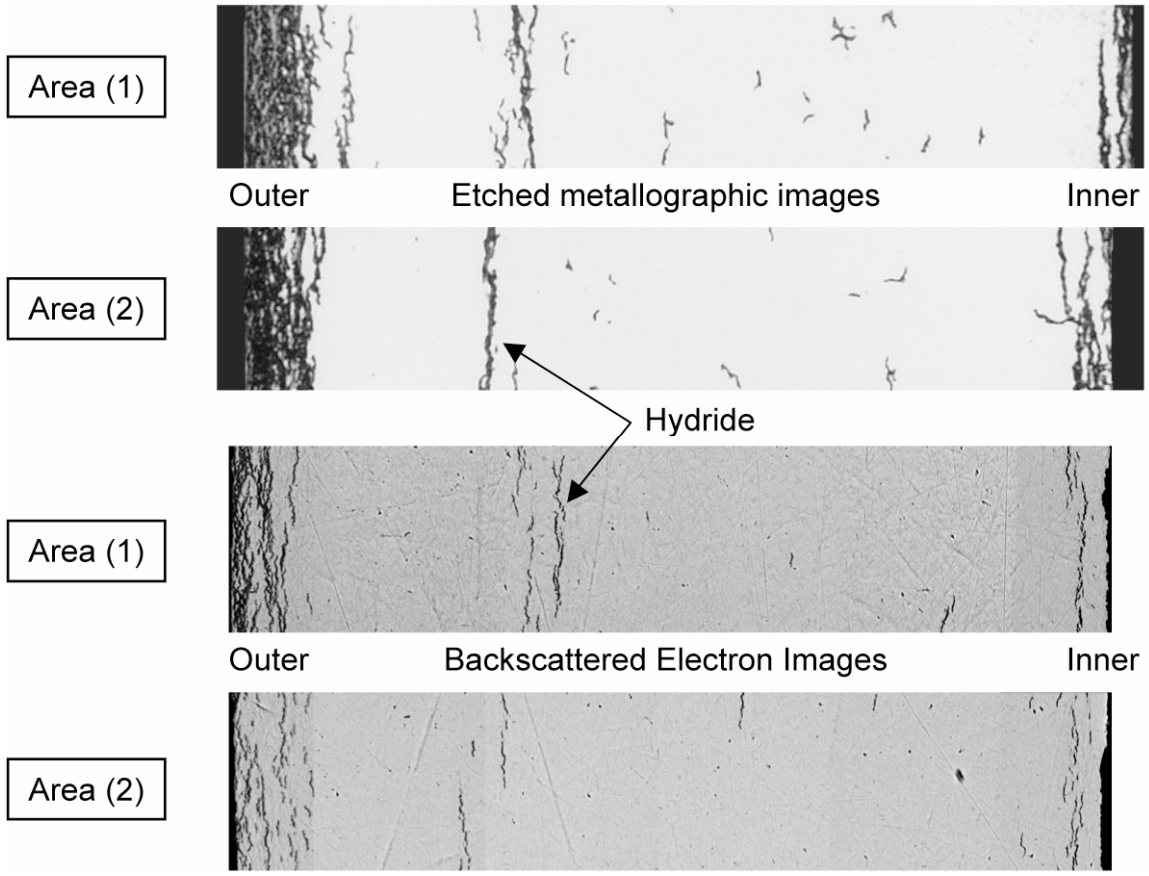

Fig.2 BEI and etched metallography image of irradiated PWR fuel cladding

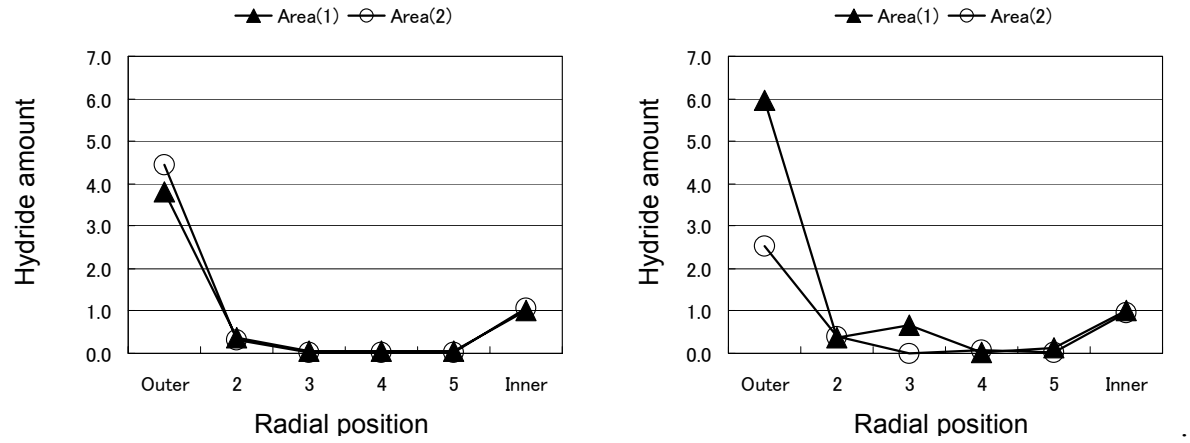

Fig.3 Hydride amount by BEI and metallographic image.
(normalized by hydride amount at innermost)

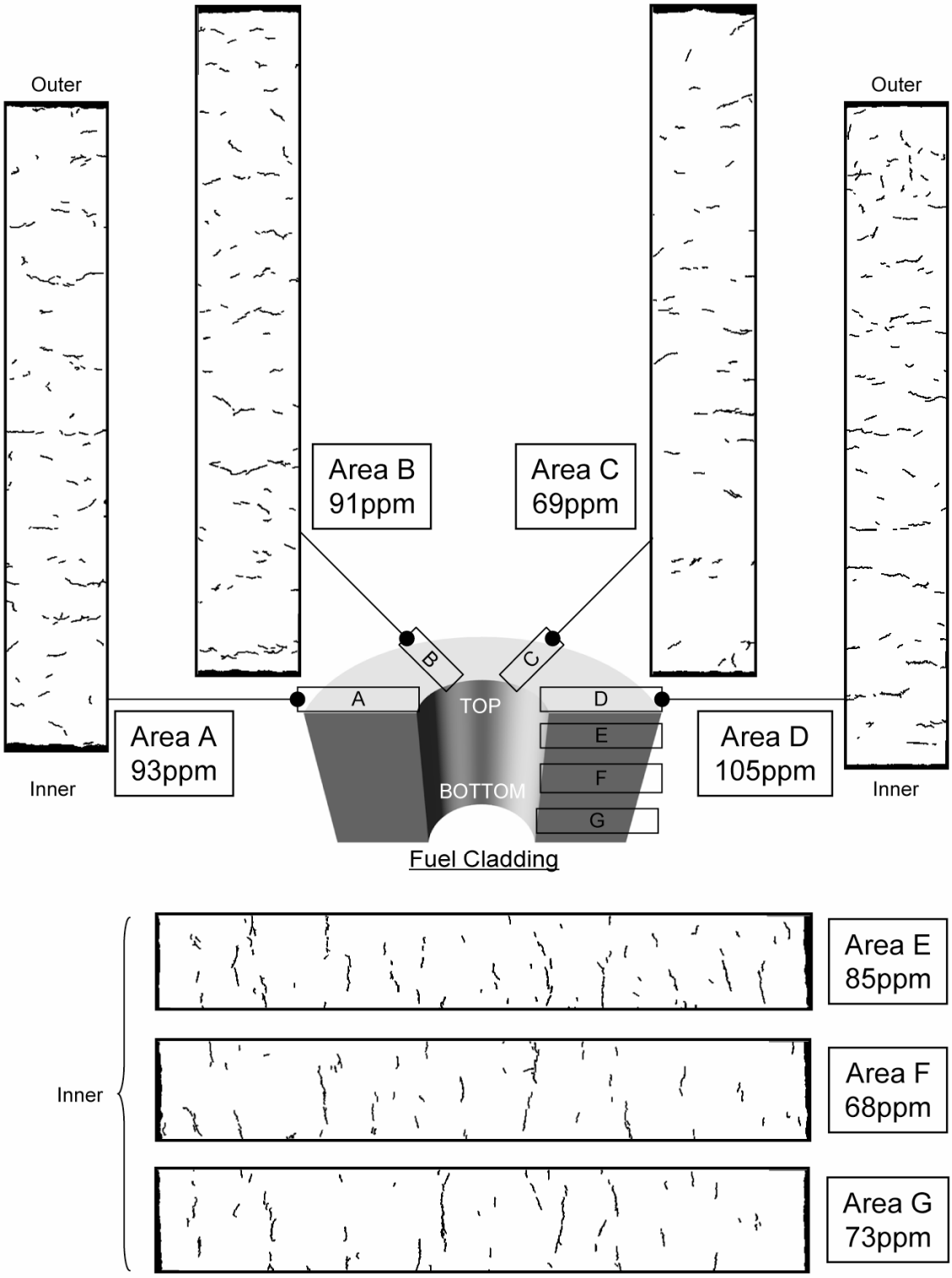

Fig.4 Hydrogen concentration of irradiated BWR fuel cladding measured by improved BEI method.

5.7 HOOP STRENGTH AND DUCTILITY EVALUATION OF IRRADIATED FUEL CLADDING

Sunki Kim [a], Jegeon Bang, Daeho Kim, Iksung Lim, Yongsik Yang, Kunwoo Song, Dosik Kim [b]

[a] *LWR Fuel Development Division, Korea Atomic Energy Research Institute*
1045 Daedeok Street, Yuseong-gu, Daejeon 305-353, Korea
[b] *Irradiated Materials Examination Facility, Korea Atomic Energy Research Institute*
1045 Daedeok Street, Yuseong-gu, Daejeon 305-353, Korea
kimsk@kaeri.re.kr

ABSTRACT

Regarding a degradation of the mechanical properties of Zr-based nuclear fuel cladding tubes under severe accident conditions such as RIA(Reactivity Initiated Accident) and LOCA(Loss of Coolant Accident), mechanical tests which can simulate the degradation of the mechanical properties properly are needed. Therefore, in this paper, modified ring tensile tests were performed in order to evaluate the mechanical properties of high burn-up fuel cladding under a hoop loading condition in a hot cell.

The mechanical properties comprise of the strength such as the YS(Yield Strength) and the UTS(Ultimate Tensile Strength) as well as the ductility such as the UE(Uniform Elongation) and the TE(Total Elongation). The tests were performed with Zircaloy-4 nuclear fuel cladding whose burn-up is approximately 65,000 MWd/tU in the temperature range of room temperature to 800°C. All the experiments were carried out at a constant strain rate of 0.01/s.

As the first step, the hoop loading grip for the ring tensile test was designed in order that a constant curvature of the specimen was maintained during the deformation, and graphite lubricant was used to minimize the friction between the outer surface of the die insert and the inner surface of the ring specimen. The specimen for the ring tensile test was designed to limit the deformation within the gauge section and to maximize the uniformity of the strain distribution. It was confirmed that the mechanical properties under a hoop loading condition can be correctly evaluated by using this test technique.

On the basis of the hoop directional tensile tests for a high burn-up Zircalay-4 cladding, the following conclusions were drawn.

First of all, the hoop directional mechanical strength of the irradiated Zircaloy-4 cladding is slightly higher than that of the unirradiated Zircaloy-4 cladding(high burn-up Zircaloy-4 cladding). While, there are significant ductility differences in both uniform elongation and total elongation between the irradiated Zircaloy-4 cladding(high burn-up Zircaloy-4 cladding) and the unirradiated Zircaloy-4 cladding, and especially, the decrease in total elongation of the irradiated cladding is more remarkable. And the mechanical ductility is abruptly degraded above 600°C, which corresponds to a design basis accident condition such as a RIA. The un-irradiated fuel cladding showed ductile fracture behaviors such as 45° shear type fracture, cup and cone type fracture, cup and cup type fracture and chisel edge type fracture, While the high burn-up Zircalay-4 cladding showed a brittle fracture behavior even at the high temperatures (e.g. over 600°C) which are achievable during a RIA.

INTRODUCTION

During a steady-state operation of light water reactors, the mechanical behavior of the zirconium-based fuel cladding degrades due to a combination of oxidation, hydriding, and radiation damage. In an effort to increase the operating efficiency through the use of longer fuel cycles, and to reduce the volume of waste associated with the core reloads, utilities have a strong incentive to increase the average discharge burn-up of the fuel assemblies. Further increases in the operating efficiency of power reactors can also be achieved by increasing the coolant outlet temperature. However, both of these changes in a reactor operation enhance the cladding degradation, which may increase the likelihood of a cladding failure during design-basis accidents.

One such postulated design-basis accident scenario is the reactivity-initiated accident(RIA) in a pressurized water reactor (PWR) caused by the ejection of a control rod from the core, which would cause a rapid increase of the reactivity and the thermal energy in the fuel [1]. The increase in fuel temperature resulting from an RIA induces a rapid fuel expansion, causing a severe pellet-cladding mechanical interaction (PCMI). This PCMI forces the cladding to experience a multiaxial tension such that the maximum principal strain is in the hoop (i.e., transverse) direction of the cladding tube. The survivability of a fuel cladding irradiated to a high burn-up under postulated RIA conditions is thus a response to a combination of the mechanics of a loading and the material degradation during a reactor operation.

While such data is available for the axial deformation behavior of cladding tubes, relatively little has been reported in the open literature on the uniaxial tension behavior in the hoop

direction of Zircaloy-4 cladding. This technique was developed in 1990s by Arsene *et al*.[2, 3] and has been applied to Zircaloy-4. And also some experimental researches on hoop-directional mechanical properties for pre-hydrided Zircaloy-4 cladding were reported using ring tensile tests[4, 5]. But, they were not applied to irradiated materials. Accordingly, it is essential to investigate the uniaxial tension behavior in the hoop direction of high burn-up Zircaloy-4 cladding. In this study, ring tensile tests are applied to obtain the data regarding the uniaxial hoop direction deformation behavior.

EXPERIMENTAL PROCEDURE

Specimen Preparation

The ring tensile specimen used in this study is a Westinghouse 17x17 type (Vantage-5H) Zircaloy-4 cladding irradiated for 3 cycles in the Ulchin Unit 2 pressurized water reactor, whose average burn-up was estimated to be approximately 65GWd/tU (Figure. 1).

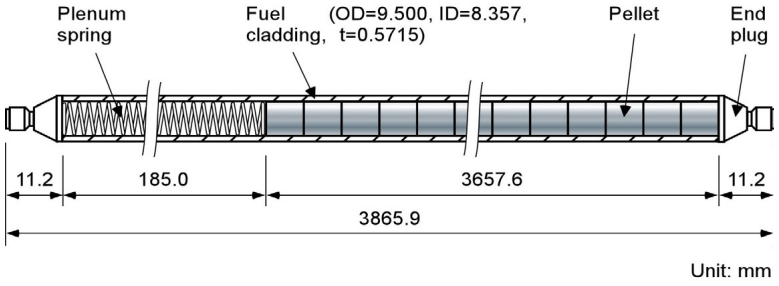

Figure 1. A schematic of Zircaloy-4 fuel rod irradiated in Ulchin Unit 2

The irradiated fuel rod was transferred to Post-Irradiation Examination Facility (PIEF) at KAERI, cut into approximately 13 cm length segments with a diamond low speed saw, and then the UO_2 pellet inside the fuel rod segment was removed by a mechanical grinding with a drill-attached defueling machine in a hot cell in Irradiated Material Examination Facility (IMEF). The specimens for the mechanical properties evaluation were fabricated with a diamond wheel grinder from the defueled cladding segments. After grinding the specimen, the ground area was polished by using a 3000 grit sandpaper and a polishing cloth with 1μm Al_2O_3 powder so that no defect is introduced during the grinding work. The fuel rod was cut into ~150 mm segment in a hot cell and then UO_2 fuel was removed using a drill-attached defueling machine. The specimens for the mechanical properties evaluation were fabricated

with a diamond wheel grinder from the defueled cladding segments in a lead-shielding glove box. Figure 2 shows the procedure for the ring tensile specimen fabrication. The dimensions and shape of the ring tensile specimen were designed in order to ensure that any deformation is limited to the gage section of the specimen, so that the uniform uniaxial hoop strain in the gage section could be at its maximal. The dimensions and a photograph of the ring tensile specimen are shown in Figure 3.

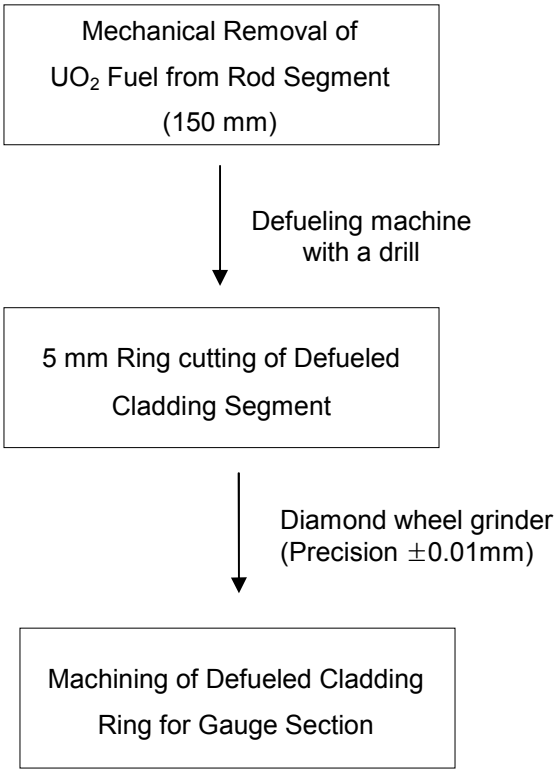

Figure 2. Procedure for the ring tensile specimen fabrication

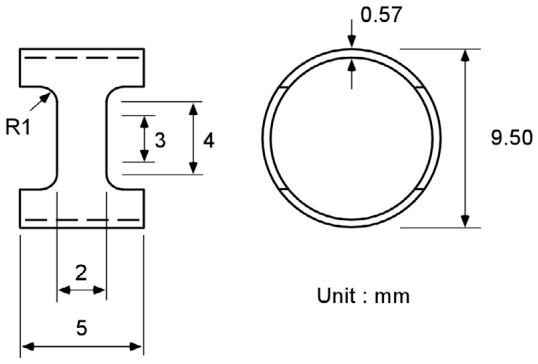

(a)

(b)

Figure 3. Ring tensile specimen (a) Dimension of the ring tensile specimen (b) Ring specimen after machining

The gage sections of the specimens were oriented at the top and bottom of the half cylinder of the grip, such that a constant specimen curvature can be maintained during a deformation. A photograph of the jig and the grip is shown in Figure 4. The interface was lubricated with a graphite-containing vacuum grease lubricant at the beginning of each test to minimize a loss of the applied load. The ring tensile tests were performed in a hot cell with the Instron Servohydraulic System, Model 8562. The tests were performed at 25, 135, 200, 300, 350, 400, 600, and 800°C, and the initial strain rate was maintained at 0.01/s. This temperature range from 25°C to 800°C was expanded, compared with the cladding temperature range(500°C~700°C) during reactivity-initiated accident(RIA). All the tests were performed in air environment.

The hydride morphologies were observed, which are shown in Figure 5. These were representative images of the hydride rim taken before the mechanical tests. As seen in the figure, a hydride rim was formed around the metal substrate/oxide interface. This hydride rim is believed to cause a decrease of the ductility of the cladding tube [5].

Figure 4. Photograph of the jig and the grip for the ring tensile specimen

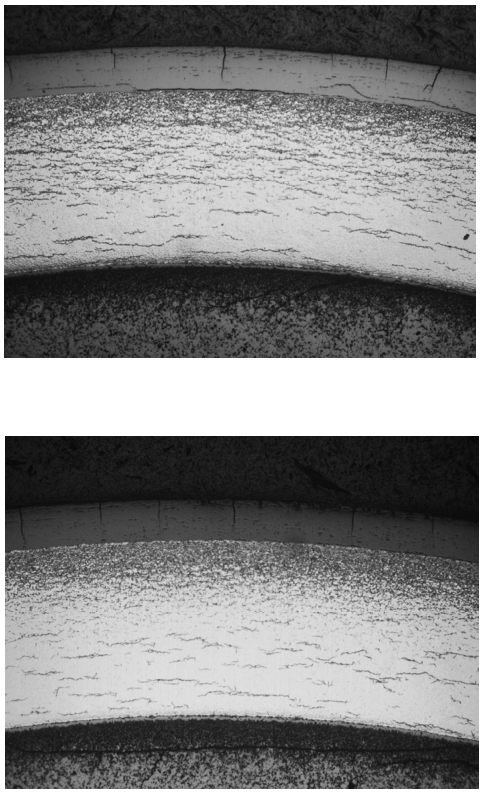

Figure 5. Optical microscopy of the Zircaloy-4 from Ulchin Unit 2

RESULTS AND DISCUSSION

To obtain the mechanical strength, the 0.2% offset YS(Yield Strength) and UTS(Ultimate Tensile Strength) were evaluated, and the UE(Uniform Elongation) and TE(Total Elongation) were also evaluated for the ductility. The hoop stress-strain curves at 400°C among hoop stress-strain correlation results various temperatures are shown in Figure 6. The hoop stress-strain behavior of the irradiated cladding specimen was compared with unirradiated cladding specimens to investigate the degradation effect of mechanical properties by irradiation in nuclear reactor. Two runs were performed for unirradiated cladding specimens in order to confirm the reproducibility of the test results. As shown in the figure, the results for the unirradiated cladding specimens shows that mechanical strengths such as yield strength and ultimate tensile strength are in accord with each other even if there is some differences in total elongation. In case of unirradiated cladding specimens, ultimate tensile strength was ~570MPa, and ultimate tensile strength of the irradiated one was ~670 MPa. While, hoop strain of the irradiated one showed much lower value(~35%) than that of the unirradiated one(~80%), compared with the hoop strain of the unirradiated one. From this result, it was observed that the ductility of the irradiated cladding is sharply decreased as the fuel burnup.

The evaluation results of the 0.2% offset YS and the UTS are shown in Figure 7. From the figure, it is confirmed that the 0.2% offset YS and the UTS abruptly decrease with an increasing temperature. The UTS was evaluated to be 942.70 MPa at RT, 678.83 MPa at 400°C, but, it is abruptly diminished to 282.64 MPa at 600°C, which is achievable in the RIA condition. Especially, it decreases to 58.30 MPa at 800°C, an extreme condition, which corresponds to 6% of the UTS at RT.

This means that the mechanical strength of the high burn-up Zircaloy-4 cladding sharply decreases in the RIA-relevant temperature ranges. The evaluation results of the UE and TE are shown in Figure 8. The results show that both the UE and TE increase with an increasing temperature. Especially, they abruptly increase at 600°C, but become lower above this temperature. This peculiar behavior was also observed in the PROMETRA test program[6] which is a mechanical property relevant test program in conjunction with the CABRI program simulating RIA. It is believed that this behavior is caused by the elongation minimum phenomenon by the dynamic strain aging of the Zircaly-4 cladding material above 600°C.

There was no significant difference in yield strength between the irradiated Zircaloy-4 cladding (high burn-up Zircaloy-4 cladding) and the unirradiated Zircaloy-4 cladding. But, in case of ultimate tensile strength, the value of the irradiated one showed slightly higher than that of unirradiated one. Therefore, it is confirmed that the hoop directional mechanical

strength of the irradiated Zircaloy-4 cladding is somewhat higher than that of the unirradiated Zircaloy-4 cladding.

From a point of view of mechanical ductility, there were significant differences in both uniform elongation and total elongation between the irradiated Zircaloy-4 cladding (high burn-up Zircaloy-4 cladding) and the unirradiated Zircaloy-4 cladding. Especially, the decrease in total elongation of the irradiated cladding was more remarkable, compared with the decrease in uniform elongation of the irradiated one.

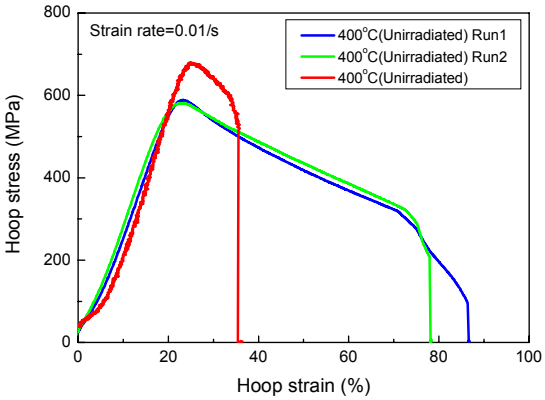

Figure 6. Hoop stress-strain curves of irradiated and unirradiated cladding at 400℃

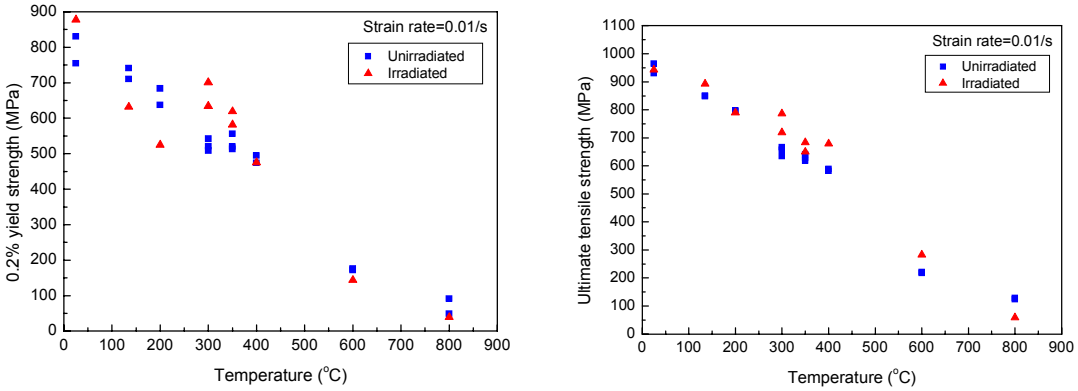

(a) *(b)*

Figure 7. Yield strength and ultimate tensile strength of the un-irradiated and high burn-up fuel cladding

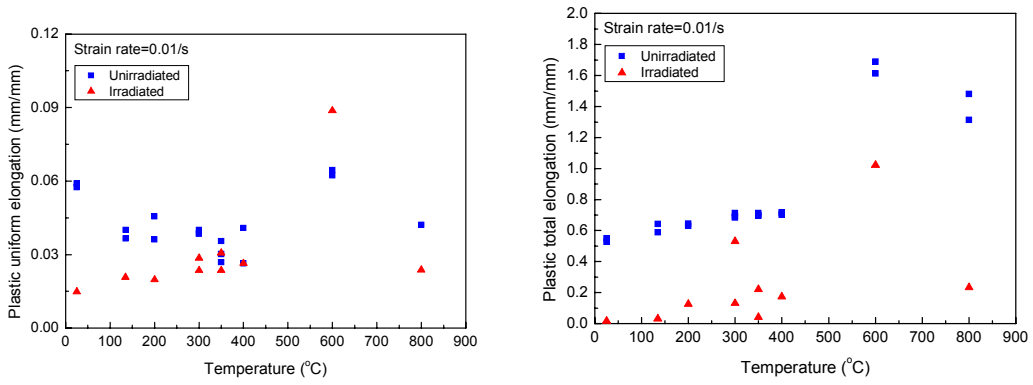

(a) *(b)*

Figure 8. Uniform elongation and total elongation of the un-irradiated and high burn-up fuel cladding

CONCLUSIONS

On the basis of the ring tensile tests for the high burn-up Zircalay-4 cladding from Ulchin Unit 2 and the as-received non-irradiated Zircalay-4 cladding, the following conclusions were drawn.

Firstly, the hoop directional mechanical strength of the irradiated Zircaloy-4 cladding is slightly higher than that of the unirradiated Zircaloy-4 cladding(high burn-up Zircaloy-4 cladding). And the mechanical strength decreases linearly with increasing temperature.

Secondly, there are significant ductility differences in both uniform elongation and total elongation between the irradiated Zircaloy-4 cladding(high burn-up Zircaloy-4 cladding) and the unirradiated Zircaloy-4 cladding, and especially, the decrease in total elongation of the irradiated cladding is more remarkable.

Thirdly, the mechanical ductility is abruptly degraded above 600°C, which corresponds to a design basis accident condition such as a RIA.

Fourthly, the un-irradiated fuel cladding showed ductile fracture behaviors such as 45° shear type fracture, cup and cone type fracture, cup and cup type fracture and chisel edge type fracture, While the high burn-up Zircalay-4 cladding showed a brittle fracture behavior even at the high temperatures (e.g. over 600°C) which are achievable during a RIA.

REFERENCES

[1] R. O. Meyer *et. al*., "A Regulatory Assessment of Test Data for Reactivity Initiated Accidents", *Nuclear Safety*, **37**(4), 271-288 (1996).

[2] S. Arsene and J. Bai, "A New Approach to Measuring Transverse Properties of Structural Tubing by a Ring Test", *Journal of Testing and Evaluation*, **24**(5), 386-391 (1996).

[3] S. Arsene and J. Bai, "A New Approach to Measuring Transverse Properties of Structural Tubing by a Ring Test—Experimental Investigation", *Journal of Testing and Evaluation*, **26**(1), 26-30 (1998).

[4] R. S. Daum, *et. al*., "Mechanical Property Testing of Irradiated Zircaloy Cladding Under Reactor Transient Conditions", *Zirconium in the Nuclear Industry : Small Specimen Test Technique : Fourth Volume,, ASTM STP 1418*, PA, 195-210 (2002).

[5] R. S. Daum, *et. al*., "On the Embrittlement of Zircaloy-4 Under RIA-Relevant Conditions", *Zirconium in the Nuclear Industry : Thirteenth International Symposium in the Nuclear Industry, ASTM STP 1423*, 702-719 (2002).

[6] X. Averty, *et. al*., "Tensile tests on ring specimens machined in M5 cladding irradiated 6 cycles" IRSN 2003/50 (2003).

5.8 PRELIMINARY IRRADIATION TEST FOR NEW MATERIAL SELECTION ON LIFETIME EXTENSION OF BERYLLIUM REFLECTOR

Taketoshi Taguchi[a], Shizuo Sozawa[a], Yoshio Hanawa[a],
Shigeru Kitagishi[b] and Kunihiko Tsuchiya[b]

[a]*Department of JMTR Operation, Neutron Irradiation Center, Japan Atomic Energy Agency*
4002, Narita-cho, Oarai-machi, Higashiibaraki-gun, Ibaraki-ken, 311-1393, Japan
[b]*Irradiation Engineering Section, Neutron Irradiation Center, Japan Atomic Energy Agency*
4002, Narita-cho, Oarai-machi, Higashiibaraki-gun, Ibaraki-ken, 311-1393, Japan
taguchi.taketoshi@jaea.go.jp, sozawa.shizuo@jaea.go.jp, hanawa.yoshio@jaea.go.jp,
kitagishi.shigeru@jaea.go.jp and tsuchiya.kunihiko@jaea.go.jp

ABSTRACT

Beryllium has been utilized as a moderator and/or reflector in Japan Materials Testing Reactor (JMTR), because of nuclear properties of beryllium, low neutron capture and high neutron scattering cross sections. At present, the amount of irradiated beryllium frames in JMTR is about 2 tons in the JMTR canal. In this study, preliminary irradiation test was performed from 162nd to 165th operation cycles of JMTR as irradiation and PIE technique development for lifetime expansion of beryllium frames. The design study of irradiation capsule, development of dismount device of irradiation capsule and the high accuracy size measurement device were carried out. The PIEs such as tensile tests, metallurgical observation, and size change measurement were also carried out with two kinds of irradiated beryllium metals (S-200F and S-65C).

INTRODUCTION

The Japan Materials Testing Reactor (JMTR) is a world-class high-energy nuclear test reactor which has been in use for 40 years at this writing. The JMTR's primary mission is to perform irradiation tests on fuels and materials, and its high-neutron flux can also be used for the production of radioisotopes. Power ramp testing of nuclear fuels is also carried out to evaluate the integrity and safety of the fuels under study [1].

Beryllium has always been used as the reflector element material in the JMTR. The core of the JMTR, which is 1560 mm in diameter and 750 mm in effective height, is divided into four regions by an H-shaped partition wall (beryllium frame), which is made of beryllium and has a 224-unit array of 77.2 mm squares arranged in a square lattice. The effective part of this element is also made of beryllium [2].

Beryllium is fabricated by the vacuum hot press. S-200F is used as the standard material and the typical purity of nuclear grade beryllium such as S-200F is 99.1%. On the other hand, beryllium reflector is irradiated at the range from 50 to 150˚C in cooling water of JMTR. At present, it is necessary to exchange the beryllium frames within every fixed period and the frames were exchanged five times up to the JMTR operation periods of 165th cycles, and the amount of irradiated beryllium frames is about 3 tons in the JMTR canal. Characteristics of irradiated beryllium are (1) internationally regulated, (2) specific chemical hazards such as BeO, (3) containing tritium and (4) activated material. Therefore, wastes of irradiated beryllium are difficult to handle and increase on and on [3].

Now, the refurbishment of the JMTR is underway, and it will run through 2011. The plan is for the new JMTR to operate through the year 2030. For the beryllium frames, it means an operational service lifetime goal of 15-20 years (180,000MWD), rather than the current five years. In order for that to happen, it will be necessary to consider fundamental changes to the frame design, starting with the choice of beryllium material grade [4].

In this study, preliminary irradiation test of beryllium metals was performed from 162nd to 165th operation cycles of JMTR as irradiation and PIE technique development for lifetime expansion of beryllium frames and the irradiation effect on the properties was also evaluated in these tests.

EXPERIMENTAL AND DEVELOPMENT OF DEVICES

The preliminary irradiation test was performed from 162nd to 165th operation cycles of JMTR as irradiation and PIE technique development for lifetime expansion of beryllium frames. The design study of irradiation capsule, development of dismount device of irradiation capsule and the high accuracy size measurement device were carried out. The PIEs such as tensile tests, metallurgical observation, and size change measurement were carried out with two kinds of irradiated beryllium metals (S-200F and S-65C).

Specimens

Two kinds of beryllium metals (S-200F and S-65C) were prepared for this study. S-200F is used as the standard material for the beryllium reflectors in the JMTR. On the other hand, S-

65C is high grade beryllium metal and is adopted as the first wall material in the International Thermonuclear Experimental Reactor (ITER). These beryllium metals are fabricated by the vacuum hot-pressing (VHP). Detail fabrication procedure is described in ref. [4]. The mechanical properties and chemical composition of beryllium metals in this study are shown in Table 1. The typical purities of S-200F and S-65C are 99.1% and 99.5%, respectively. The amount of BeO is more than 1% in S-200F and the amount of BeO is less than 1% in S-65C.

Three kinds of test specimens were fabricated for the tensile test, impact test and bending measurement test. Configurations of these specimens are shown in Fig.1. The tensile test specimens and impact test specimens are the standard size in the JMTR irradiation test. On the other hand, the bending measurement specimens are the special size.

Table 1 Mechanical properties and chemical composition of beryllium metals

	Irradiation Samples		
Grade	S-200F*1	S-65C*1	S-65C*2
Fabrication method	**VHP**	**VHP**	**VHP**
Grain size (μm)	–	–	10.5
Mechanical properties			
Tensile strength (MPa)	339(Long)	330(Long)	379(Long)
0.2% yield strength (MPa)	265(Long)	255(Long)	279(Long)
Elongation (%)	3.9(Long)	3.7(Long)	4.2(Long)
Elements (wt%)			
Be	**99.1**	**99.4**	**99.5**
BeO	**1.1**	**0.7**	**0.5**
Al	0.04	0.02	0.02
C	–	–	0.02
Fe	0.10	0.06	0.06
Mg	0.013	< 0.01	< 0.01
Si	0.03	0.03	0.02
Other elements	–	–	< 0.04

*1:Tensile specimens and Impact specimens, *2:Bend measuring specimens

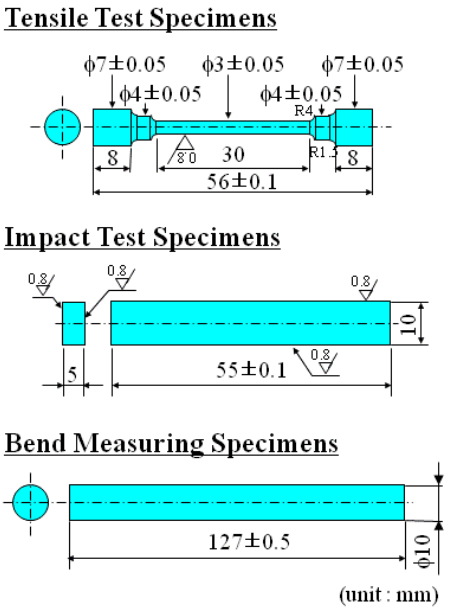

Fig. 1 Configurations of beryllium specimens.

Irradiation Conditions and Irradiation Capsule Fabrication

Two kinds of beryllium specimens were irradiated from 162nd to 165th operation cycles of JMTR. Irradiation temperatures were selected at 50˚C and 150~200˚C. Target fast neutron fluence was also fixed at 1×10^{25} /m^2. Distribution of fast neutron flux in JMTR is shown in Fig.2. Thus, the irradiation hole was selected at K-10 (fuel region) in the JMTR. Average fast neutron flux and thermal neutron flux were about 1×10^{18} and 2×10^{18} /m^2/s in this hole, respectively.

Photograph of irradiation capsule is shown in Fig.3. Two types of inner capsules were fabricated for this irradiation tests. One is the open-typed inner capsule called “leaky capsule”.

The specimens are directly cooled by the JMTR primary coolant (about 50˚C). The other is the sealed typed inner capsule. The specimens are irradiated in the inert gas atmosphere such as helium gas. The thermocouples were not installed in this capsule. Irradiation temperature will be calculated by the code.

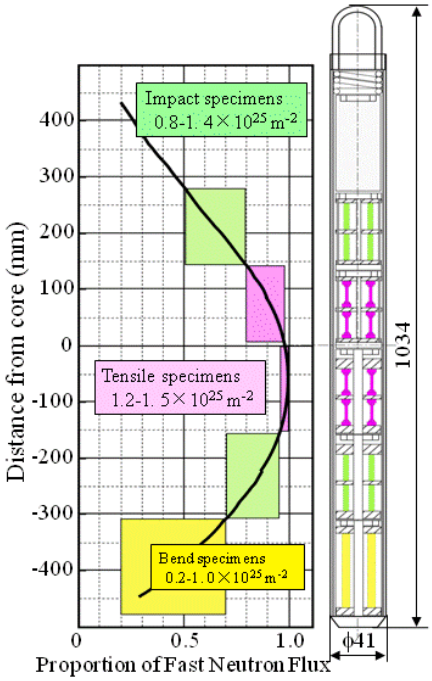

Fig. 2 Distribution of fast neutron flux in JMTR.

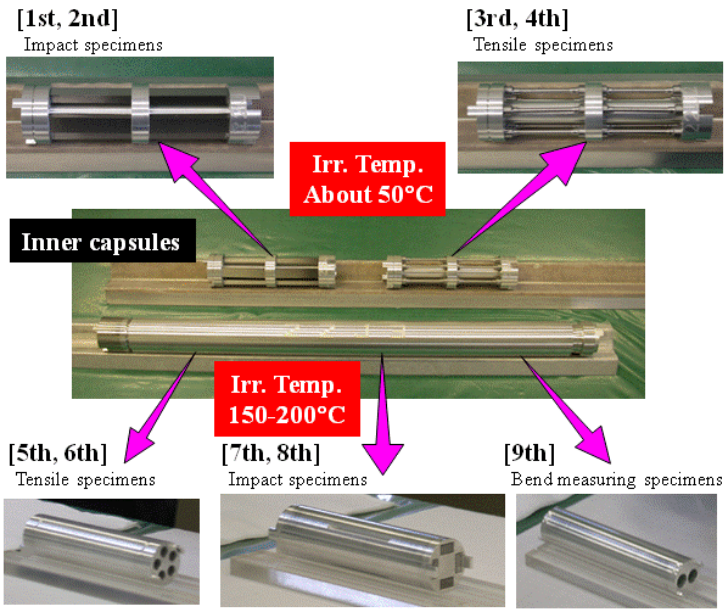

Fig. 3 Photograph of irradiation capsule.

Dismounting Device of Irradiation Capsules

Tritium is generated in the irradiated beryllium specimens. Tritium has to be recovered when the beryllium specimens are produced from the irradiation capsule. Thus, the dismounting device of the sealed typed inner capsules was developed for recovery of tritium. Outline of this device is shown in Fig.4.

Tritium is generated by the following reactions;

$^{9}Be + n \rightarrow {}^{4}He + {}^{6}He$ ···· (n, α) reaction ···· (1)

$^{6}He \rightarrow {}^{6}Li$ ···· β decay ···· (2)

$^{6}Li + n \rightarrow {}^{4}He + {}^{3}H$ ···· (n, α) reaction ···· (3)

Tritium generation was evaluated in the beryllium specimens installed in the sealed typed inner capsule. The amount of tritium generated in the specimens is about 1.3×10^{11} Bq. From the reference data [5], the amount of tritium release irradiated at 200˚C is about 7.2×10^{9} Bq in the sealed typed inner capsule. From the amount of tritium release and the leakage of the

developed device, tritium concentration in the hot cell is about 2.6×10^{-3} Bq/cm^3 and this value is less than the controlled tritium concentration of the exhaust (5×10^{-3} Bq/cm^3). It is possible to dismantle the sealed typed inner capsule by this device.

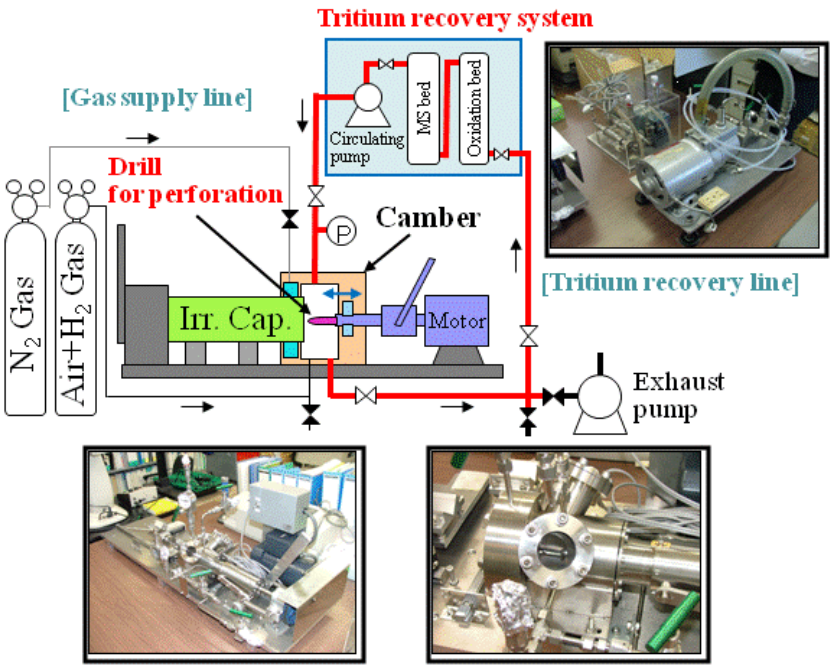

Fig.4 Outline of dismounting device of the sealed typed inner capsules.

High Accuracy Size Measurement Device

In this case of the irradiated beryllium, it is expected that the swelling is a cause in the size. It is necessary to measure the size change and bending size of the beryllium specimens after neutron irradiation. Thus, the high accuracy size measurement device was developed. Outline of this device is shown in Fig.5. This device is composed of the laser and motorized stage. Comparison with conventional point and target point for development of this device is shown in Table 2. Measuring procedure was fixed by the preliminary measuring tests using un-irradiated materials.

Post Irradiation Examinations

After neutron irradiation, tensile tests including fracture observation and bending measurement test were carried out. The tensile tests were carried out in air at 22˚C. A crosshead speed was 0.1mm/min and the fracture surfaces were observed by a scanning electron microscopy (SEM) after the tensile tests. On the other hand, bending measurements were used the columnar specimens by the developed device.

Table 2 Comparison with conventional point and target point for development of high accuracy size measurement device.

Items	Conventional	Target
Procedure of measurement	Vernier caliper, Micrometer	Laser and moterized stage
Handling in hot cell	Difficulty	Ease
Accuracy	~0.5mm	~1μm
Measuring point	Size change	Size change, bending size

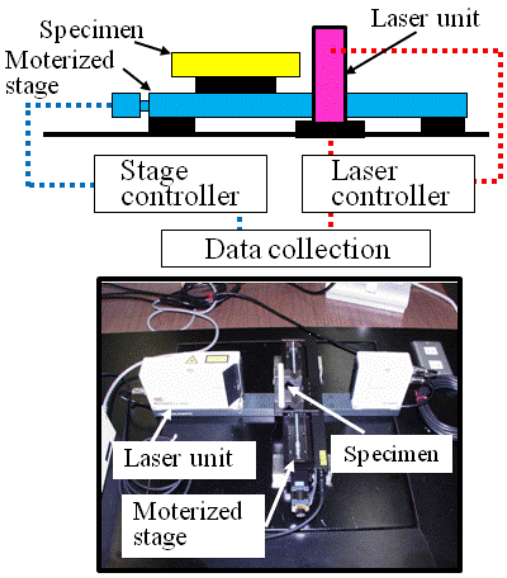

Fig.5 Outline of high accuracy size measurement. device.

RESULTS AND DISCUSSION

Irradiation Conditions

The irradiation temperature of the beryllium specimens in the sealed typed inner capsule was calculated by the numerically integrated elements for system analysis (NISA). Density, thermal conductivity and thermal expansion of beryllium and structural materials of irradiation capsule were given as the important values in this calculation. Peak g-heating was 7.5W/g in K-10 hole. From the results, irradiation temperature of the beryllium specimens was the range from 190 to 200˚C and test temperature was contented with the target value.

Actual fast neutron (E>1MeV) and thermal neutron were determined by Fe wire and Al-Co wire as fluence monitors. From the results, fast neutron fluence and thermal neutron fluence were about 1.3×10^{25} and 2.4×10^{25} /m^2, respectively.

Tensile tests

The tensile tests of S-200F and S-65C were carried out at 22 and 200˚C before neutron irradiation. Strain-stress curves of beryllium specimens before neutron irradiation are shown in Fig.6. The results of tensile tests of beryllium specimens before neutron irradiation are shown in Table 3. The tensile properties of S-65C were almost similar to those of S-200F at 22˚C. On the other hand, the elongation of S-65C was larger than that of S-200F at 493K.

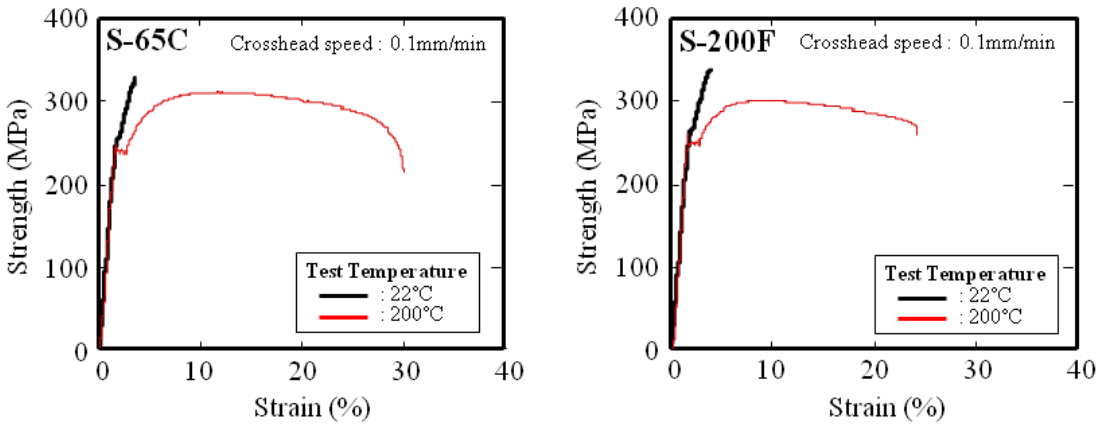

(a) S-65C specimen *(b) S-200F specimen*

Fig.6 Strain-stress curves of beryllium specimens before neutron irradiation.

Table 3 Results of tensile tests of beryllium specimens before neutron irradiation.

	S-65C		S-200F	
	22°C	200°C	22°C	200°C
Tensile Strength (MPa)	330	311	339	301
Yield Strength (MPa)	255	241	265	250
Elongation (%)	3.7	30	3.9	24

Table 4 Results of S-200F and S-65C specimens irradiated at 50°C.

- Irr. Temperature : ~50°C (water temperature)
- Neutron Fluence : 1.5×10^{25} m^{-2} (E>1.0MeV)

	S-65C	S-200F
Tensile test condition	25°C, Air atmosphere	25°C, Air atmosphere
Fracture strength	392 MPa (av.)	344 MPa (av.)
Elongation	2.8%	2.4%
Aspect of specimen after tensile test	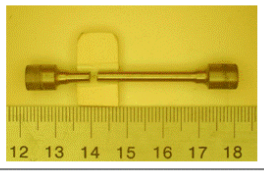	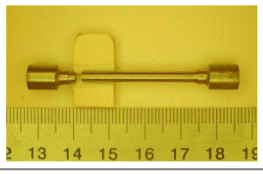
SEM photograph of fracture surface	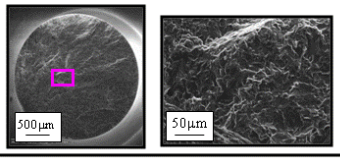	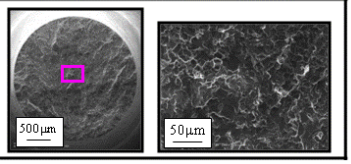

The tensile tests of irradiated S-200F and S-65C were carried out at 22˚C. The results of S-200F and S-65C irradiated at 50˚C are also shown in Table 4. The tensile properties of irradiated S-200F varied widely from high and low. On the other hand, the tensile strengths of the irradiated S-200F and S-65C were almost larger than those of un-irradiated S-200F and S-65C at 22˚C, respectively. The irradiated S-200F and S-65C were very embrittle and the hardening.

Bending Measurement

The high accuracy size measurement device was developed for bending measurement of the irradiated beryllium. The preliminary measuring tests were carried out with the ceramic standard gauge, titanium rod and un-irradiated beryllium. Each specimen was put on the V gauge block and driving speed of the motorized stage was set up. Schematic diagram of measuring procedure is shown in Fig.7.

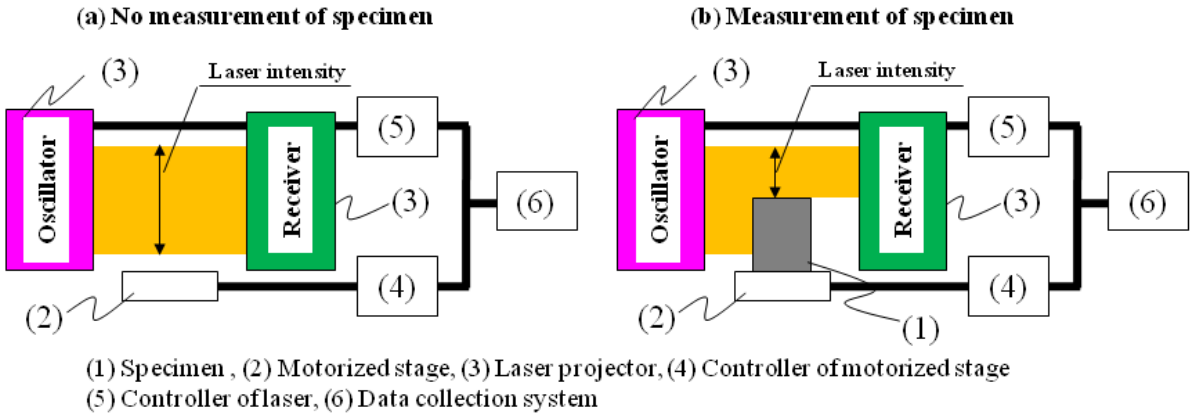

Fig.7 Schematic diagram of measuring procedure.

From the preliminary tests, the accuracy of size measurement was achieved about 1μm when driving speed is 1 μm/step at both ends of the specimens. Thus, measuring procedure was fixed as follows;

(1) Driving speed is 1 μm/step at both ends of the specimens (about 2mm).

(2) Driving speed is 100 μm/step at the center of the specimens except both ends.

(3) Measuring points are two directions such as 0 and 90˚.

The results of beryllium specimens before/after neutron irradiation are shown in Fig.8. In these figures, no bending and swelling of S-65C specimen were observed at the neutron irradiation condition (~1×10^{25} /m^2, ~200˚C).

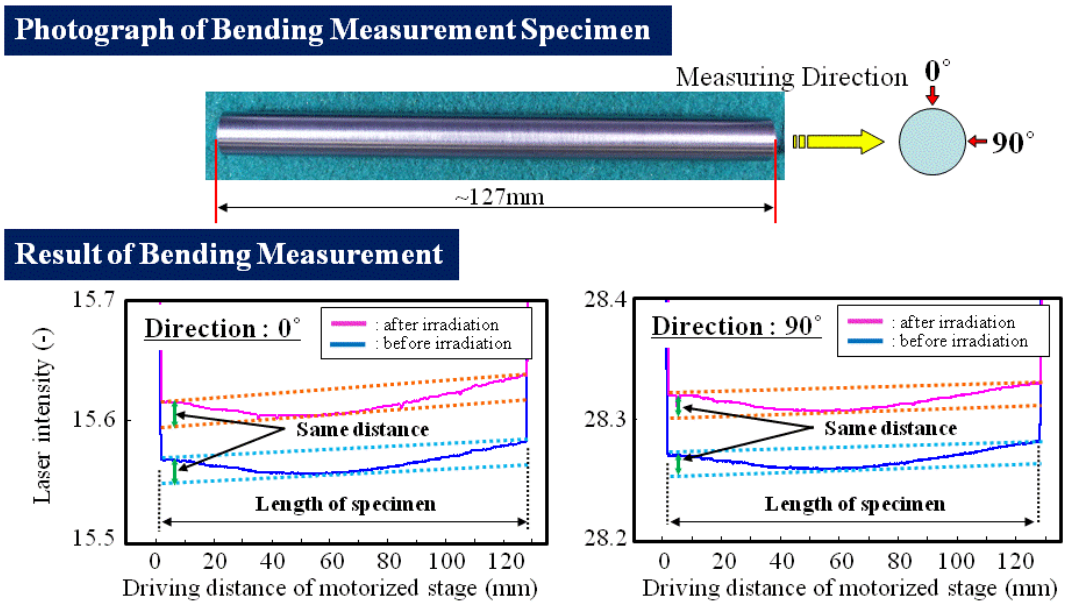

Fig.8 Results of beryllium specimens before/after neutron irradiation.

CONCLUSIONS

Preliminary irradiation test of beryllium materials was performed for lifetime expansion of beryllium frames. The development of test devices and PIEs of the irradiated beryllium specimens were carried out in this test. The main results are as follows;

1) The dismounting device of irradiation capsules was developed for recover of tritium and tritium concentration released from the capsule was able to reduce to the controlled tritium concentration in the exhaust.
2) The high accuracy size measurement device of irradiated specimens was developed and the accuracy of size measurement achieved about 1μm.
3) PIEs such as tensile tests, bending measurement and metallurgical observation were carried out and basic irradiation data of beryllium materials were obtained for lifetime expansion.

In this preliminary test, we succeeded in the irradiation and PIE technique development for lifetime expansion of beryllium frames. In future plan, detail PIEs such as tensile test at 200˚C, impact tests and metallogical observation are to be carried out and the irradiation effects on the properties are to be evaluated in these tests.

REFERENCES

[1] Japan Atomic Energy Agency, *JMTR Japan Materials Testing Reactor brochure* (year unknown) pp. 3-7.
[2] Japan Atomic Energy Research Institute, *Conceptual Design of the Japan Materials Testing Reactor*, (1964) p. 1056.
[3] K. Tsuchiya, G. Longhurst, V. Chakin, I. Tazhibayeva, F. Druyts, C. Dorn, H. Kawamura, *Problems and Future Plan on Material Development of Beryllium in Materials Testing Reactors*, International Symposium on Material Testing Reactors, JAEA-Oarai, Japan, July 16-17, 2008, to be published in JAEA-Conf.
[4] C. K. Dorn, K. Tsuchiya, D. H. Hashiguchi, A. B. Sayer, W. J. Hawas, H. Kawamura, *Material Selection for Extended Life of The Beryllium Reflectors in the JMTR*, International Symposium on Material Testing Reactors, JAEA-Oarai, Japan, July 16-17, 2008, to be published in JAEA-Conf.
[5] D. L. Baldwin, O. D. Slagle, D. S. Gelles, J. Nucl. Mater., 179-181 (1991) 329-334.

5.9 MULTISCALE MODELING SIMULATIONS OF POINT DEFECT PRODUCTION IN NEUTRON-IRRADIATED IRON

Junhyun Kwon[a] and Jung-Ki Shin[b]

[a] *Nuclear Materials Research Division, Korea Atomic Energy Research Institute*
1045 Daedeok-daero, Yuseong, Daejeon 305-353, Korea
[b] *Dept. of Physics, Hannam University, Daedeok, Daejeon 306-791, Korea*
jhkwon@kaeri.re.kr and sjk0327@hotmail.com

A computer simulation and an experimental method were applied to determine a point defect concentration in reactor pressure vessel (RPV) steels irradiated by neutrons. The steel samples had the basic composition of SA508-3 type steels of which the RPV for commercial nuclear power plants are made. The samples were neutron irradiated at 250^{o}C at a fluence of 1.69×10^{19} n/cm^2 ($E_n > 1.0$ MeV). For estimating the concentration of the point defects in the steels, we used computer simulation methods, including a molecular dynamics (MD) computation and a point defect kinetics model calculation. In order to obtain the primary damage parameters, MD simulations of the displacement cascades in Fe were performed. Then, we calculated the point defect concentrations by using the defect kinetics model and the MD calculation results. In parallel with the computation, we undertook a measurement of the positron annihilation lifetimes (PAL) of the irradiated samples. The PAL test results showed that a certain amount of single vacancies were present in the irradiated steels. The vacancy concentration from the PAL measurement was found to be 7.3×10^{-7} /atom, while that from the computational approach was 1.8×10^{-6} /atom. In spite of some uncertainties about the kinetic and materials parameters, a fair agreement between the two methods was obtained.

2008 KAEI/JAEA Joint Seminar on Advanced Irradiation and PIE Technologies
Daejeon, Korea, Nov. 5-7, 2008

Multiscale Modeling Simulations of Point Defect Production in Neutron-Irradiated Iron

Junhyun Kwon & Jung-Ki Shin
Korea Atomic Energy Research Institute
Nuclear Materials Research Division
2008. 11. 7

KAERI
Korea Atomic Energy Research Institute

Outline

- Introduction
  - Radiation effects on materials
- Quantification of point defect production
  - Experimental method
    - ~ Positron annihilation lifetime (PAL) measurement
  - Computational method
    - ~ Molecular dynamics calculation
    - ~ Point defect kinetics model
- Results
  - Determination of point defect (vacancy) concentration
- Summary

KAERI

2

Introduction

- *Radiation Effects on Materials*

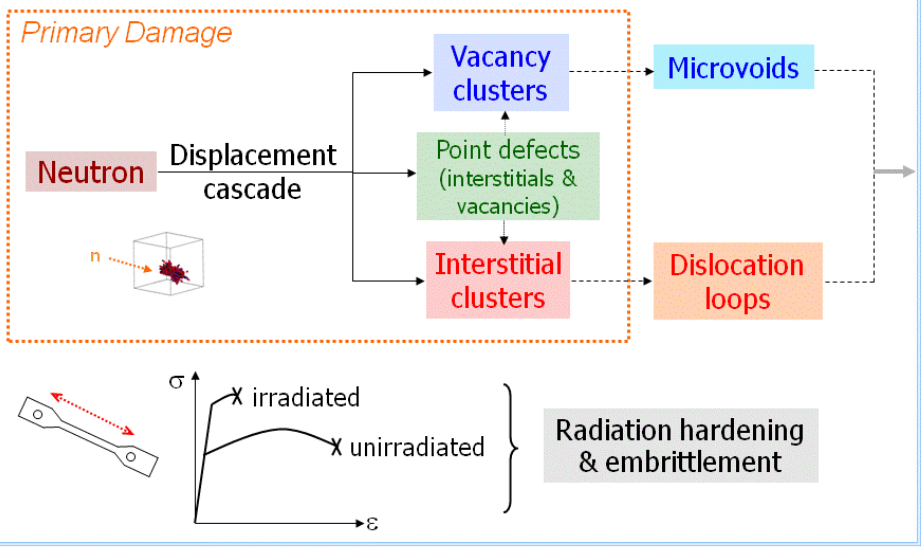

KAERI

Radiation Damage to Materials

- *Degradation of neutron-irradiated pressure vessel steels*

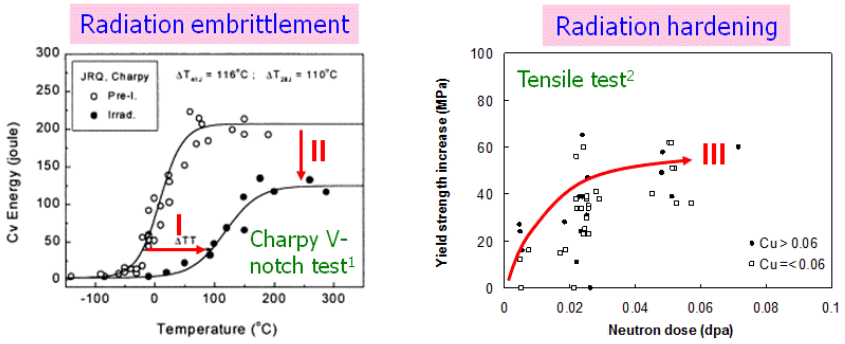

I : increase in Charpy transition temperature shift (TTS)
II : decrease in upper shelf energy (USE)
III : increase in yield strength (σ_{ys})

KAERI

1 B.S. Lee et. al. Int. J. Pres. Ves. & Piping 77, 10 (2000) pp.599-604.
2 C. Brillaud et. al. ATM STP 1125 (1992) pp.23-49.

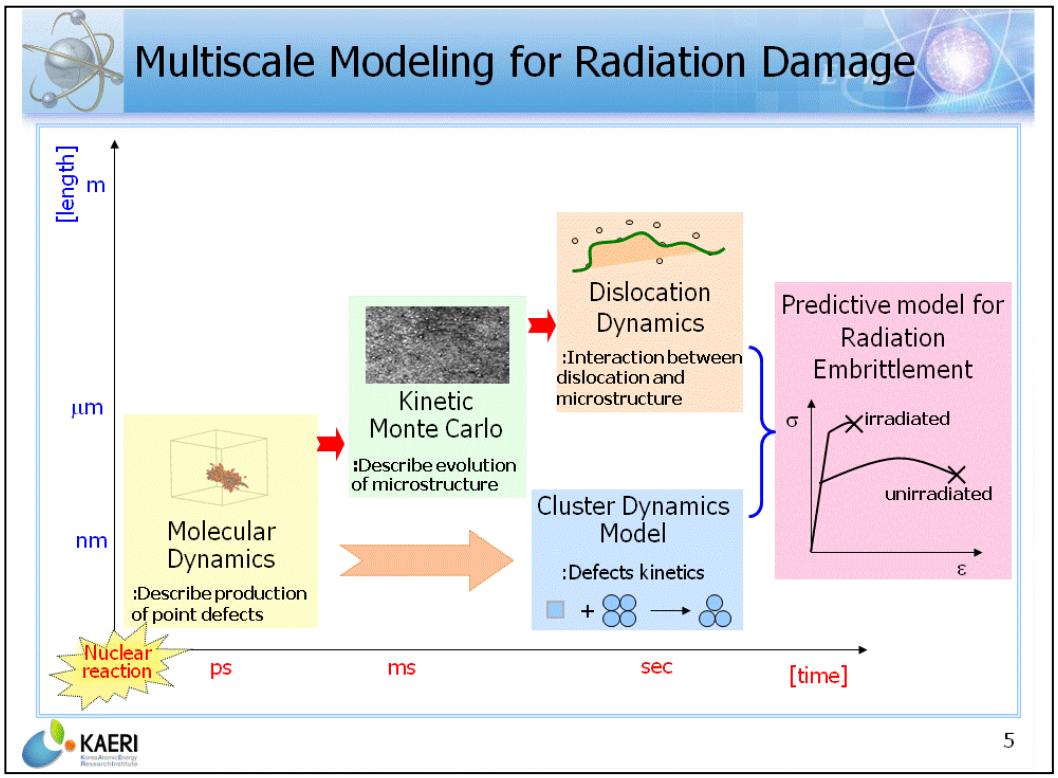
Multiscale Modeling for Radiation Damage
[length]
m
μm
nm
Molecular Dynamics
:Describe production of point defects
Kinetic Monte Carlo
:Describe evolution of microstructure
Dislocation Dynamics
:Interaction between dislocation and microstructure
Cluster Dynamics Model
:Defects kinetics
Predictive model for Radiation Embrittlement
σ
irradiated
unirradiated
ε
Nuclear reaction
ps
ms
sec
[time]
KAERI
5

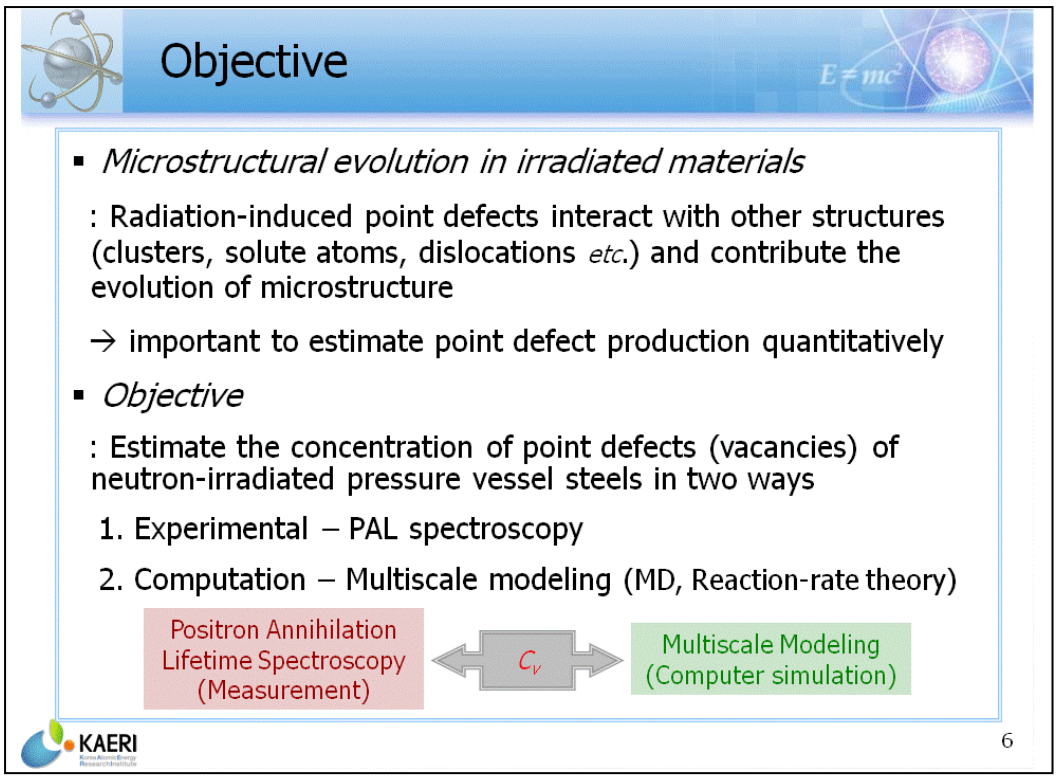
Objective
▪ Microstructural evolution in irradiated materials
: Radiation-induced point defects interact with other structures (clusters, solute atoms, dislocations etc.) and contribute the evolution of microstructure
→ important to estimate point defect production quantitatively
▪ Objective
: Estimate the concentration of point defects (vacancies) of neutron-irradiated pressure vessel steels in two ways
1. Experimental – PAL spectroscopy
2. Computation – Multiscale modeling (MD, Reaction-rate theory)
Positron Annihilation Lifetime Spectroscopy (Measurement)
C_v
Multiscale Modeling (Computer simulation)
KAERI
6

Experimental

- *Materials of interest*
  - Reactor pressure vessel steels (SA508 series)

Mn	Ni	Mo	Si	Cr	P	S	Cu	Fe
1.24	0.92	0.49	0.24	0.21	0.007	0.002	0.03	Bal.

(unit: w/o)

- *Irradiation conditions*
  - Neutron irradiation in a research reactor, HANARO

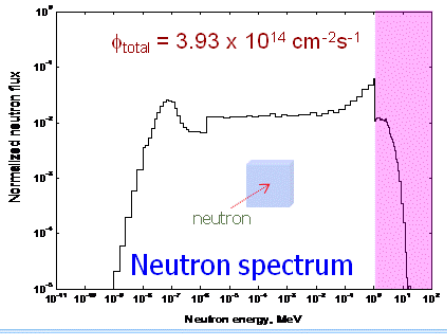

- Irradiation temperature : 280°C
- Fast neutron fluence (E_n>1.0 MeV) = 1.69 x 10^{19} cm^{-2} (~0.02 dpa)
- Specimen size : 10x10x1 mm^3

KAERI

7

Experimental - PALS

- *Positron Annihilation Lifetime Spectroscopy*

- By detecting the β^+-annihilation gamma, possible to obtain information on character & relative density of the *open-volume defects* in the samples (radiation-induced *vacancies*)

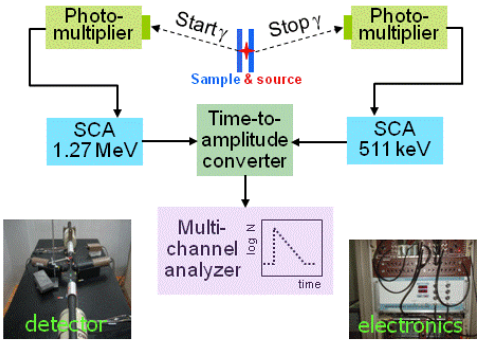

[Experimental setup for PALS]

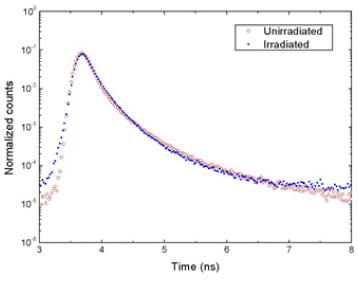

[Measured PAL Spectra]

KAERI

8

Experimental - PALS

- *PAL Data Analysis (by PALSFIT S/W)*

	Unirradiated	Irradiated	
Lifetime τ_1 (ps)	99.6 ± 1.1	81.6 ± 3.5	← β^+ annihilation at the bulk
Intensity I_1 (%)	**58.7 ± 1.2**	**28.1 ± 2.3**	
Lifetime τ_2 (ps)	150 ± 0.0	150 ± 0.0	← β^+ annihilation at dislocations
Intensity I_2 (%)	**41.3 ± 1.2**	**64.7 ± 4.5**	
Lifetime τ_3 (ps)	-	186 ± 0.0	← β^+ annihilation at vacancies
Intensity I_3 (%)	-	**7.2 ± 2.3**	
Average τ (ps)	***120.4*** →	***133.4***	

→ Neutron irradiation to PV steels induces the formation of small-size vacancies (~ single vacancies) [τ_v* for Fe = 170 to 190 ps]

→Estimate the concentration of vacancies (C_v) from PAL measurement data and positron trapping model...

$$C_v^{PAL} = 7.3 \times 10^{-7} \text{ /atom}$$

KAERI

9

Computational Model

- *Point defect kinetics*

→ Describe mathematically the interactions of point defects with defects such as point defects, their clusters, dislocations, grain boundaries...

→ Obtain information on primary damage from the molecular dynamics (MD) simulation ~ Input to point defect kinetics model

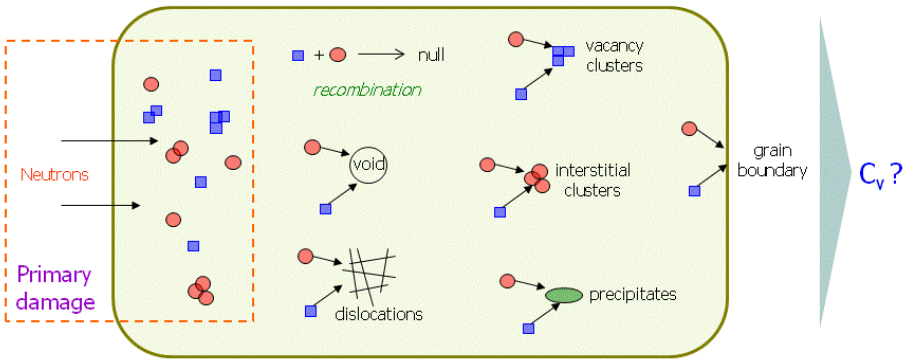

KAERI

10

Computational Model

- *Basic Neutron Damage Calculation*

1. Neutron damage calculation using the SPECTER code
2. Obtain primary damage parameters for the MD simulation

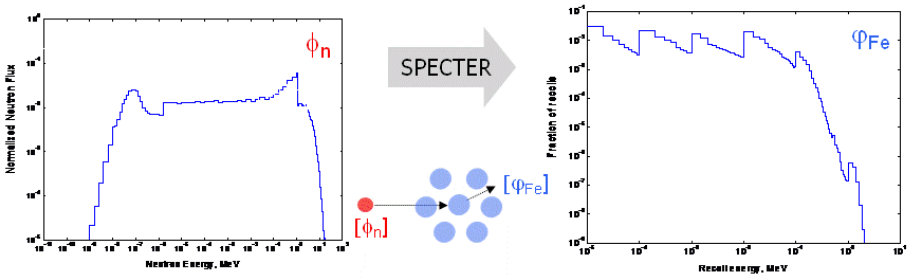

Neutron spectra of HANARO

Recoil spectra for Fe

- Average PKA energy : 4.7 keV
- Displacement rate : 1.04 x 10^{-7} dpa/s

Input to MD calculations

KAERI

11

Molecular Dynamics Calculation

- *MD calculations for simulating primary damage*

→ Investigate the distribution of residual point defects in the primary damage state

→ Simulation of displacement cascade in Fe using the MD code (MOLDY)

- block size ~ 40x40x40 a_o^3
- PKA energy ~ 4.7 keV
- temperature ~ 280°C

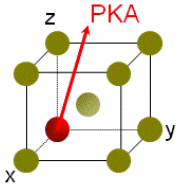

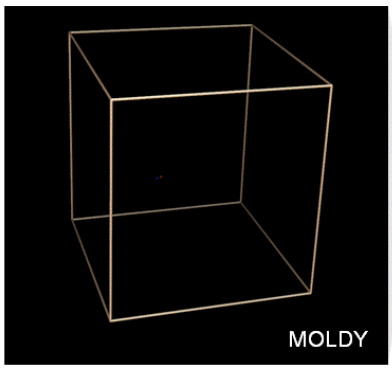

- cascade efficiency (η) = 0.42
- interstitial clustering fraction (f_{id}) = 0.31
- vacancy clustering fraction (f_{vd}) = 0.21

KAERI

12

Point Defect Kinetics

- *Point defect kinetics model*

→ Describe rate of changes in the spatially-averaged point defect concentrations (C_i, C_v)

$$\frac{dC_i}{dt} = P_i - RC_iC_v - D_iS_i^TC_i \qquad \frac{dC_v}{dt} = P_v - RC_iC_v - D_vS_v^TC_v$$

P_i, P_v: point defect production rate (i~ interstitial / v~ vacancy)
R : recombination constant between i and v
D_i, D_v: diffusion coefficient for point defects
S^T_i, S^T_v: total sink strength for the absorption of point defects (dislocations, grain boundaries)
where, $P_i = \eta\,(1-f_{icl})\,G_{dpa}$ ← from MD simulation results

→ Steady state solution ($dC_v/dt=0$)

$$C_v = \frac{-\Xi + \sqrt{\Xi^2 + 4RP_iD_iS_i^TD_vS_v^T}}{2RD_iS_i^T} \qquad \Xi = RP_v + D_iS_i^TD_vS_v^T - RP_i$$

KAERI 13

Point Defect Kinetics

- *Materials and kinetic parameters for RPV steels*

→ Input data for solving the rate equations

Parameter	Value
Irradiation temperature (°C)	250
Displacement rate (dpa/s)	1.043×10^{-7}
Cascade efficiency	0.42
Interstitial clustering fraction	0.308
Vacancy clustering fraction	0.213
Vacancy pre-exponential factor (cm^2/s)	0.5
Vacancy migration energy (eV)	1.25
Interstitial pre-exponential factor (cm^2/s)	0.05
Interstitial migration energy (eV)	0.25
Dislocation vacancy bias	1
Dislocation interstitial bias	1.25
Effective grain diameter (cm)	0.001
Dislocation density (/cm^2)	1.1×10^{10}
Lattice constant of iron (cm)	2.87×10^{-8}

From SPECTER

From MOLDY

$C_v = 1.8 \times 10^{-6}$ /atom

KAERI 14

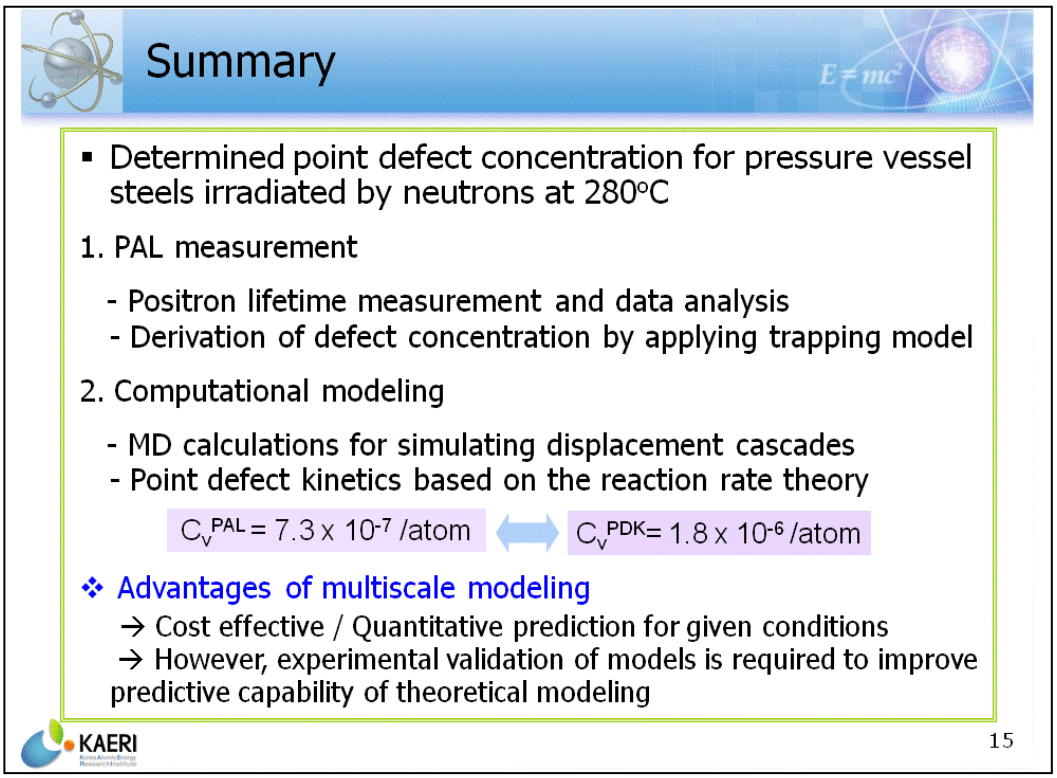
Summary
E = mc²
▪ Determined point defect concentration for pressure vessel steels irradiated by neutrons at 280°C
1. PAL measurement
- Positron lifetime measurement and data analysis
- Derivation of defect concentration by applying trapping model
2. Computational modeling
- MD calculations for simulating displacement cascades
- Point defect kinetics based on the reaction rate theory
$C_v^{PAL} = 7.3 \times 10^{-7}$ /atom
$C_v^{PDK} = 1.8 \times 10^{-6}$ /atom
❖ Advantages of multiscale modeling
→ Cost effective / Quantitative prediction for given conditions
→ However, experimental validation of models is required to improve predictive capability of theoretical modeling
KAERI
15

5.10 MEASUREMENT OF DEFORMATION OF FBR FUEL ASSEMBLY WRAPPER TUBE BY AN INNOVATIVE TECHNIQUE

Shinji Sasaki, Kazuyuki Abe and Tsuyoshi Nagamine

Fuels and Materials Department, Japan Atomic Energy Agency
4002 Narita-cho, O-arai-machi, Higashi-ibaraki-gun, Ibaraki 311-1393, Japan

ABSTRACT

An innovative technique to measure the deformation of irradiated wrapper tube for FBR fuel assembly was developed, and installed in the hot cell of the Fuels Monitoring Facility in JAEA. In order to confirm the performance of this instrument, a number of measurements were carried out on the wrapper tubes irradiated to high fluence in the experimental fast reactor Joyo.

In the instrument used until now, only three face to face distances in the hexagonal wrapper tube have been measured along the axial direction. On the other hand, in the instrument developed in this technique the face to face distances could be continuously measured along the lateral direction on the outer surfaces of wrapper tube. Using data obtained by this technique, the detailed analyses of deformation can be done throughout a whole wrapper tube.

INTRODUCTION

The fuel assembly of fast breeder reactor (FBR) consists of fuel rods bundle and a hexagonal wrapper tube packing them. This wrapper tube expands and deforms by the swelling, creep and so on during irradiation in FBR[1][2]. This deformation of wrapper tube has an effect on the integrity of wrapper tube. It is, therefore, very important to examine the deformation performance of wrapper tube.

Until now, the deformation of wrapper tube has been inspected by measuring the distance between a face and its opposite face of hexagonal wrapper tube (face to face distance) at three points on their outer surfaces. The maximum value in the measured data, most of which was appeared at laterally central position, was treated as the deformation value. These

measurements were repeated between two other pairs of faces. Furthermore, these measurements were carried out at an interval of 10 mm along the axial direction.

In this study, the face to face distance was measured continuously along lateral direction on the outer surfaces of hexagonal wrapper tube. That is, the continuous measurement of the face to face distance was laterally carried out from one corner to another corner of hexagonal wrapper tube. In addition, the corner to corner distance was measured between a corner and its corresponding corner the outer surfaces of hexagonal wrapper tube. This upgrades in the face to face measurement and the corner to corner measurement made it possible to analyze an more detailed deformation.

OUTLINE OF INSTRUMENT

Fig.1 shows a schematic diagram of instrument developed in this study. In this figure, the faces and corners of hexagonal wrapper tube are delineated by the marked F1 to F6 and C1 to C6, respectively. During the measurement, the fuel assembly is fixed and the distance, D, between the surfaces of bases where two probes are fixed (based surface) is held to be constant. Then, the lengths of two probes, l_l, and l_r, from their left and right based surfaces are measured. Thus, the face to face distance, l_f and corner to corner distance, l_c are measured by the following equation,

$$l_f \quad \text{or} \quad l_c = D - l_l - l_r,$$

The deformation of two kinds of wrapper tubes of fuel assemblies were measured, which were irradiated to high fluence in the experimental FBR “Joyo”. First type of fuel assembly was used as the core assembly in JOYO MK-Ⅱ and its maximum fluence was 9.90×10^{26}n/m^2 (E$\geqq$0.1MeV), and second one was doubly wrapped assembly specially developed for the purpose of irradiation to high fluence and its maximum fluence was 2.23×10^{27}n/m^2 (E$\geqq$0.1MeV). The main specifications of them are showed in Fig.2 and Table 1.

First, two measurement probes move laterally on an outer face F1 and its opposite face F4 and the face to face distance can be continuously measured between both faces. Next, the two measurement probes were rotated counterclockwise by 30 degrees and move upward along two corners between the faces F1 and F2 and F4 and F5 to measure the corner to corner distance between C1 to C4. After then, two measurement probes were rotated counterclockwise by 30 degrees and the face to face distance was measured between the faces F2 and F5. Additionally, the face to face distance between two faces F3 and F6, and the corner

to corner distances between C2 and C5, C3 and C6 were measured by repeating similar procedures.

These measurements were carried out along the axial direction at predetermined positions. This instrument was installed in hot cell because the irradiated fuel assembly had strong radioactivity. Then, a number of measurements were done on the wrapper tubes of fuel assemblies irradiated to high fluence in the experimental FBR,"Joyo".

RESULTS AND DISCUSSION

Fig.3 shows typical deformations obtained at the axially central positions of core fuel regions on two kinds of wrapper tubes used for Joyo Mk-Ⅱ core fuel assembly and Joyo special fuel assembly. Fig.4 indicates an analysis method of data obtained. In this figure, $l_f(0)$ is the distance between two faces (minimum face to face distance) near the corners where no significant bowing deformity is seen. Δl_f is given by the following equations, expressing the degree of bowing deformity.

$$\Delta l_f = l_l(c) - l_l(0), \text{ or } \Delta l_f = l_r(c) - l_r(0),$$

where $l_l(c)$ or $l_r(c)$ is the length of probe from its left or right based surface at the laterally central position of wrapper tube. $l_l(0)$ or $l_r(0)$ is the length from its left or right based surface near the corner where no significant bowing deformity is seen.

Fig. 5 shows the values of $l_f(0)$ as a function of axial distance from the bottom of fuel assembly obtained on two kinds of wrapper tubes. The dashed lines indicates the region of the face to face distance before irradiation. It is shown that the no significant change is seen in the wrapper tube used for the core fuel assembly (Fig. 5(a)), but a remarkable deformation can be observed in the inner wrapper tube used for the special fuel assembly irradiated to the higher fluence (Fig.5(b)). In addition, it should be noted that deformation is large in the axially central region where the fluence is high, but are small at the bottom and top of core fuel region where the fluence are low.

Fig. 6 shows the extents of bowing deformities, Δl_fs, as a function of axial distance from the bottom of fuel assembly obtained on all (six) faces of two kinds of wrapper tubes. It is illustrated that the change in the extent of bowing deformity on any face is nearly same of the wrapper tube used for core fuel assembly (Fig.6(a)), but it is irregular, depending on the distance from the bottom of fuel assembly and face measured in the inner wrapper tube used for special fuel assembly.

Fig. 7 shows the corner to corner distance obtained on two kinds of wrapper tubes. Also in these results, the deformation is larger in the inner wrapper tube used for the special assembly irradiated to the higher fluence than in the wrapper tube used for the core fuel assembly.

A plan to theoretically understand the data obtained in this study is under progress. In this plan, the irradiation fluence, coolant pressure, creep, swelling and so on are taken into consideration.

CONCLUSION

A new technique was developed in the measurement of face to face distance and corner to corner of wrapper tube used for the FBR fuel assembly. These distances can be continuously measured along the lateral direction on the faces of hexagonal wrapper tube. In addition, these measurements were carried out along the axial distance from the bottom of fuel assembly at the predetermined position. From the data obtained, the detailed analyses of face to face distance and corner to corner could be realized. Furthermore, it made possible that the extent of bowing deformity on the any face of hexagonal is analyzed.

REFERENCE

[1] E. R. Gilbert, et al. “Irradiation creep data in support of LMFBR core design”, J. Nucl. Mater. No. 65, PP266-278

[2] T. Asaga, et al. “Evaluation of driver fuel performance in the Joyo Mk-II core”, J. Nucl. Mater. No. 204, PP102-108

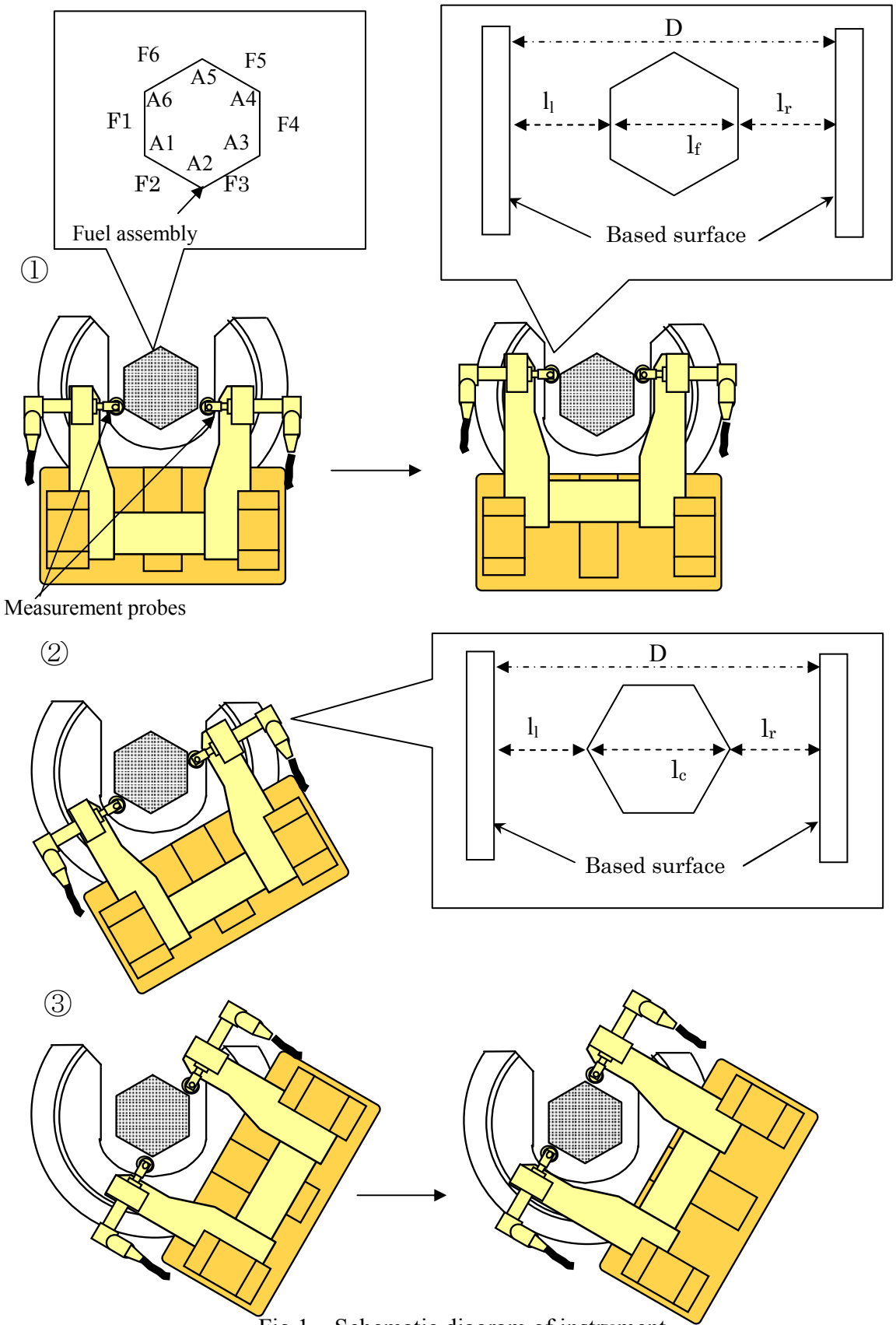

Fig.1 Schematic diagram of instrument

Table 1 Specification of Joyo MK-II core fuel assembly and Joyo special fuel assembly.

Assembly type	Joyo MK-II core fuel assembly	Joyo special fuel assembly.
Length	2970mm	2970mm
Core fuel length	550mm	550mm
Face to face distance of wrapper tube (outer surface)	78.5mm	78.5mm (Outer wrapper tube)
		66.4mm (Inner wrapper tube)
Thickness of wrapper tube	1.9mm	1.9mm (Outer wrapper tube)
		1.7mm (Inner wrapper tue)
Total number of fuel pins	127 pins	61 pins
Maximum neutron fluence (E≧0.1MeV)	$9.90 \times 10^{26} n/m^2$	$2.23 \times 10^{27} n/m^2$

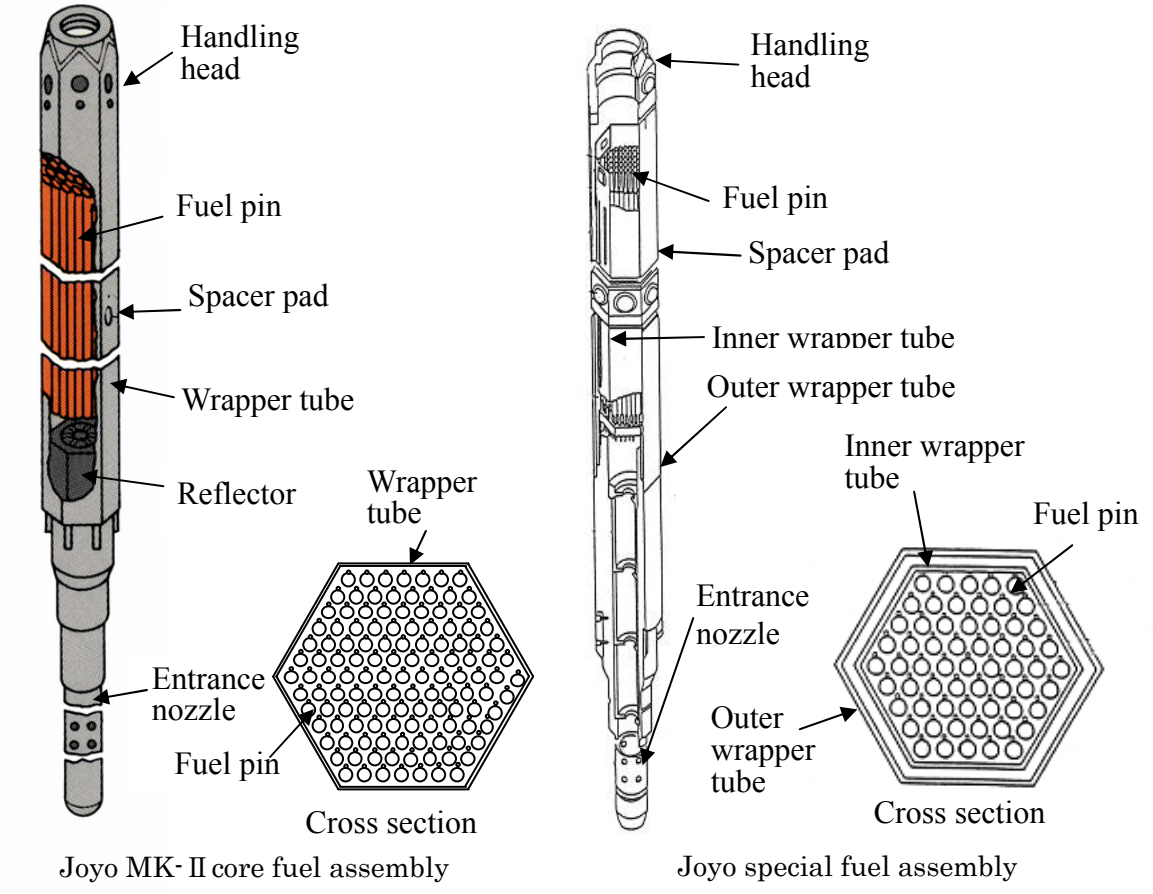

Fig.2 Outline of fuel assemblies

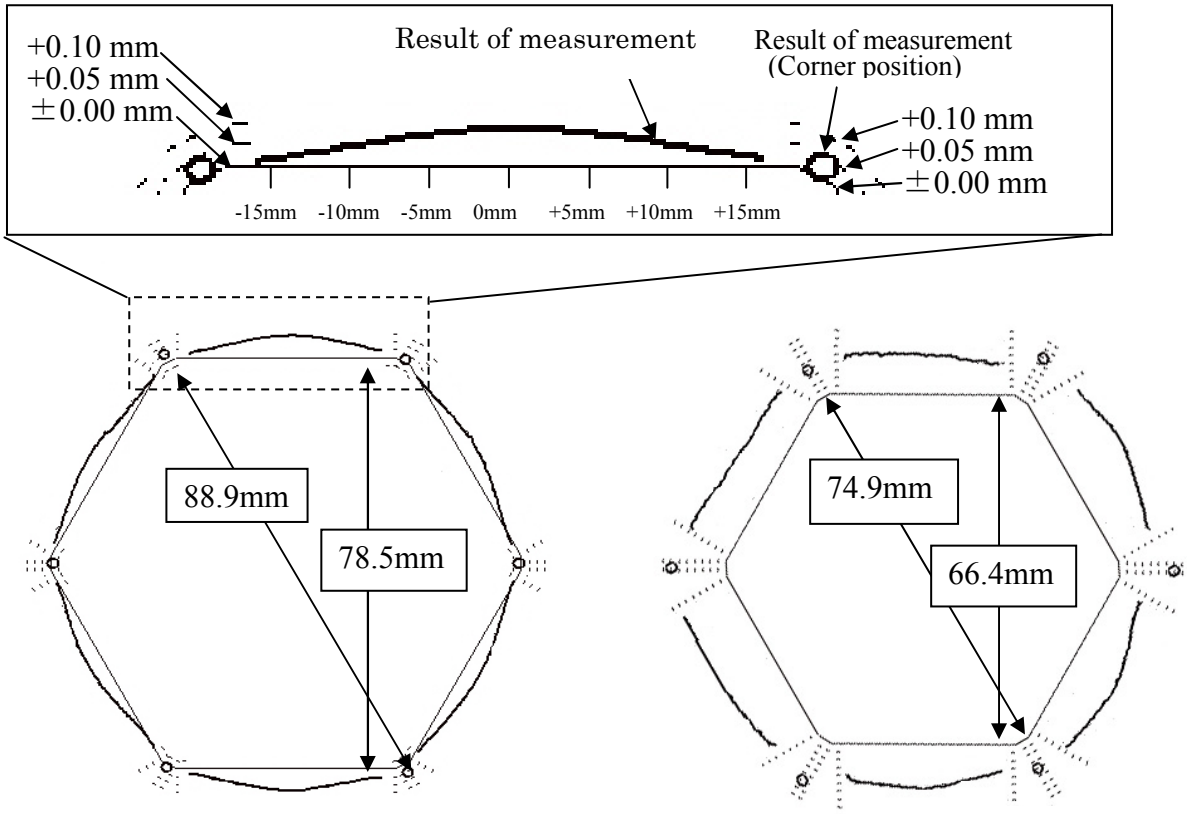

Joyo MK-Ⅱ core fuel assembly
wrapper tube.
(Maximum fluence:9.90×10^{26}n/m^2
:E≧0.1MeV)

Joyo special fuel assembly
inner wrapper tube.
(Maximum fluence:2.23×10^{27}n/m^2
:E≧0.1MeV)

Fig.3 Deformations of wrapper tubes at the axially central position of core fuel region.

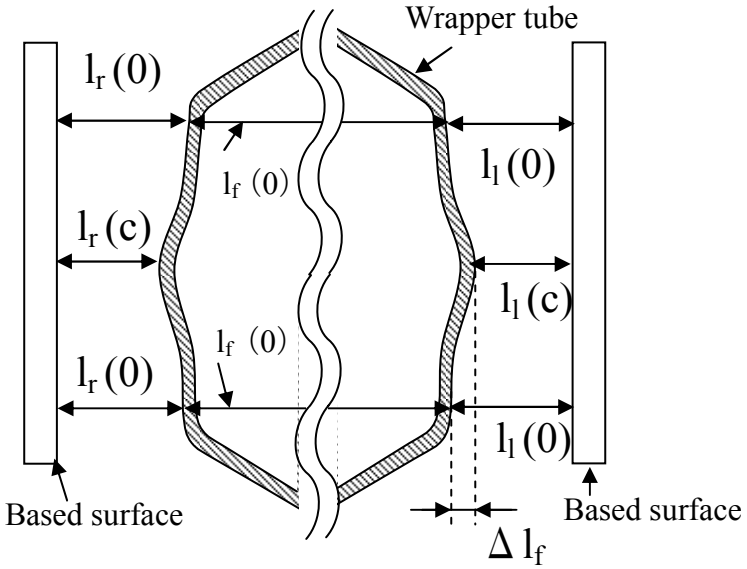

Fig.4 An analysis method of data obtained

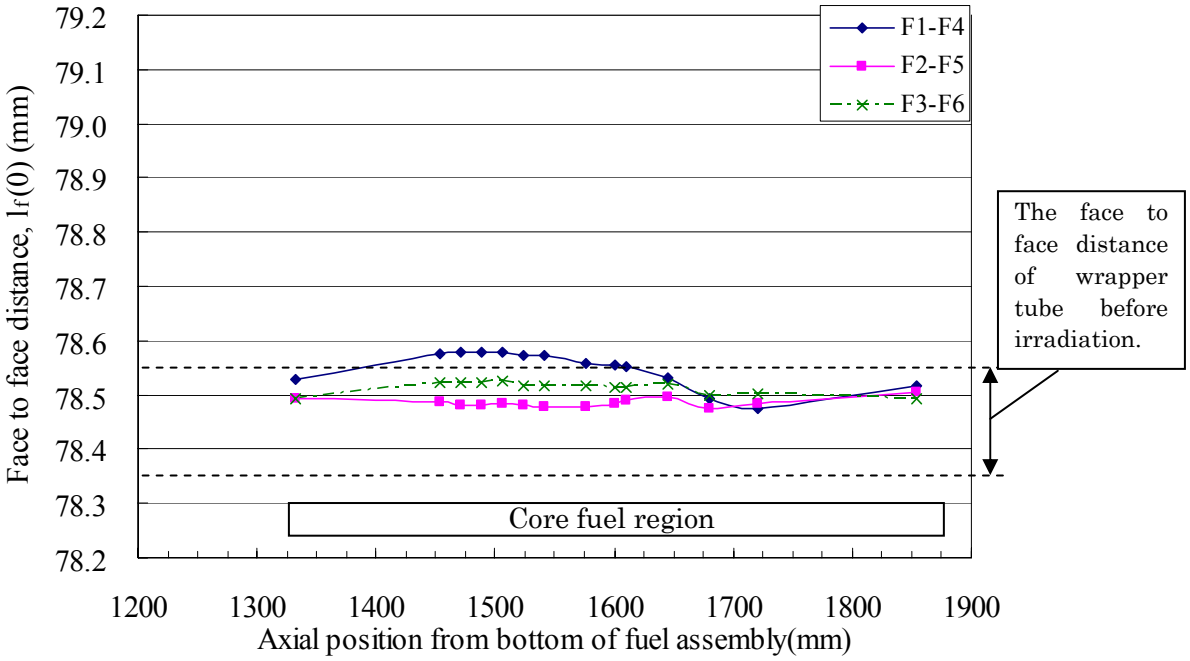

Fig.5(a) Wrapper tube of Joyo core fuel assembly
(Maximum fluence:9.90×10^{26}n/m^2 E≧0.1MeV)

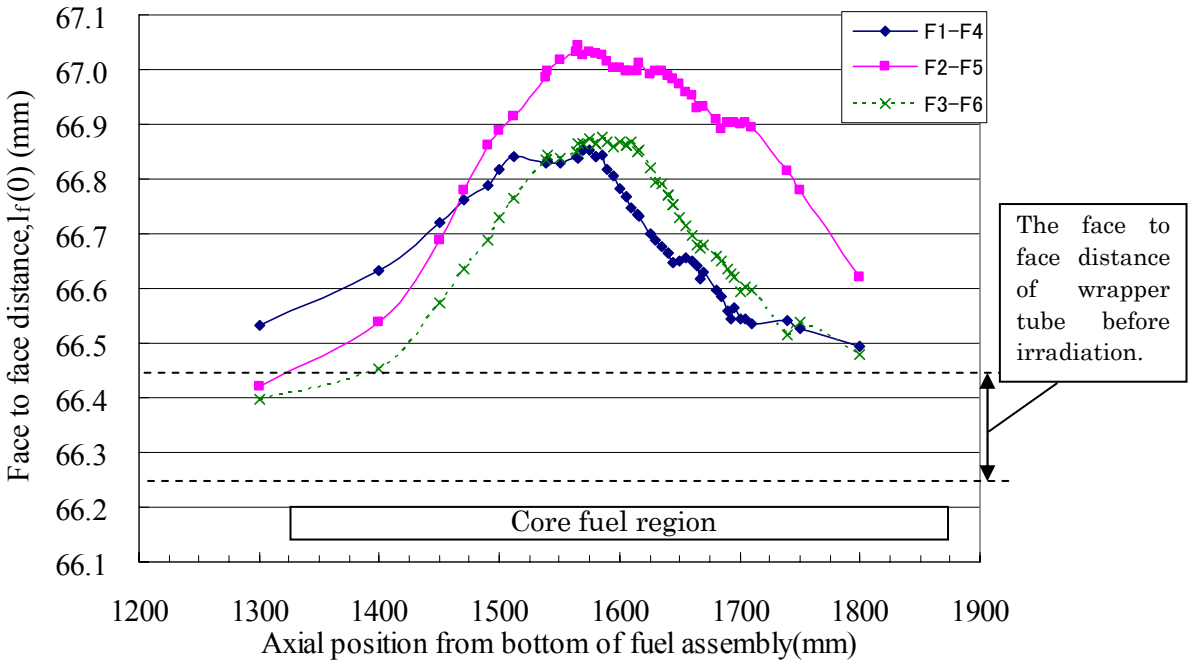

Fig.5(b) Inner wrapper tube of Joyo special fuel assembly
(Maximum fluence:2.23×10^{27}n/m^2: E≧0.1MeV)

Fig.5 Face to face distance, $l_f(0)$, along axial direction

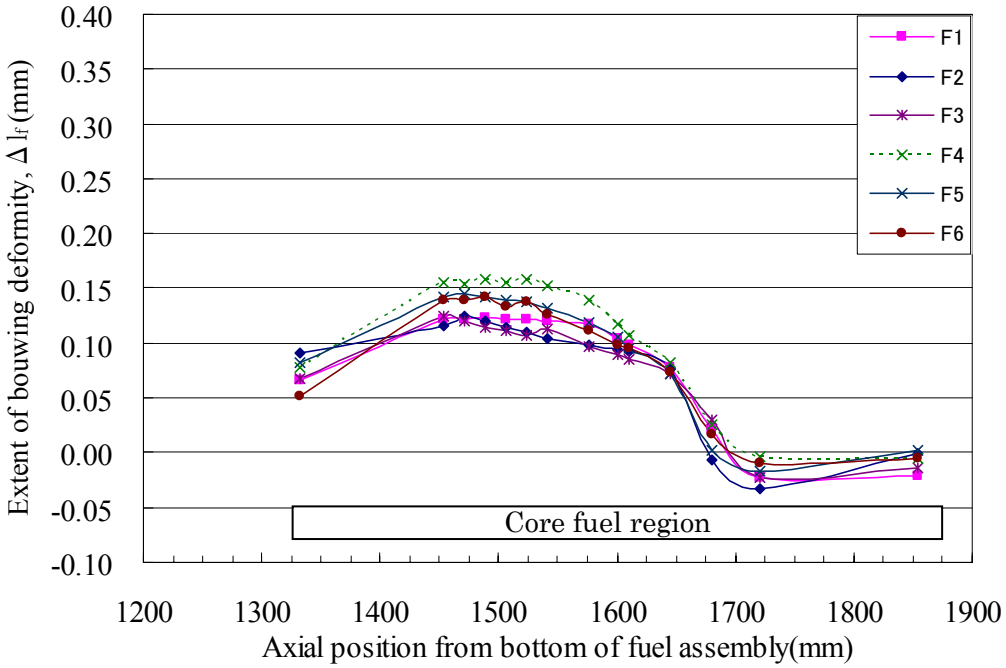

Fig.6(a) Wrapper tube of Joyo fuel assembly
(Maximum fluence:9.90×10^{26}n/m^2 E≧0.1MeV)

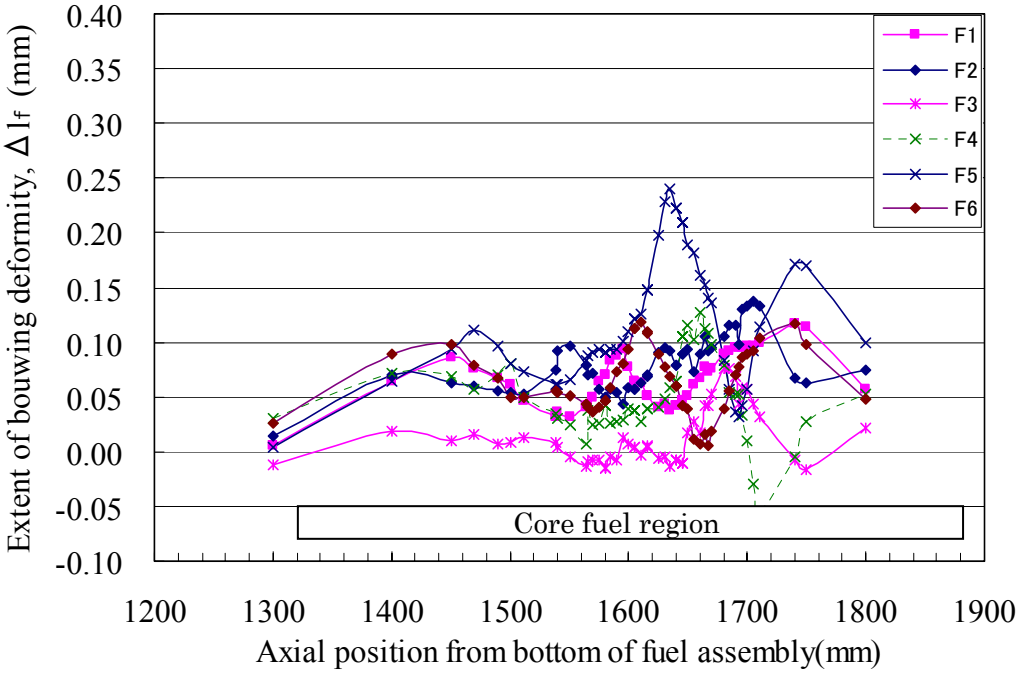

Fig.6(b) Inner wrapper tube of Joyo special fuel assembly
(Maximum fluence:2.23×10^{27}n/m^2: E≧0.1MeV)

Fig.6 Extent of bowing deformity, Δl_f, along axial direction

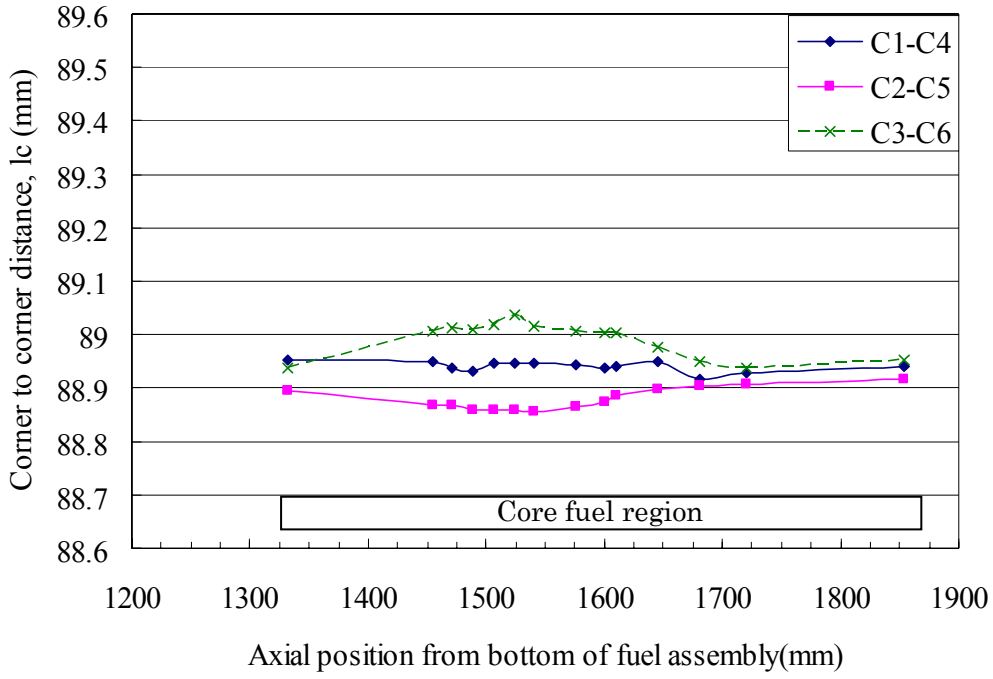

Fig.7(a) Wrapper tube of Joyo core fuel assembly
(Maximum fluence:9.90×10^{26}n/m^2 E≧0.1MeV)

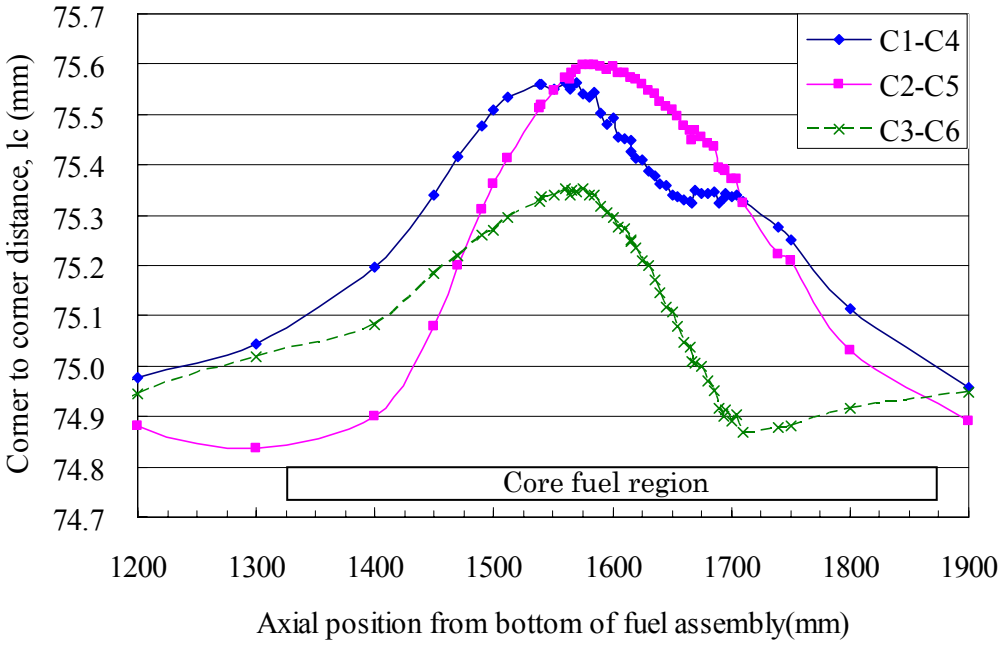

Fig.7(b) Inner wrapper tube of Joyo special fuel assembly
(Maximum fluence:2.23×10^{27}n/m^2: E≧0.1MeV)

Fig.7 Corner to corner distance, lc, along axial direction

5.11 TRANSIENT BURST TECHNIQUES AND RESULTS OF THE EXAMINATION FOR IRRADIATED PNC316 STEEL

Toshihiko Inoue, Ryuichiro Ogawa, Naoaki Akasaka, and Kenji Nishinoiri

Materials Monitoring Section, Fuels and Materials Department,
Oarai Research and Development Center, Japan Atomic Energy Agency
4002, Narita-cho, Oarai-machi, IBARAKI, 311-1393, JAPAN
inoue.toshihiko@jaea.go.jp, ogawa.ryuichiro19@jaea.go.jp,
akasaka.naoaki@jaea.go.jp, and nishinoiri.kenji@jaea.go.jp

ABSTRACT

In fast reactors, deformation behavior and failure strength of fuel cladding tubes (CTs) under loss of coolant flow (LOF) events are important evaluation items of reactor safeties. It has calculated that the primary temperature peak of CTs under such events reaches 720 ℃ or more from 650 ℃ in a short time, e.g. 2-3 seconds. Transient burst tests simulate this phenomenon, and they measure failure temperature of the CTs, as heating under a constant pressure. In this paper CTs behavior was evaluated during the primary phase of an LOF event and transient bust test were made for neutron irradiated PNC316 CTs. The CTs specimens were irradiated in the experimental fast reactor JOYO. Post irradiation examination (PIE) results for transient burst test specimens showed failure temperatures were between 930 and 1,030 ℃ at a hoop stress of 98 MPa. For higher hoop stresses, the rupture temperatures were lower. The failure temperatures of irradiated and un-irradiated CTs were within 10% of the average measurement value at each hoop stress. The failure temperature of the irradiated CTs had no extreme degradation by comparison to the failure temperature of the un-irradiated CTs.

INTRODUCTION

In fast reactors, if events such as a flow reduction of liquid sodium coolant will occur, or an excessive reactor thermal power occur, the CTs with inner pressure caused by fission products will be heated. The loading temperature and inner pressure (as hoop stress) exceed the normal conditions of reactor operation. These CTs may possibly rupture because they already have

decreased strength through normal use (with under 69 MPa and at under 650 ℃). The degree of strength change of the CTs depends on the rising condition of the temperature and inner pressure (as hoop stress), the event type (e.g. LOF event) and the time phase of the event (e.g. primary temperature peak). The mechanical behavior and the strength of the CTs under LOF events are important evaluation items of reactor safeties. The primary peak temperature in such a case is a strict condition for the CTs. This peak temperature has been calculated to reach 720 ℃ or more from 650 ℃ within seconds in a prototype fast reactor. The mechanical behavior of the CTs, while reaching the primary peak temperature, can be simulated by transient burst examinations which detect the failure temperature of the CTs as heating under constant pressure.

This paper describes the procedure for the transient burst test, and their results, obtained from post irradiation examinations (PIEs) of the irradiated PNC316 CTs specimens.

EXPERIMENTAL

Experimental apparatus

The transient burst tests were carried out using equipment that was specially installed in the hot cell of the Materials Monitoring Facility in the Oarai Research and Development Center. This equipment consisted of two sets of components: heating device components and high pressure device components. The experiments were carried out by using these two devices as experimental parameters. Figure 1 shows a schematic diagram of the transient burst test apparatus and figure 2 shows the vessel in the hot cell.

The heating device could heat specimens up to 1,600 ℃ by direct resistance heating, and heating rate could be controlled from 5 ℃/s to 100 ℃/s in vacuum vessel which was kept in a vacuum condition under 1 Pa. The temperature of the centrally located specimen was measured with platinum-rhodium thermocouples. The thermocouples were welded onto the specimen by resistance welding. The measured temperatures were fed back into the temperature control system. The temperature control system controlled the electric current to keep the desired heating rate. The maximum pressure supplied by the high pressure device was 80 MPa which was the set load pressure at the specimen. The pressure medium was argon gas (pure grade: over 99.99 %). The argon gas (14.7 MPa) is pressurized to the test pressure by a compression machine in the operation area, and a Heise pressure indicator was used to show the test pressure. The CTs specimen was filled with pressurized argon gas in the hot cell by passing the gas through pipes. A laser-based measurement device was used to get the outer diameter of the CTs at one point in the middle area which was generally at the rupture point.

An electrical pole and a modified-Swagelok® fitting were attached to each end of a specimen (figure 3). One end of each electric pole was connected to a high-pressure pipe through which the internal pressure of high-purity argon gas was supplied from outside to the hot cell at room temperature. The specimens and its attachments were mounted in the transient burst test apparatus, and argon gas was introduced into the specimen to the test pressure as hoop stress. Argon gas was maintained at the test pressure during the test. The specimen was heated until failure from 400 ℃ (preliminary heating temperature by manual operation) at the desired heating rate, as from 5 ℃/s to 100 ℃/s in the vacuum vessel. The rupture temperature was measured and the outer diameter at the mid-point in the longitudinal direction of the specimen was also measured continuously until rupture.

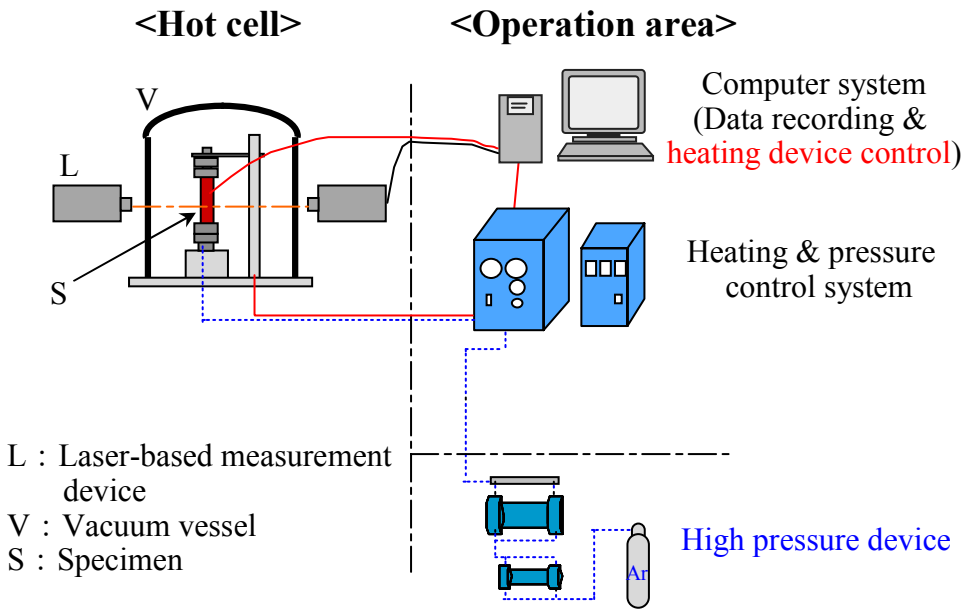

Figure 1 Schematic diagram of the transient burst test apparatus.

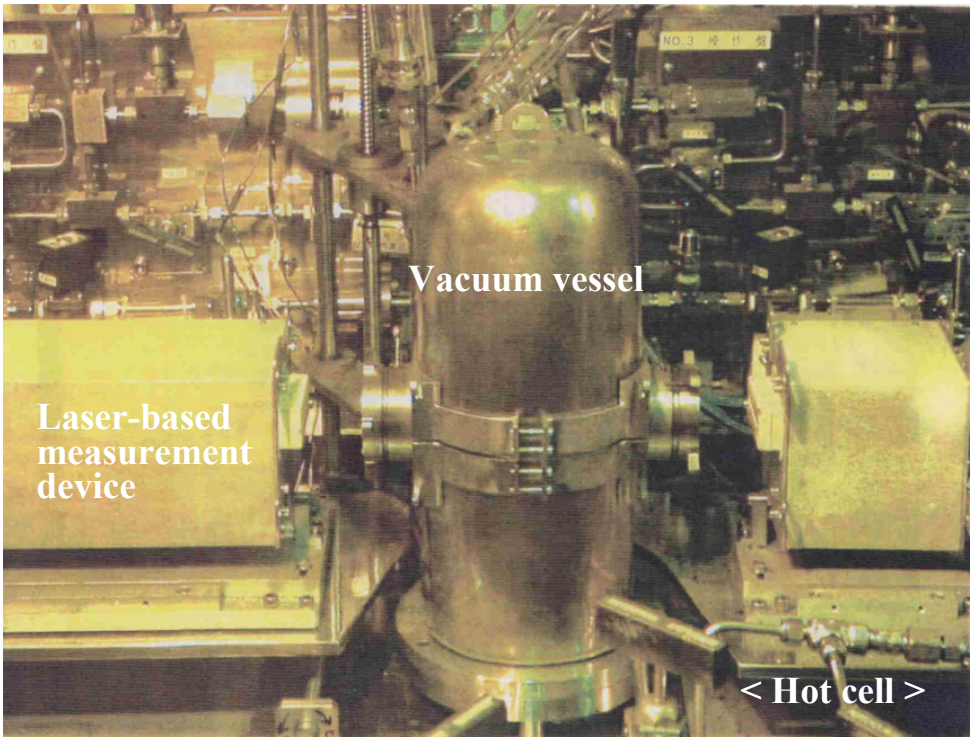

Figure 2 Photo showing the transient burst test apparatus in the hot cell.

The transient burst Test

The test specimens were modified 316 stainless steel (PNC316) CTs. The cold working levels were 18-20%. Chemical composition of PNC316 is shown in table 1. The outer diameters of the specimens were 5.5 mm (0.35 mm thickness) and 6.5 mm (0.47 mm thickness) and their length was 80 mm.

The test conditions of irradiated PNC316 stainless steel CTs specimens are described below. The heating rate was constant at 5 ℃/s, and the constant pressure levels were 49, 98, 147, 196, 216, and 294 MPa, as hoop stress. The test specimens had been irradiated in JOYO at irradiation temperatures between 400 and 730 ℃, and at fast neutron (E > 0.1 MeV) doses ranging from 11 to 115 dpa (25×10^{26} n/m^2).

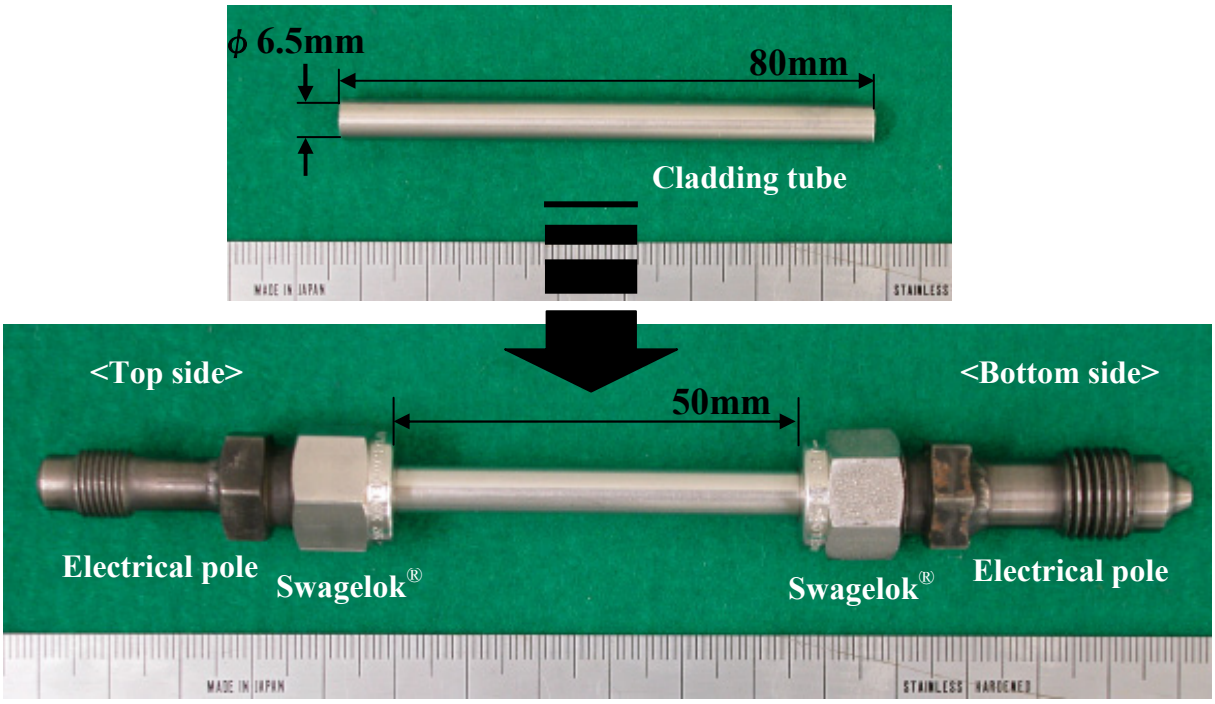

Figure 3 Photos of a specimen and its attachments prior to the transient burst test.

Table 1 Chemical composition of PNC316 stainless steel (wt%)

	C	Si	Mn	P	Ni	Cr	Mo	B	Ti	Nb	Fe
PNC316	0.052 - 0.054	0.78 - 0.82	1.72 - 1.83	0.028 - 0.029	13.45 - 13.84	16.22 - 16.52	2.35 - 2.49	0.0031 - 0.0039	0.078 - 0.080	0.079 - 0.080	Bal.

RESULTS AND DISCUSSION

The transient burst results are plotted in figure 4 for irradiated and un-irradiation test specimens. The filled symbols show results of fuel pin CTs, and open symbols show results of material-irradiated CTs. The line is the nominal line of un-irradiated results and horizontal bars show the range of rupture temperature results. There was no difference between the irradiated specimen results and the un-irradiated specimen results. And there was no difference in the results for 5.5 mm (fuel pin) and 6.5 mm (fuel pin and material-irradiated) outer diameters of specimens. The results of transient burst tests showed that the burst temperature decreased monotonically from 1,100 ℃ to 800 ℃ with an increase in hoop stress from 49 MPa to 294 MPa. This phenomenon was confirmed in both irradiated and un-

irradiated specimens. The rupture time (test time) decreased from 140 seconds to 80 seconds by increasing the hoop stress from 49 MPa to 196 MPa, as the measurement test time was starting from 400 ℃ (preliminary heating). The measured rupture time and the time calculated from figure 4 were almost the same. The rupture temperature of specimens with high irradiation fluence or high irradiation temperature was a little lower than that of un-irradiated specimen. The decrease was about 50 ℃ at 98 MPa test pressure. This small change seemed to be caused by fluence over $20x10^{26}$ n/m^2 (E>0.1 MeV) or irradiation temperature over 700 ℃. The failure temperatures of irradiated CTs specimens were within the 10% of measured values at each hoop stress. On the other hand, the failure temperatures of un-irradiated CTs specimens were within the 5% of measured values at each hoop stress. The failure temperature of irradiated CTs specimens had no extreme degradation compared to the failure temperature of un-irradiated CTs specimens.

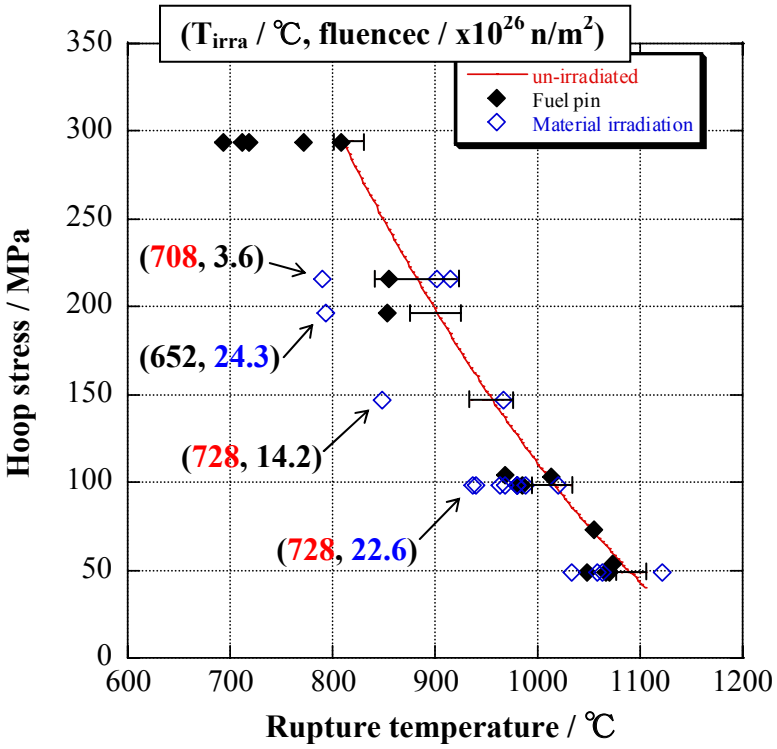

Figure 4 The relationship between hoop stress and failure temperature of PNC 316 CTs.

The photos of irradiated transient burst specimens after the test (figure 5) showed the ruptured area was in their middle, which was about the same as the maximum heating area.

The fracture mode of specimens depended on hoop stress. As the hoop stress was higher, the fracture mode became violent in both irradiated and un-irradiated specimens. The fracture mode at test hoop stress of 49 MPa was fissure type. On the other hand, the fracture mode at 196 MPa was a violent type (figure 5).

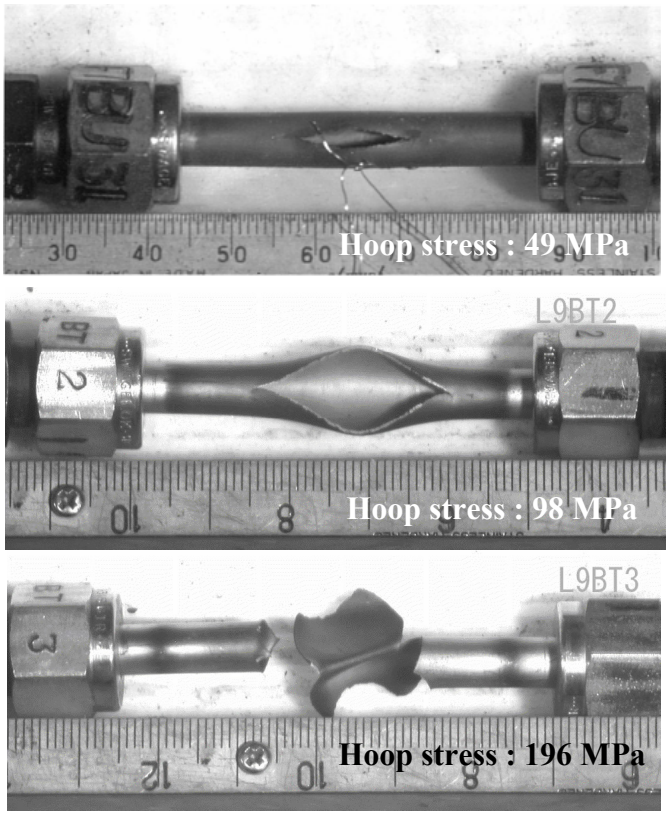

Figure 5 Photos of irradiated specimens after transient burst tests.

CONCLUSIONS

The mechanical behavior of modified 316 stainless steels steel (PNC316) CTs during thermal transients (in the primary peak of LOF events) was investigated. Hoop stress of 49 to 294 MPa at a heating rate of 5 ℃/s were test conditions. The findings are as follows:

(1) There was no difference between the results of irradiated and un-irradiated specimens.
(2) As the hoop stress was higher, the fracture mode became violent.
(3) The failure temperatures decreased monotonically with an increase in hoop stress.
(4) The failure temperatures of irradiated and un-irradiated CTs specimens were within

10% of average measured values at each hoop stress.

(5) The failure temperature of irradiated CTs specimens had no significant changes when compared to the failure temperature of un-irradiated CTs specimens.

The transient burst test techniques may be used to evaluate the deformation behavior of CTs in detail. This will lead to database construction for PIEs and promote CTs material development.

REFERENCES

[1] H.Yamada, Journal of Nuclear Materials 78 (1978), pp.24-32.

[2] I. Shibahara, T. Omori, Y. Sato, S. Onose, and S. Nomura, 16th Effects of Radiation on Materials (ASTM STP 1175, 1993), pp.664.

[3] A. Uehira, S. Mizuta, S. Ukai, R.J. Puigh, Journal of Nuclear Materials 283-287 (2000), pp.396-399.

[4] Y. Yano, T. Yoshitake, S, Yamashita, N. Akasaka, S. Onose, and H. Takahashi, Journal of Nuclear Materials 367-370 (2008), pp.127-131.

5.12 IN-REACTOR FUEL PERFORMANCE EXAMINATION TECHNOLOGY IN KOREA

Jungcheol Shin, Jungtack Kwon and Jaeik Kim

Korea Nuclear Fuel, 493 Duckjin-Dong, Yuseong-Ku, Daejeon 305-353, Korea
jcshin@knfc.co.kr

In order to develop an advanced nuclear fuel, a series of poolside examination (PSE) is needed to confirm in-pile behavior of the fuel for commercial production. For this purpose, KNF has developed a PSE equipment to measure in-reactor fuel performance. In general, PSE is performed a variety of measurements in assembly and single rod state, such as visual inspection, fuel assembly length growth, bowing and twist, rod-to-rod spacing, spacer grid width, fuel rod diameter, and fuel rod oxide thickness at the end of each cycle of irradiation during plant outage periods. After the completion of fuel life, selected rods are extracted from the fuel assembly for individual fuel rod measurement. This paper describes the technologies of PSE and outlines the principles of measurements for it use.

2008 KAERI/JAEA Joint Seminar
on Advanced Irradiation and PIE Technologies
November 5-7, 2008, Daejeon, Korea

FUEL PERFORMANCE EXAMINATION TECHNOLOGY IN KOREA

November 7, 2008

Jung Cheol, Shin

Nuclear Fuel Service Team

CONTENTS

1. Overview of Fuel Performance Examination
2. Scope of Poolside Examination
3. System Architecture of Video Imaging Processing
   3.1 FA Length and Grid Altitude Measurement
   3.2 Shoulder Gap Measurement
   3.3 Fuel Rod-to-Rod Gap Measurement
   3.4 FA Bowing Measurement
   3.5 FA Twist Measurement
4. Spacer Grid Width Measurement
5. Fuel Rod Diameter Measurement
6. Fuel Rod Oxide Layer Thickness Measurement
7. Single Fuel Rod Measurement

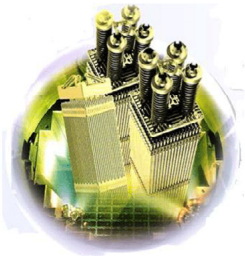

Overview of Fuel Performance Examination

- Verification of In-Reactor Fuel Performance for Confirmation of Design Criteria
- Evaluation of Fuel Design Modes & Codes for Development of Advanced Fuels
- Development of New Fuel Design using Database of Fuel Performance

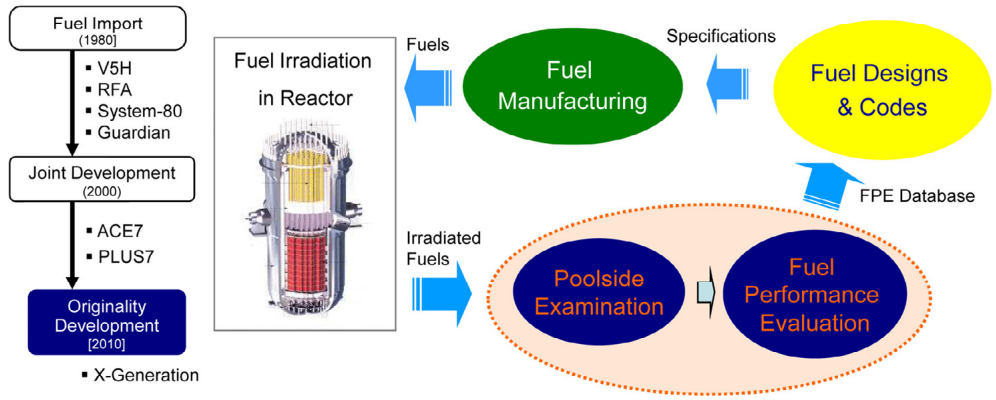

[Development of Fuel in Korea]

※Essential Technique of New Advanced Nuclear Fuel Development

Scope of Poolside Examination

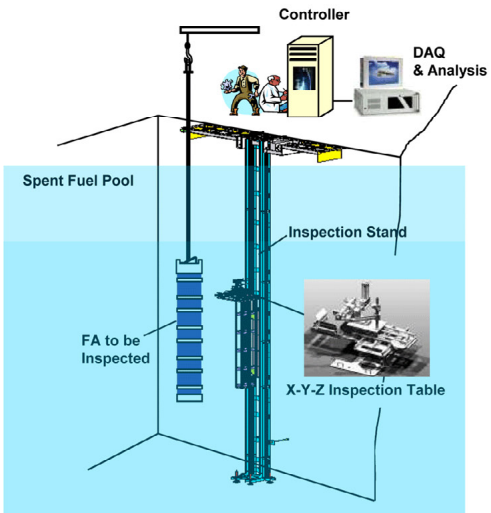

[Layout of Poolside Examination]

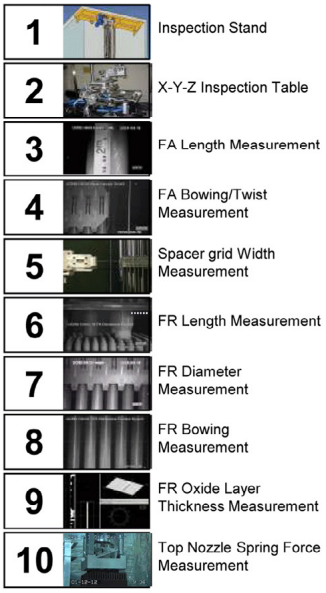

System Architecture of Video Imaging Processing

Assembly Dimensional Measurement System using Video Image Processing

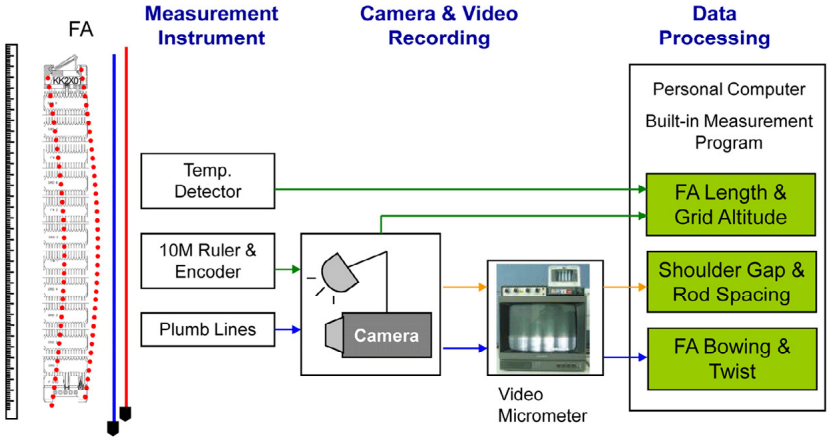

Shoulder Gap Measurement

Fuel Rod Growth is induced from Shoulder Gap Measurement.

The thickness of the top nozzle adapter plate is measured as reference value in number of pixels by video micrometer, and compared by the as-built data.

The shoulder gap is detected successively between the two positions of horizontal lines generated by the video micrometer.

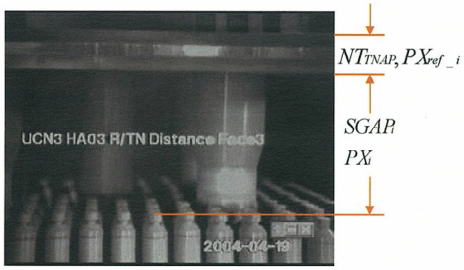

- Shoulder Gap corresponding to the rod #i is given by

$$SGAP_i = NT_{TNAP} \frac{PX_i}{PX_{ref\_i}}$$

- Estimated Accuracy : ±0.5㎜
- Test Result

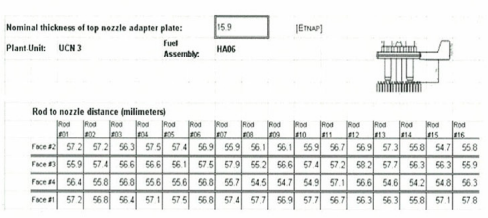

Shoulder Gap Measurement

Fuel Rod Growth is induced from Shoulder Gap Measurement.

The thickness of the top nozzle adapter plate is measured as reference value in number of pixels by video micrometer, and compared by the as-built data.

The shoulder gap is detected successively between the two positions of horizontal lines generated by the video micrometer.

- Shoulder Gap corresponding to the rod #i is given by

$$SGAP_i = NT_{TNAP} \frac{PX_i}{PX_{ref\_i}}$$

- Estimated Accuracy : ±0.5㎜
- Test Result

Nominal thickness of top nozzle adapter plate: 15.9 [ETNAP]

Plant Unit: UCN 3 Fuel Assembly: HA06

Rod to nozzle distance (millimeters)

	Rod #01	Rod #02	Rod #03	Rod #04	Rod #05	Rod #06	Rod #07	Rod #08	Rod #09	Rod #10	Rod #11	Rod #12	Rod #13	Rod #14	Rod #15	Rod #16
Face #2	57.2	57.2	56.3	57.5	57.4	56.9	55.9	56.1	56.1	55.9	56.7	56.9	57.3	55.8	54.7	55.8
Face #3	55.9	57.4	56.6	56.6	56.1	57.5	57.9	55.2	56.6	57.4	57.2	58.2	57.7	56.3	56.3	55.9
Face #4	56.4	55.8	56.8	55.6	55.6	56.8	56.7	54.5	54.7	54.9	57.1	56.6	54.6	54.2	54.8	56.3
Face #1	57.2	56.8	56.4	57.1	57.5	56.8	57.4	57.7	56.9	57.7	56.7	56.3	56.3	55.8	57.1	57.8

Fuel Rod-to-Rod Gap Measurement

Rod-to-rod spacing is measured to identify fuel rod bowing.

The nominal outer diameter of a rod is denoted the reference value in rod spacing measurement.

The rod spacing is difference between the two positions of the vertical line generated by the video micrometer and, if necessary, the correction of image tilt is applied by the measurement program.

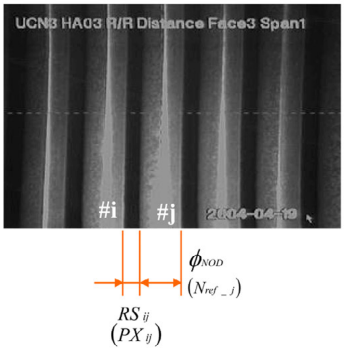

- The rod-to-rod gap between rod #i and #j is given by

$$RS_{ij} = \phi_{NOD} \frac{PX_{ij}}{PX_{ref\_j}}$$

- Estimated Accuracy : ±0.1㎜
- Test Result

Plant Unit: UCN 3 Fuel Assembly: HA06

Rod to rod spacing (millimeters) after operating correction

Face #1	Rod #01 → Rod #02	Rod #02 → Rod #03	Rod #03 → Rod #04	Rod #04 → Rod #05	Rod #05 → Rod #06	Rod #06 → Rod #07	Rod #07 → Rod #08	Rod #08 → Rod #09	Rod #09 → Rod #10	Rod #10 → Rod #11	Rod #11 → Rod #12	Rod #12 → Rod #13	Rod #13 → Rod #14	Rod #14 → Rod #15	Rod #15 → Rod #16	average	min
Span #10	3.3	3.2	3.4	3.3	3.2	3.3	3.3	3.4	3.3	3.2	3.3	3.3	3.4	3.2	3.3	3.30	3.16
Span #9	3.4	3.4	3.3	3.6	3.4	3.5	3.4	3.5	3.4	3.7	3.5	3.6	3.5	3.6	3.6	3.50	3.26
Span #8	3.6	3.5	3.5	3.4	3.4	3.5	3.5	3.5	3.4	3.3	3.3	3.4	3.4	3.4	3.2	3.43	3.21
Span #7	3.5	3.6	3.6	3.7	3.4	3.6	3.5	3.6	3.6	3.5	3.7	3.5	3.6	3.5	3.5	3.56	3.44
Span #6	3.6	3.6	3.4	3.5	3.6	3.5	3.5	3.5	3.5	3.4	3.4	3.5	3.2	3.3	3.3	3.45	3.22
Span #5	3.3	3.4	3.4	3.4	3.4	3.5	3.5	3.5	3.3	3.4	3.4	3.5	3.3	3.5	3.3	3.40	3.27
Span #4	3.3	3.5	3.4	3.4	3.2	3.5	3.2	3.3	3.2	3.2	3.1	3.1	3.2	3.2	3.1	3.27	3.11
Span #3	3.3	3.5	3.4	3.2	3.4	3.3	3.5	3.5	3.4	3.1	3.3	3.4	3.4	3.4	3.3	3.35	3.12
Span #2	3.1	3.1	3.2	3.3	3.2	3.3	3.0	3.3	3.3	3.1	3.2	3.3	3.0	3.1	2.7	3.14	2.74
Span #1	3.2	3.2	3.1	3.1	3.2	3.1	3.2	3.2	3.1	3.0	3.0	2.9	3.2	2.9	3.2	3.10	2.85
															min		2.74

FA Bowing Measurement

The assembly bowing is defined as the deviation of the assembly centerline from the line between top and bottom nozzle.

The plumb line is approached to the right face of the assembly. The camera is moved with the elevator to detect the right edge of the grid and the close plumb line.

In case the assembly is bowed, some different distances of the plumb line to the assembly are measured by means of the camera and video micrometer.

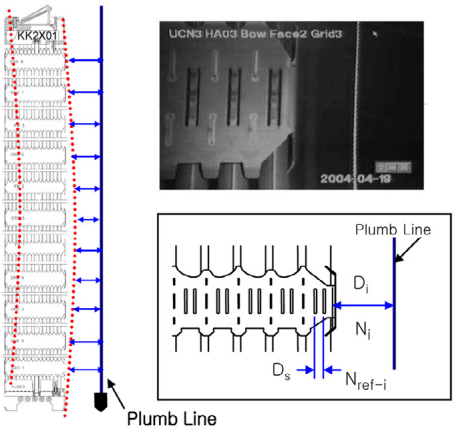

- The distance from the edge of the grid #i to the vertical line is

$$D_i = \frac{N_i}{N_{ref-i}} D_s$$

- Estimated Accuracy : ±0.5㎜
- Test Result

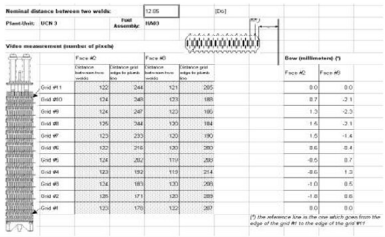

FA Twist Measurement

The assembly twist is defined as torsion of the different assembly cross sections against the top or bottom nozzle.

Before the twist measurement, the calibration is conducted to set the angle corresponding to the graduation read on the horizontal ruler at the specified distance.

Then the camera is shifted, while recording the image, along axis X at low speed until it moves past the two plumb lines and the latter converge. Repeat the operation for the bottom nozzle.

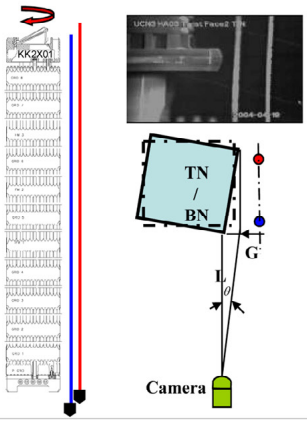

- The angle corresponding to the graduation read is

$$\theta_i = \frac{180}{\pi} arctg \left[\frac{G_i - \frac{G_{11} + G_1}{2}}{L} \right]$$

- Estimated Accuracy : ±0.5°
- Test Result

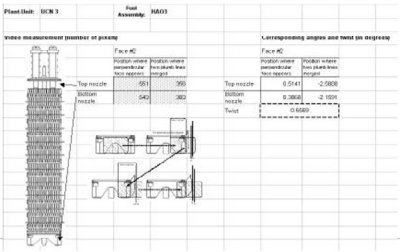

Spacer Grid Width Measurement

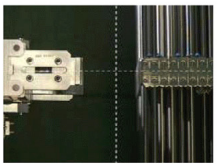

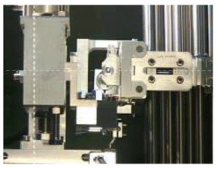

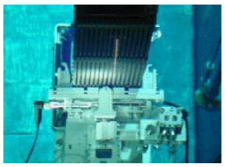

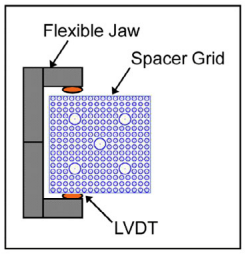

Spacer width is measured to identify an amount of transversal irradiation growth of a fuel using a linear variable differential transformer (LVDT)-based system that measures the distance between two jaws positioned on each side of the measured grid.

- Estimated Accuracy : ±0.15㎜

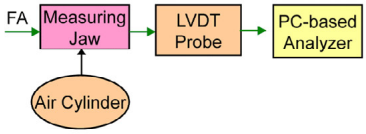

[System Diagram]

Fuel Rod Diameter Measurement

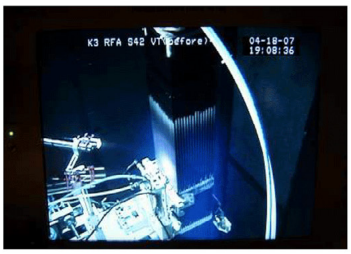

The continuous axial diameter of peripheral fuel rods in a fuel assembly is measured by LVDT which is made up of two fingers between adjacent pairs of spacers.

A calibration rod with different rod diameters is used to calibrate the system.

- Estimated Accuracy : ±10㎛

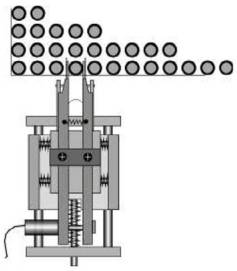

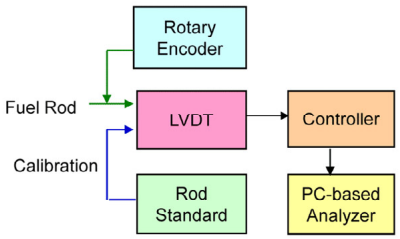

[System Diagram]

Fuel Rod Oxide Layer Thickness Measurement

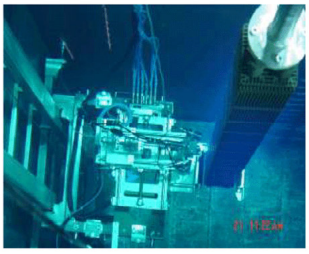

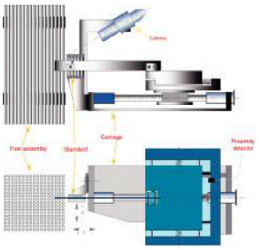

Oxide layer thickness is measured in order to verify oxide and corrosion behavior during operation.

The equipment consists of an eddy current probe mounted on the X-Y table, an eddy current measuring instrument unit, and a computer-based data acquisition system.

To measure the oxide thickness of interior rods without fuel rod removal from an assembly, the eddy current probe is sufficiently thin permitting pass through into the channels between rods.

▪ Estimated Accuracy : ±5.0㎛

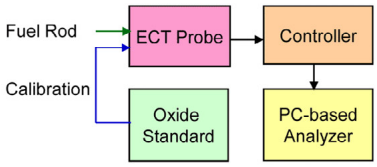

[System Diagram]

Single Fuel Rod Measurement

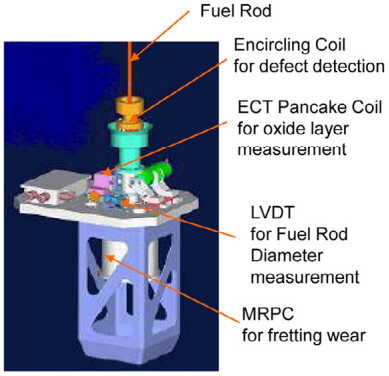

For the single rod measurement, selected rods are extracted from the fuel assembly, after removing the top or bottom nozzle from the assembly.

The equipment consists of three types of eddy current coils, a pair of LVDT, an encoder and camera. In order to be able to identify the position of possible defects, an encoder is applied with roller that runs along the rod during the measurement.

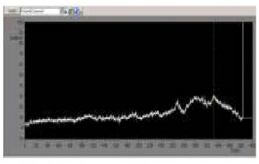

[Oxide Layer Measurement]

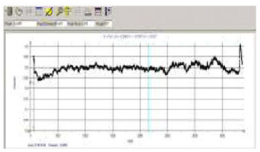

[Rod Diameter Measurement]

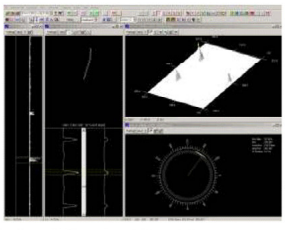

[Defect & Fretting Wear Measurement]

THANK YOU !!!

KNF

5.13 PERFORMANCE EVALUATION OF LARGE U-Mo PARTICLE DISPERSED FUEL IRRADIATED IN HANARO

Ho Jin Ryu, Jong Man Park, Seok Jin Oh, Se Jung Jang, Byung Ok Yu, Choong Seong Lee, Chul Gyo Seo, Hee Taek Chae, Chang Kyu Kim

Advanced Research Reactor Fuel Fabrication, Korea Atomic Energy Research Institute
150 Deokjin-dong, Yuseong-gu, Daejeon 305-353, Korea

U-Mo/Al dispersion fuel is being developed as advanced fuel for research reactors. Irradiation behavior of U-Mo/Al dispersion fuel has been studied to evaluate its fuel performance. One of the performance limiting factors is a chemical interaction between the U-Mo particle and the Al matrix because the thermal conductivity of fuel meat is decreased with the interaction layer growth. In order to overcome the interaction problem, large-sized U-Mo particles were fabricated by controlling the centrifugal atomization conditions.

The fuel performance behavior of U-Mo/Al dispersion fuel was estimated by using empirical models formulated based on the microstructural analyses of the post-irradiation examination (PIE) on U-Mo/Al dispersion fuel irradiated in HANARO reactor. Temperature histories of U-Mo/Al dispersion fuel during irradiation tests were estimated by considering the effect of an interaction layer growth on the thermal conductivity of the fuel meat.

When the fuel performances of the dispersion fuel rods containing U-Mo particles with various sizes were compared, fuel temperature was decreased as the average U-Mo particle size was increases. It was found that the dispersion of a larger U-Mo particle was effective for mitigating the thermal degradation which is associated with an interaction layer growth.

국가 미래 에너지를 책임지는 연구원

Performance Evaluation of Large U-Mo Particle Dispersed Fuel Irradiated in HANARO

Ho Jin Ryu, Jong Man Park, Seok Jin Oh, Se Jung Jang,
Byung Ok Yu, Choong Seong Lee, Chul Gyo Seo,
Hee Taek Chae, Chang Kyu Kim

KAERI

KAERI-JAEA Joint Seminar on
Advanced Irradiation and PIE Technologies
Daejeon, Nov. 5-7, 2008

한국원자력연구원
Korea Atomic Energy Research Institute

Research Reactor Fuel

한국원자력연구원
Korea Atomic Energy Research Institute

- HEU fuel (~93wt%)
  - U_3O_8/Al dispersion fuel: 1.3 gU/cm^3 (18 vol.%)
    - *HFIR (ORNL, 85 MW)*
  - UAl_x/Al dispersion fuel: 1.0~1.6 gU/cm^3 (37 vol.%)
    - *ATR (INL, 250 MW)*

- LEU fuel (<20wt%)
  - U_3Si_2/Al dispersion fuel: 4.8 gU/cm^3
    - *HFR, OPAL, OSIRIS, JMTR*
  - U_3Si/Al dispersion fuel: 3.15gU/cm^3
    - *HANARO*

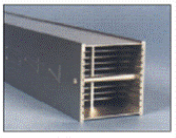

- Advanced fuel (high uranium density ~8gU/cm^3)
  - U-Mo/Al dispersion fuel
  - Qualification (RERTR Program): ~2011

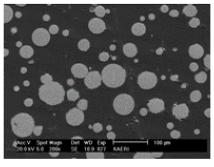

Dispersion Fuel Performance

한국원자력연구원 Korea Atomic Energy Research Institute

- Low U-density fuel: 75~150°C
  - Maintain BOL structures and properties
- High U-density fuel: high temperature operation
  - Significant interdiffusion reaction between U-Mo and Al
- Interaction Layer➔ $(U,Mo)Al_3$ ~$(U,Mo)Al_7$
  - Low conductivity (7~15 W/mK)➔ fuel temperature increase
  - Low density ➔ fuel volume expansion

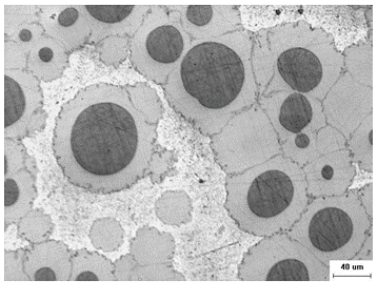

Microstructure of Irradiated U-7Mo/Al

Thermal behavior of U-Mo/Al dispersion fuel should be evaluated.

HANARO Fuel

한국원자력연구원 Korea Atomic Energy Research Institute

- Rod-type dispersion fuel (6.35mm in diameter)
  - U_3Si/Al dispersion fuel: 3.15gU/cm^3
- Heat transport of rod-type dispersion fuel
  - inferior to plate-type fuel (large ΔT)
  - sensitive to thermal conductivity changes

Performance evaluation for U-Mo/Al dispersion fuel is necessary.

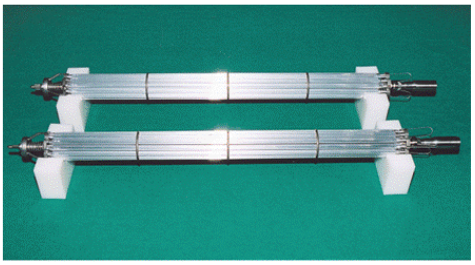

KOMO Irradiation Tests (HANARO)

한국원자력연구원 Korea Atomic Energy Research Institute

	Fuel Composition	Fuel Particle Size(μm)	Matrix	U-loading (g-U/cc)	Max. LP (kW/m)	Max. BOL T. (°C)	Max. BU (at%U^{235})	Status
KOMO-1	U-7Mo U-9Mo	<150	Al 1050	3.4 and 6.0	112	276	~13	Irr. Stopped (Fuel Failure) 2001.7~8
KOMO-2	U-7Mo U-9Mo	mostly <150	Al 1050	4.0 and 4.5	108	196	68	Irr. Test + PIE Completed 2002.1-2003.1
KOMO-3	U-7Mo U-7Mo-1Zr U-7Mo-0.2Si	105-210 210-300 300-425	Al 1050 Al-0.4Si Al-2Si	4.5	95	181	66	Irr. Test Completed 2006.2-2007.7 PIE in Progress
KOMO-4	U-7Mo U-7Mo-1Zr U-7Mo-1Ti	Mostly 210-300	Al 1050 Al-2Si Al-5Si Al-8Si	4.5 and 5.0	110	200	~40	Planned in 2008

Analysis Procedures

한국원자력연구원 Korea Atomic Energy Research Institute

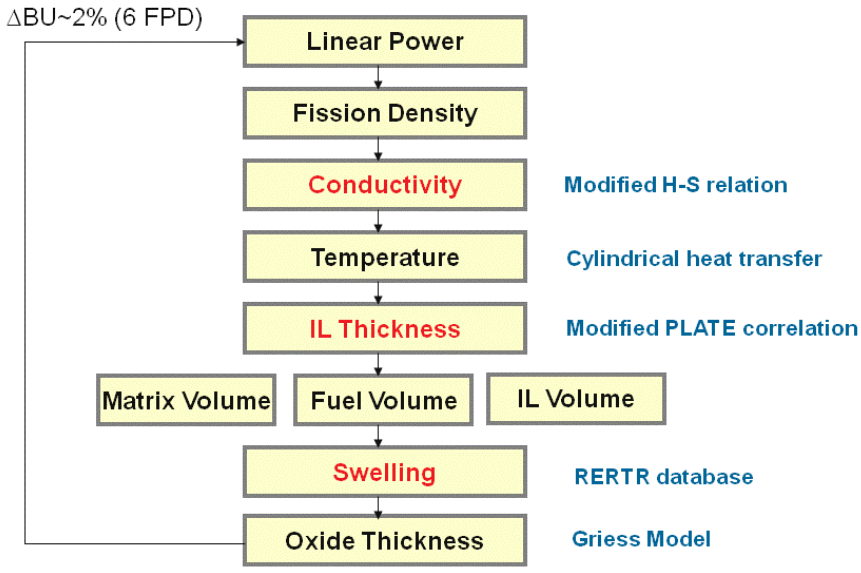

Interaction Layer Growth

한국원자력연구원 Korea Atomic Energy Research Institute

$$Y^2 = A \cdot f_r^{1/2} \exp\left(-\frac{Q}{RT}\right) t$$

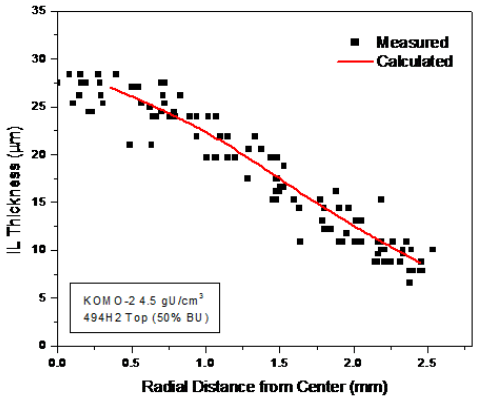

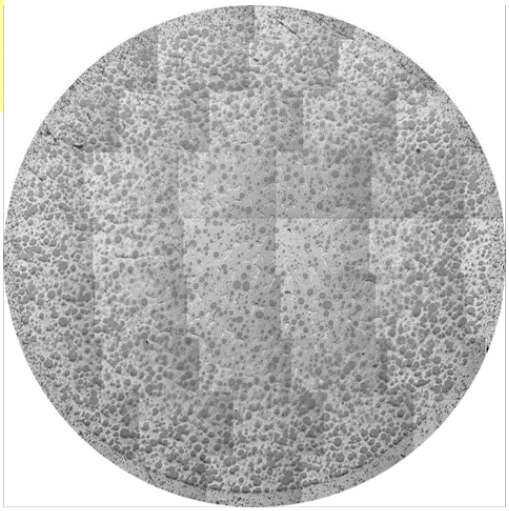

Microstructure from KOMO-2 PIE (U-7Mo/Al)

Effects of U-Mo Particle Size

한국원자력연구원 Korea Atomic Energy Research Institute

Fuel Centerline Temperature

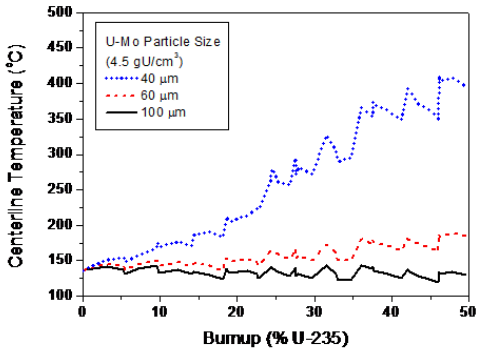

Interaction Layer Thickness

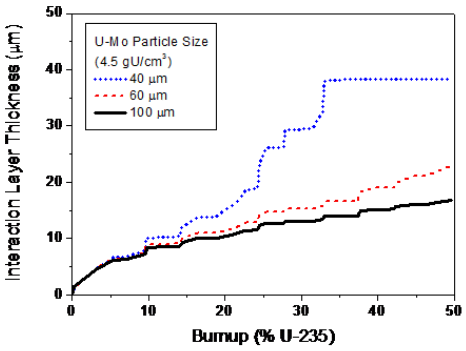

- Fuel temperature decreases with U-Mo particle size
- Interaction layer thickness decreases with U-Mo particle size

PIE (U-Mo Particle Size Effect)

한국원자력연구원 Korea Atomic Energy Research Institute

- Fine U-Mo particle: active interaction
- Coarse U-Mo particle: less interaction

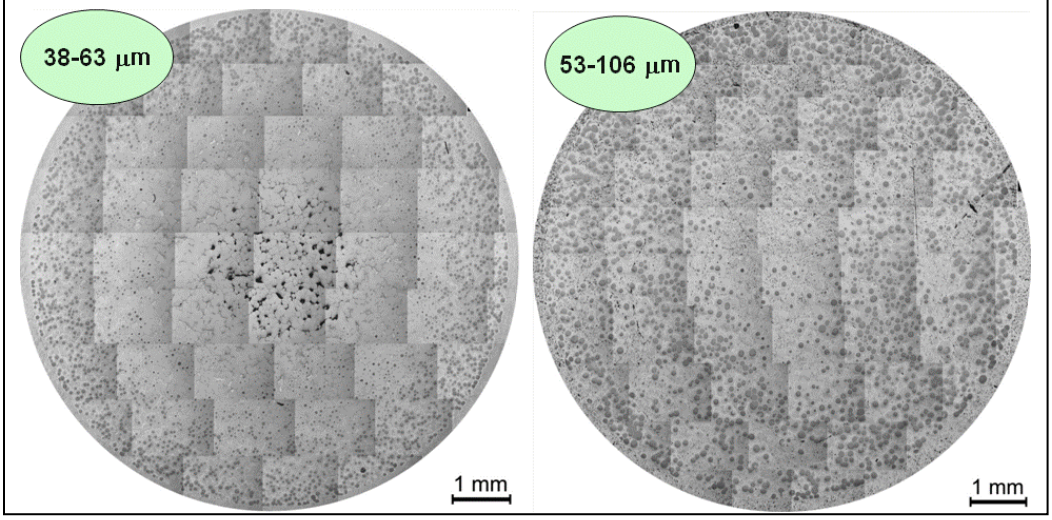

Large U-Mo Particle

한국원자력연구원 Korea Atomic Energy Research Institute

- KAERI has developed large-sized atomized particles: 150~760 μm
- Larger than 200 μm is used for KOMO-3 test

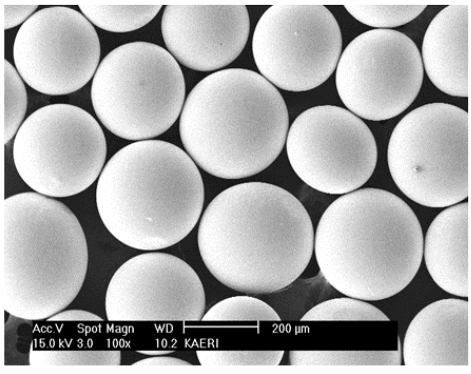

Atomized U-Mo Powder

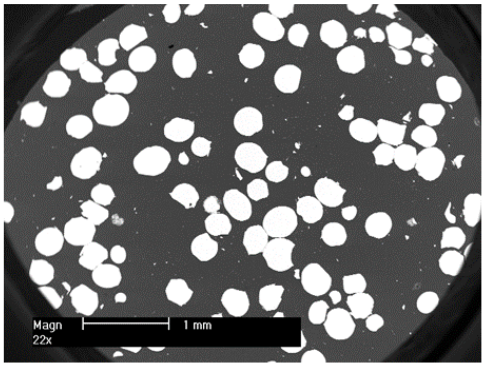

U-Mo/Al Dispersion Fuel

PIE of KOMO-3 (Size Effect)

한국원자력연구원 Korea Atomic Energy Research Institute

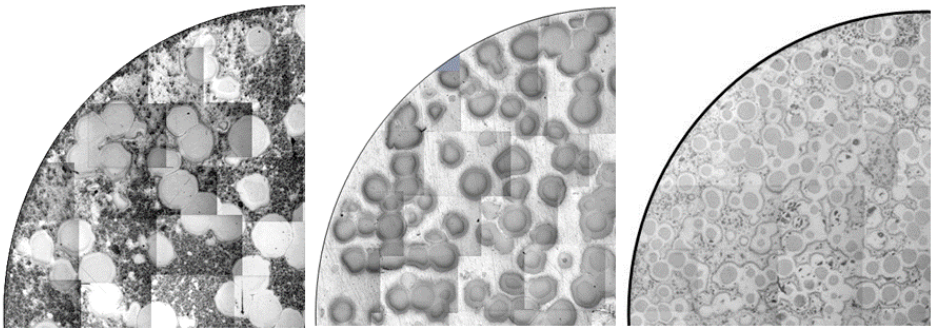

U-7Mo/Al(4.5gU/cc)
300-425 μm
ΔV/V = 10.6%
LP = 98.5 kW/m
T_{max}(BOL) = 181°C
BU = 64.8 at%

U-7Mo/Al(4.5gU/cc)
210-300 μm
ΔV/V = 10.4%
LP = 90.3 kW/m
T_{max}(BOL) = 170°C
BU = 63.2 at%

U-7Mo/Al(4.5gU/cc)
105-210 μm
ΔV/V = 12.0%
LP = 94.0 kW/m
T_{max}(BOL) = 175°C
BU = 63.9 at%

PIE Results of KOMO-3

한국원자력연구원 Korea Atomic Energy Research Institute

Interaction Layer Thickness

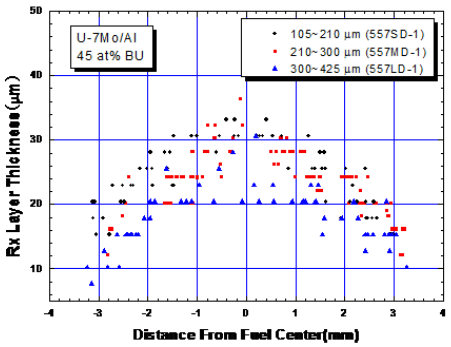

Fuel Meat Swelling

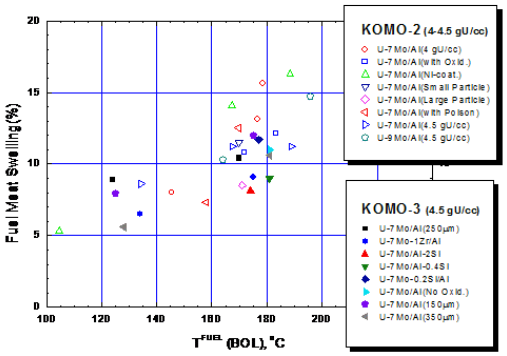

- Larger U-Mo particle showed thinner interaction layer
- KOMO-3 fuel showed less swelling that KOMO-2 fuel because of smaller IL fractions.

Volume Fraction and Temperature

한국원자력연구원 Korea Atomic Energy Research Institute

Volume Fraction

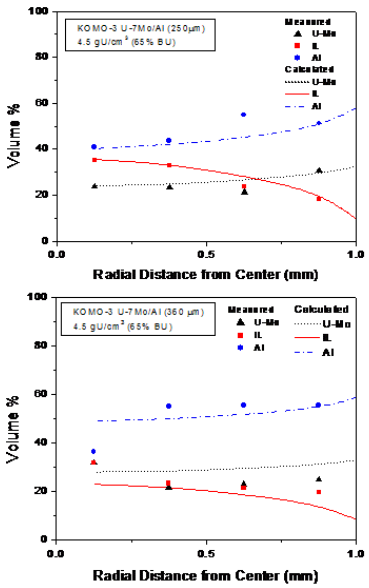

Fuel Temperature History

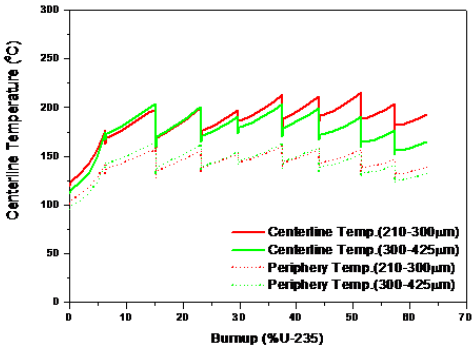

- Prediction model for rod-type fuel (Ryu, NET 2008)
- Larger U-Mo particle dispersion fuel showed lower fuel temperature ➔ lower interaction

Conclusions

한국원자력연구원 Korea Atomic Energy Research Institute

◆ Performance evaluation of U-Mo/Al dispersion fuel showed that the fuel temperature is a strong function of U-Mo particle size

◆ U-Mo/Al fuel containing a large-sized U-Mo particle powder (210-300μm) in KOMO-3

➢ *smaller IL interface fraction than the KOMO-2 appears to affect advantageous irradiation performance by reducing fuel temperatures*

→ *Use of large-sized U-Mo particles is a promising method to solve the interaction problem in dispersion fuel*

5.14 BURNUP DETERMINATION OF A HIGH BURNUP PWR FUEL BY NEODYMIUM AND CESIUM ISOTOPE MONITOR METHODS BASED ON ISOTOPE DILUTION MASS SPECTROMETRIC MEASUREMENTS

Jungsuk Kim, Youngshin Jeon, Soondal Park, Sunho Han, Yeongkeong Ha and Kyuseok Song

Nuclear Chemistry Research Division, Korea Atomic Energy Research Institute
150 Deokjin-dong, Yuseong-gu, Daejeon 305-353, Korea
njskim1@kaeri.re.kr, ysjeon@kaeri.re.kr, nsdpark@kaeri.re.kr, hansh@kaeri.re.kr, nykha@kaeri.re.kr and sks@kaeri.re.kr

ABSTRACT

Destructive methods were used for the burnup determination of a PWR nuclear fuel irradiated to a high burnup in power reactors. The total burnup was determined from a measurement of the Nd and Cs isotope burnup monitors. The methods included U, Pu, ^{148}Nd, ^{145}Nd+^{146}Nd, total of the Nd isotopes, and ^{133}Cs and ^{137}Cs determinations by the isotope dilution mass spectrometric method (IDMS) by using quadrupole spikes (^{233}U, ^{242}Pu, ^{150}Nd and ^{133}Cs). The methods involved two sequential anion exchange resin (AG 1X8 and 1X4) separation procedures and a Cs purification with a cation exchange resin (AG 50WX4) separation procedure. The effective fission yield was calculated from the weighted fission yields averaged over the irradiation period. The results obtained by the Nd and Cs isotopes from the mass spectrometric measurement were compared with those by the ORIGEN code.

INTRODUCTION

The burnup of important fissile isotopes and the composition of an irradiated fuel depend on the nature of the fuel and on the conditions of an irradiation. A detailed knowledge of these

quantities is useful for reactor work as well as for the effective utilization of a nuclear fuel. Various methods have been developed to measure a burnup both by non-destructive and destructive techniques. Destructive method, which is based on the determination of specific nuclides, e.g. U, Pu and ^{148}Nd (or ^{137}Cs) by a chemical analysis after an appropriate separation of the heavy elements and a monitoring of the fission product, is widely used as a reference method to measure the burnup of a spent fuel[1-3]. A mass spectrometric isotope dilution analysis of ^{137}Cs with ^{133}Cs as an isotopic diluent would overcome a ^{134}Cs interference[4]. All the isotopic compositions for the fission product Cs involving the stable ^{133}Cs, and radioactive ^{134}Cs, ^{135}Cs and ^{137}Cs can be measured using mass spectrometric techniques. The stable fission product method is almost independent of the irradiation history and as such it is capable of a high overall accuracy. Of the many stable nuclides formed in a fission, Nd satisfys most of the necessary requirements for a good burnup monitor[5].

The aim of the present work is to determine the total burnup by using various Nd and Cs isotope monitors for the same samples from PWR fuels irradiated to a high burnup in power reactors and dry processed fuels irradiated in the Hanaro reactor at KAERI, and to compare the results, so as to determine the respective validity of the methods. In this paper experiments are described for a dissolution of an irradiated fuel sample for a burnup measurement, as well as for a determination of the isotope compositions of U, Pu and the fission products Nd and Cs after their separation by the ion exchange separation techniques from a fuel sample, and a determination of the elements in an irradiated fuel by the isotope dilution mass spectrometric method by using ^{233}U, ^{242}Pu, ^{150}Nd and ^{133}Cs as spikes.

EXPERIMENTAL

Chemicals and instruments

Certified ^{233}U (99.470 atom%) and ^{150}Nd (96.13 atom%) spikes were obtained from Oak Ridge National Laboratory (ORNL). These spike solutions were prepared by dissolving their oxides in 8 M HNO_3-0.01 M HF. Certified ^{242}Pu spike solution (99.9033 atom%, IRMM-044) was obtained from the Institute for Reference Materials and Measurements. The ^{133}Cs spike solution was obtained with monoisotopic standard solutions from Spex Industries Inc.. The concentrations of the spike solutions were prepared by calibrating them with a standard solution. The PWR nuclear fuels used in this work were irradiated to a high burnup in two power reactors, with an enrichment of 4.2 w/o, and then cooled for the post-irradiation analyses. The dry processed fuels were fabricated with a spent PWR fuel which was irradiated in a power reactor, with an enrichment of 3.2 w/o[6]. The isotopic compositions of U, Pu, Nd and Cs separated from the irradiated fuel samples were determined by using a

thermoionization mass spectrometer (TIMS) of the Finnigan MAT 262 type.

Irradiated fuel dissolution, separation and mass spectrometric measurement

Basic processes in the PIE analytical laboratory for the burnup determination are shown in Figure 1. An aliquot of the diluted fuel solution was placed in a capped vial and transferred from the shielded facility into a glove box by a pneumatic transfer system. Chemical separation was carried out for both the unspiked and the spiked sample solutions in the same experimental conditions in a glove box without any heavy shieldings. Two portions were subjected to a determination of the U, Pu, Nd and Cs isotopes in the sample with and without a spike addition followed by the sequential anion and cation exchange separation procedures. Each sample solution of U, Pu, Nd and Cs in the range of μg to ng was loaded onto a triple rhenium filament and then measured. The mass discrimination bias factor and the contribution of natural Nd for all the Nd isotopes measured was corrected[5].

Calculation of the total burnup.

Total burnup by using different Nd and Cs isotope monitors, F_t, was calculated by the following equation (1)[5,7] :

$$F_t = \frac{N/Y}{N/Y + N(U) + N(Pu)} \times 100 \text{ (atom\% fission)} \qquad (1)$$

where N : number of atoms of the monitor Nd or Cs isotope in the irradiated fuel solutions,
Y : effective fission yield of the monitor Nd or Cs isotope from the fissile elements,
N(U), N(Pu) : number of U and Pu atoms in the irradiated fuel solution, respectively
Y value is provided by the average weighted fission yield calculated according to the equations in reference[8].

RESULT AND DISCUSSION

Determination of the isotopic composition.

Isotopic compositions of U, Pu, Nd and Cs in each isolated fraction, followed by the separation procedures, were measured by a thermoionization mass spectrometer. The contributions of various isobars to the Nd and Cs fractions were identified by monitoring the mass peaks from 140 to 149 and from 130 to 138, respectively. After the mass spectrometric

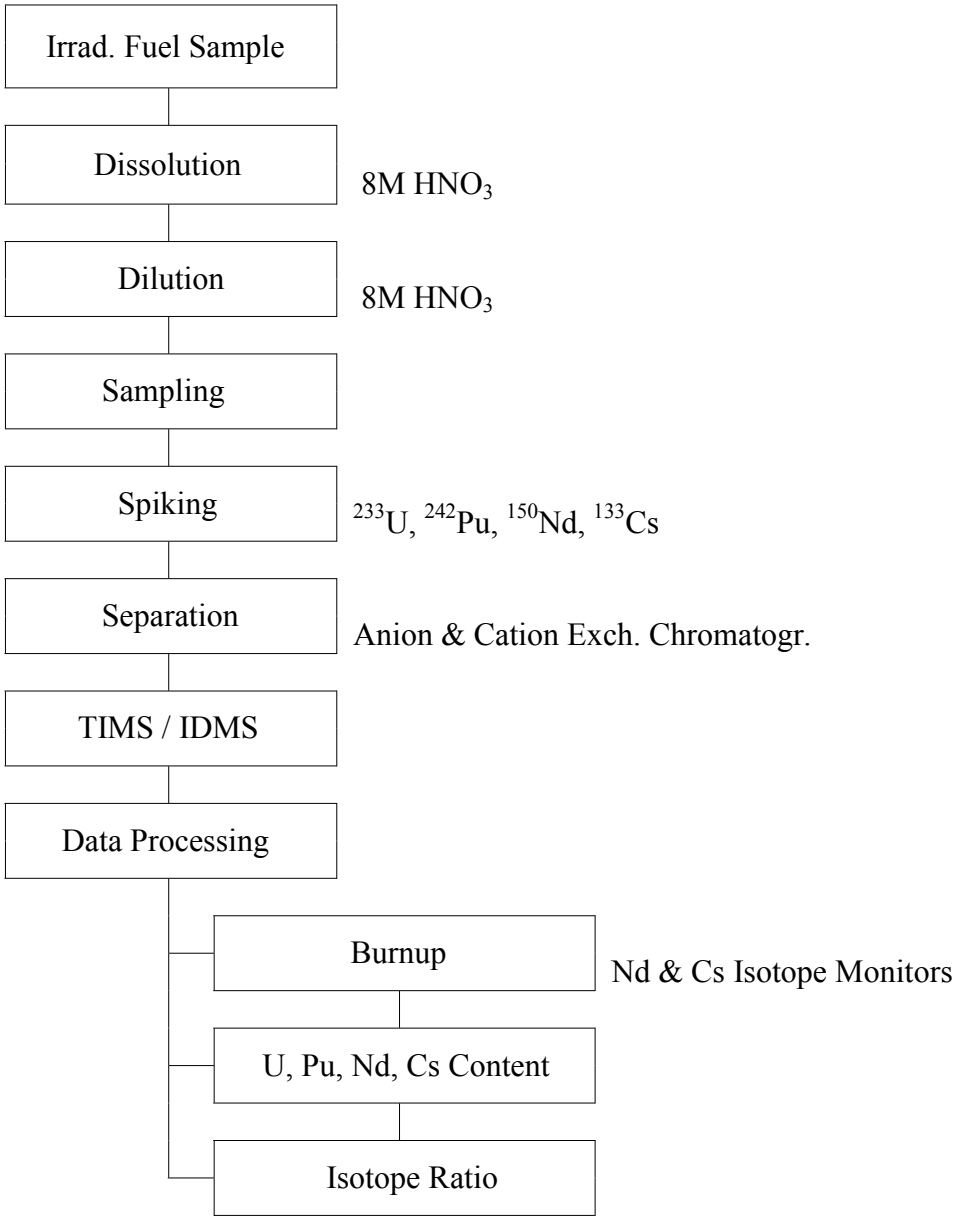

Fig. 1. Basic processes in the PIE analytical laboratory.

measurement of each isolated portion from the spiked and unspiked sample solutions, the concentrations of U, Pu, Nd, and Cs in the sample solutions were determined by the isotope dilution method (IDMS). A major advantage of IDMS is that a quantitative recovery of the elements concerned is not required. Tables 1 and 2 show the isotopic compositions of Nd and Cs in the irradiated fuel samples measured by the TIMS, respectively. Data in the tables show some difference between the two types of fuel samples. Table 3 shows the atomic ratios of $^{134}Cs/^{137}Cs$ and $^{133}Cs/^{137}Cs$ in the high burnup PWR fuel samples measured by a mass

spectrometry. The measured atomic ratios are in good agreement with the calculated ones, which were obtained by correcting the elapsed time for a measurement with the values by the ORIGEN 2 code. On the other hand, the $^{134}Cs/^{137}Cs$ ratios from 0.003 to 0.007 and the $^{133}Cs/^{137}Cs$ ratios from 1.14 to 1.16 in the dry processed fuel samples are lower and higher than those in the high burnup PWR fuel samples, respectively, as determined from the data in Table 2. Table 4 shows the contents of Cs and its isotopes in the high burnup PWR and the dry processed fuel samples determined by IDMS, which were calculated for the date of

Table 1. Isotopic compositions of the neodymium separated from the high burnup PWR and dry processed fuel samples

	Atom%[a)]						
Isotope	K-1	K-2	K-3	D3-1	D4-1	D4-2	D4-3
Nd-143	15.2491	15.6765	18.6918	17.0964	15.7388	13.7360	19.5489
Nd-144	36.9872	36.4770	33.8404	35.3464	36.5292	38.3352	33.2011
Nd-145	15.3062	15.3068	16.1287	16.2364	16.3759	17.8040	17.0812
Nd-146	18.7205	18.7131	17.8392	17.7295	17.6687	17.6099	16.8934
Nd-148	9.2930	9.3249	9.1490	9.0927	9.2356	8.8115	9.0390
Nd-150	4.4440	4.5017	4.3508	4.4986	4.4517	3.7034	4.2364

D4-2 : SIMFUEL

[a)] corrected for contribution due to natural contamination and mass discrimination.

Table 2. Isotopic compositions of the cesium separated from the high burnup PWR and dry processed fuel samples

	Atom%					
Isotope	K-1	K-2	K-3	D3-1	D4-1	D4-3
Cs-133	40.9079	40.4928	41.0620	48.0852	48.2740	50.0186
Cs-134	1.7671	1.6788	1.3819	0.1410	0.3015	0.1318
Cs-135	13.2682	13.7967	15.9399	10.4316	9.0987	6.3566
Cs-137	44.0567	44.0317	41.6162	41.3423	42.3258	43.4930

Table 3. Isotopic ratios of Cs for the high burnup PWR fuel samples

	K-1		K-2		K-3	
Ratio	Meas.	Calc.	Meas.	Calc.	Meas.	Calc.
Cs-134 / Cs-137	0.0401 (1.000)	0.0380 (0.948)	0.0381 (1.000)	0.0379 (0.995)	0.0332 (1.000)	0.0319 (0.961)
Cs-133 / Cs-137	0.9285 (1.000)	0.9352 (1.007)	0.9196 (1.000)	0.9347 (1.016)	0.9867 (1.000)	0.9919 (1.005)

Cs-134 / Cs-137 (Meas. for dry processed fuel) : 0.003 to 0.007
Cs-133 / Cs-137 (Meas. for dry processed fuel) : 1.14 to 1.16
Meas. : measured by mass spectrometric method,
Calc. : corrected for elapsed time to measurement with the calculated values from ORIGEN 2.

Table 4. Quantities of Cs in the high burnup PWR and dry processed fuel samples determined by an isotope dilution mass spectrometry

	Cs(mg)/g-fuel					
Isotope	K-1	K-2	K-3	D3-1	D4-1	D4-3
Cs-133	1.6493	1.6610	1.3847	0.1480	0.2939	0.1362
Cs-134	0.0718	0.0694	0.0470	0.0004	0.0018	0.0004
Cs-135	0.5430	0.5744	0.5456	0.0326	0.0562	0.0176
Cs-137	1.8297	1.8605	1.4456	0.1311	0.2654	0.1220
Total	4.0938	4.1653	3.4229	0.3121	0.6173	0.2762

performance of the experiment. Mass spectrometric isotope dilution analysis of ^{137}Cs with ^{133}Cs as an isotopic diluent would overcome a ^{134}Cs interference for a counting by the gamma spectrometric method. The Cs contents in the high burnup PWR fuel samples are much more than those of the dry processed fuels. It is assumed that semi-volatile elements such as Cs are removed during a refabrication of the dry processed fuels from the spent PWR fuels.

Determination of the total burnup

Walker[9] reported that the variance in the ^{148}Nd isotopic abundance is greater than that of ^{145}Nd+^{146}Nd and even ^{150}Nd, each of which are slightly affected by the neutron capture processes. That is, the calculated number of fissions exceeded the actual number of fissions because of an excess ^{148}Nd being produced from a capture on ^{147}Nd. The magnitude of this error is a function of the flux and fluence. This is especially significant for constant prolonged high flux irradiations. However, a significant fraction of the reactor down time will reduce the magnitude of the capture effect. Another approach is to use a different monitor such as ^{145}Nd+^{146}Nd, because the sum of ^{145}Nd and ^{146}Nd appears to be invariant to the neutron flux and fluence. Table 5 gives the total burnup determined by the Nd isotope monitors, that is, ^{148}Nd, ^{145}Nd+^{146}Nd, and the total of the Nd isotopes, together with the corresponding results calculated by the ORIGEN 2 code for the dry processed fuel samples. The number of fissions by the ^{148}Nd monitor, was calculated with a correction for the excess ^{148}Nd produced from the capture on ^{147}Nd, where the correction factor was calculated on the basis of a continuous reactor operation according to the ASTM E 321-96 standard[5]. The data obtained by using other Nd isotope monitors, ^{145}Nd+^{146}Nd, and the total of the Nd isotopes, are in agreement, to within a deviation of 3.3% of that by the ^{148}Nd monitor. The data calculated by the ORIGEN 2 code is also in good agreement with that by the ^{148}Nd monitor. The use of other Nd isotopes in the determination of the burnup for a nuclear fuel can be used to verify the value obtained for ^{148}Nd. In addition, no additional separation work or mass spectrometric analysis is necessary. The agreement on the number of fissions calculated from the isotopes sensitive to a fuel composition confirms the fissile isotope content.

Table 5. Total burnup determined by the Nd isotope monitor methods for the dry processed fuel samples

	GWD/MTHM			
	Nd-148	Nd-(145+146)	Nd-Total[a)]	Calculated[b)]
D3-1	39.87±1.25 (1.000)	39.70±1.24 (0.996)	40.06±1.25 (1.005)	38.90 (0.976)
D4-1	41.80±1.31 (1.000)	41.66±1.30 (0.997)	41.74±1.30 (0.999)	42.20 (1.010)
D4-2	3.31±0.10 (1.000)	3.26±0.10 (0.987)	3.20±0.10 (0.967)	3.30 (0.997)
D4-3	31.15±0.97 (1.000)	30.81±0.96 (0.989)	31.00±0.97 (0.995)	30.60 (0.982)

a) 143+144+145+146+148+150,
b) calculated from ORIGEN 2.

Table 6. Total burnup determined by the Nd and Cs isotope monitor methods for the high burnup PWR fuel samples

	GWD/MTU				
	Nd-148	Nd-(145+146)	Nd-Total[a)]	Cs-133	Cs-137
K-1	61.20±1.91 (1.000)	59.48±1.86 (0.972)	59.86±1.87 (0.978)	65.51±2.05 (1.070)	66.34±2.07 (1.084)
K-2	61.45±1.92 (1.000)	61.48±1.92 (1.000)	61.20±1.91 (0.996)	62.43±1.95 (1.016)	64.39±2.01 (1.048)
K-3	49.46±1.55 (1.000)	49.39±1.54 (0.999)	49.38±1.54 (0.998)	49.55±1.55 (1.002)	49.99±1.56 (1.011)

a) 143+144+145+146+148+150.

The measured atoms of the radioactive Cs monitor isotopes (^{137}Cs) should be corrected for a decay during and after an irradiation according to the equation in reference [4]. Table 6 shows the total burnup values for the high burnup PWR fuel samples determined by the Nd and Cs isotope monitor methods, which are based on IDMS. From the presented data, it can be seen that the values obtained by the Nd isotope monitors are in very good agreement with each other and show less than a 2.8% variation between them. The results obtained by the ^{133}Cs and ^{137}Cs monitor methods for the K-2 and K-3 samples are in agreement to within a range of 4.8% with those obtained by using ^{148}Nd as a fission monitor. However, the total burnup values obtained by using the Cs isotope monitors for the K-1 sample showed a relative difference of more than 7% with that obtained by the ^{148}Nd monitor method. It is assumed that this error from the radioactive Cs isotopes is attributable to an uncertainty in the physical constants and an inaccurate knowledge of the irradiation history. In our laboratory, the

Gamma (^{137}Cs monitor) spectrometric method for determining a total burnup has been carried out experimentally. This method is based on a non-isolation of ^{137}Cs from a solution of an irradiated fuel and a U determination by IC-ICP-MS (ion chromatography-inductively coupled plasma mass spectrometry), therefore it has been used for a fast determination of a total burnup[2,3]. The IDMS technique by using TIMS will be applied to calibrate the number of ^{137}Cs atoms by the radiometric method. The in-pile decay corrections necessitate an accurate knowledge of the fuel power history.

CONCLUSIONS

The burnup of high burnup PWR and dry processed fuel samples by using Nd and Cs isotope monitors can be determined simultaneously by the isotope dilution mass spectrometric method by using quadrupole spikes. The advantage of considering a whole set of Nd isotopes primarily lies in a confirmation of the value obtained for ^{148}Nd. The number of Cs atoms and their isotopic compositions obtained by the IDMS technique can be used to calibrate those by the radiometric method. The Nd and Cs isotope patterns provide information on the real irradiation characteristics which are necessary for evaluating a fuel's performance in a reactor. A comparison between independently determined burnup values provides a check on the validity of the results

REFERENCES

[1] J. S. Kim, S. H. Han, M. Y. Suh, K. S. Joe, T. Y. Eom, J. Korean Nucl. Soc., 21(4) (1989),p. 277.
[2] J. S. Kim, Y. S. Jeon, K. S. Choi, B. C. Song, S. H. Han, W. H. Kim, J. Korean Nucl. Soc., 33(4) (2001), p. 375..
[3] J. S. Kim, Y. S. Jeon, S. D. Park, B. C. Song, S. H. Han, J. G. Kim, Nucl. Eng. & Technol., 38(3) (2006), p. 301.
[4] Annual Book of ASTM Standards 12.02, E219-80 (Reapproved 1985), (1987), p. 57.
[5] Annual Book of ASTM Standards 12.02, E321-96, (1996).
[6] K. C. Song, M. S. Yang, J. H. Park, et al., KAERI/RR-2543/2005, Korea Atomic Energy Research Institute, (2005).
[7] J. Krtil, F. Sus , A. Hermann, Radiochem. Radioanal. Lett., 48(3-4) (1981), p. 209.
[8] P. De Regge, R. Boden, J. Radioanal. Chem., 35 (1977), p. 173.
[9] W. H. Walker, "Fission Product Data for Thermal Reactors," Atomic Energy of Canada Limited Report AECL-3037, Part 1 and 2, Chalk River Nuclear Laboratory, (1972).

5.15 MICRO GAMMA SCANNING ON THE HIGH BURNUP PWR FUEL SAMPLES

Hyoung-Mun Kwon, Hang-Seog Seo, Hyung-Kwon Lee, Duck-Kee Min, Yong-Bum Chun

Post Irradiation Examination Facility, Korea Atomic Energy Research Institute
1045 Daedeok-daero, Yuseong-gu, Daejeon 305-353, Korea
django@kaeri.re.kr

ABSTRACT

The ratio of Cs-137 and Cs-134 provides important clues about the nuclear fuel burnup. However, Cesium has a tendency to be released from the fuel pellet with increasing burnup and the distribution of Cesium has a bathtub shape along the radial direction of a fuel pellet due to the self-shielding effect in neutron spectrum. The distribution of the radioactive nuclides affects the gamma spectra measuring in the lateral face of a spent fuel rod. That should be corrected in estimating the fuel burnup. This study aims to measure the distribution of nuclides as a preceding work of correcting the burnup estimation for Cs ditribution. In order to measure the radial distribution of Cs-137 and Cs-134, disk type samples were prepared from the PWR spent fuel rods, and the micro gamma scanning was performed on the samples.

INTRODUCTION

A gamma spectroscopy has been used widely as a nondestructive method for evaluating the burnup of PWR spent fuels. For over 15 years, a gamma scanning of disk type samples from spent fuel pellets has been conducted in the Post Irradiation Examination Facility (PIEF) of Korea Atomic Energy Research Institute (KAERI). Cs release has been observed in 3 samples among the results of about 30 samples for 5 years.

The ratio of Cs-137 and Cs-134 measured in the lateral face of a spent fuel rod provides important clues about the nuclear fuel burnup. However, the pellet periphery has relatively higher activity due to the self-shielding effect of a neutron spectrum[1], and also a cesium release occurs by axial migration in the grain boundary porosity range in the central region of a fuel pellet. Cesium behaves similarly to xenon at a temperature above 1200 °C as both are

gaseous. Below 1200 °C, cesium is a relatively immobile liquid and forms a film on grain faces[2].When gamma-ray emitted from a spent fuel rod is measured to estimate the axial burnup, a correction for the self-absorption and the radial distribution of a gamma-ray source should be considered.

This paper aims to measure the distribution of nuclides and to determine the Cs release rate as a preceding work for correcting the burnup estimation for a Cs release and a self-shielding. In order to measure the radial distribution of Cs-137 and Cs-134, disk type samples were prepared from PWR spent fuel rods, and a micro gamma scanning was performed on the samples.

RADIAL DISTRIBUTION OF NUCLIDES

Relative full energy peak efficiency

According to the frequently applied power-law model, the relative full energy peak efficiency for an incoming gamma-ray and its energy can be represented as follows,

$$\varepsilon \propto E^{p}$$

Where ε is the full energy peak efficiency for a gamma-ray of energy E, and p is an empirical constant. The ratio of the energy efficiency for any two gamma-ray lines from two distinct nuclides can be written as

$$\frac{\varepsilon_i}{\varepsilon_j} = \left(\frac{E_i}{E_j}\right)^{p} = \frac{C_i}{C_j}\frac{F_i}{F_j}\frac{\Gamma_j}{\Gamma_i}$$

Where C is the net peak counts, Γ is the gamma decay probability per decay of any nuclide, and F is the cumulative correction factor[3]. The final objective in this study is to find F values in case of the axial gamma scanning. The cumulative correction factor is considered to depend on sample condition and the distribution of a gamma-ray source. This paper shows the fundamental experiment data and MCNP estimation to determine p and F.

Experiment

Axial and radial micro gamma scanning was carried out on a commercial PWR rod, using a high purity Ge detector (HPGe) with each slit of 25.0 mm × 0.5 mm and 0.5 mm × 0.5 mm. Operation of the scanning mechanism and data acquisition and analysis are done by an on-line computer.

The commercial PWR rod for the resent experiment has a rod average burnup, 51.7 GWd/tU. Two samples were taken at the axial upper (sample A) and lower (sample B) regions

corresponding to high and low burnup. The thickness of the specimens of this rod for the section gamma scanning is 3.0 mm and the pellet outer diameter is 8.22 mm. In the radial gamma scanning, the energies of gamma-ray were at 604.721 keV for Cs-134, 661.657 for Cs-137 and 511.8605 keV for Ru-106.

The micro gamma scanning was carried out by two operational modes: Multi-Channel Scaling (MCS) and Multi Channel Analysis (MCA). The MCS acquisition mode is used for applications requiring a measurement of the intensity versus time. The event counting can also be based on analog signals processed by the Single Channel Analyzer (SCA) in the predefined Region of Interest (ROI), which corresponds to the gamma-ray energy band [4]. When a scanning is started, the MCS begins and the sample stage control system is simultaneously operated according to the predefined radial scanning condition. Therefore, the radial position could be substituted for the time of MCS. However, the intensity from the MCS mode is different from the net peak count from the MCA mode, which is proportional to the quantity of the gamma-ray source. It is necessary to correct the intensity for a background count and dead time.

In order to correct the intensity from the MCS mode, it was compared with the net peak count from the MCA mode of the equivalent radial position. Dwell time of each scanning point is 1,500 sec for Cs-134 and Cs-137, and 3,000 sec for Ru-106 in the MCS mode. Spectra of each point were measured in live time 1,000 sec in the MCA mode. In the MCS mode, predefined ROIs were at the 982 ~ 1010 channels for Cs-137, the 902 ~ 925 channels for Cs-134, and the 764 ~ 782 channels for Ru-106.

It appears that the relative standard deviations (RSD) of the MCA and MCS intensity ratios were at around 1.0 % in the case of Cs-137 661.7 keV and Cs-134 604.7 keV. However, Ru-106 presented a relatively higher RSD.

As a result of the intensity correction, the distributions of the net peak count rate for three gamma-ray lines were obtained as shown as figure 1. Cs-release did not occurred in both sample A and B. Ru-106 was used as an indicator of a Cs-release because it has an immobile characteristic at a typical PWR operation temperature.

Cs-134 661.7 keV line has a higher intensity than the Cs-134 604.7 keV line at lower part of the fuel rod, sample A. While on the other, the reverse happened at the upper part of the fuel rod, sample B. It is related with the irradiation condition, cooling time, and half life of the nuclides.

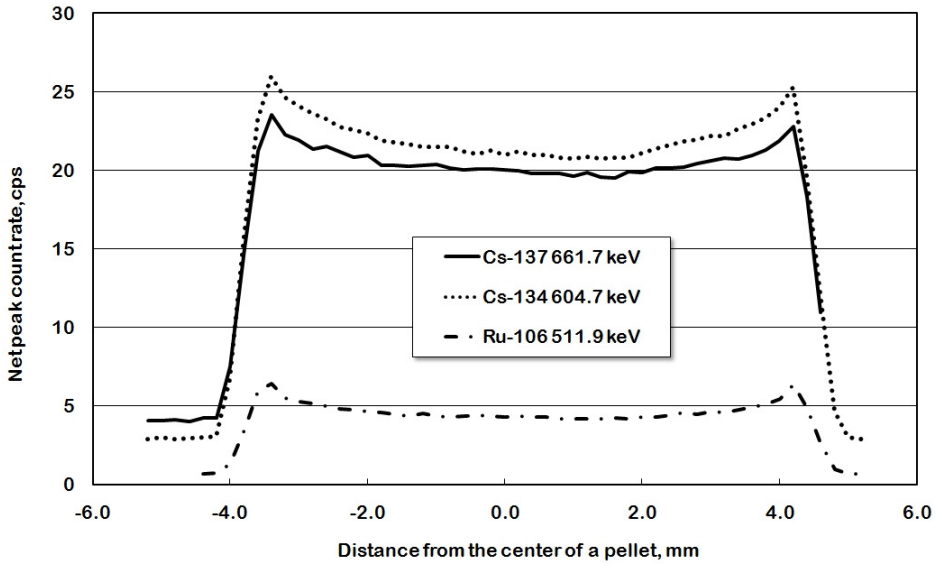

(a) Sample A

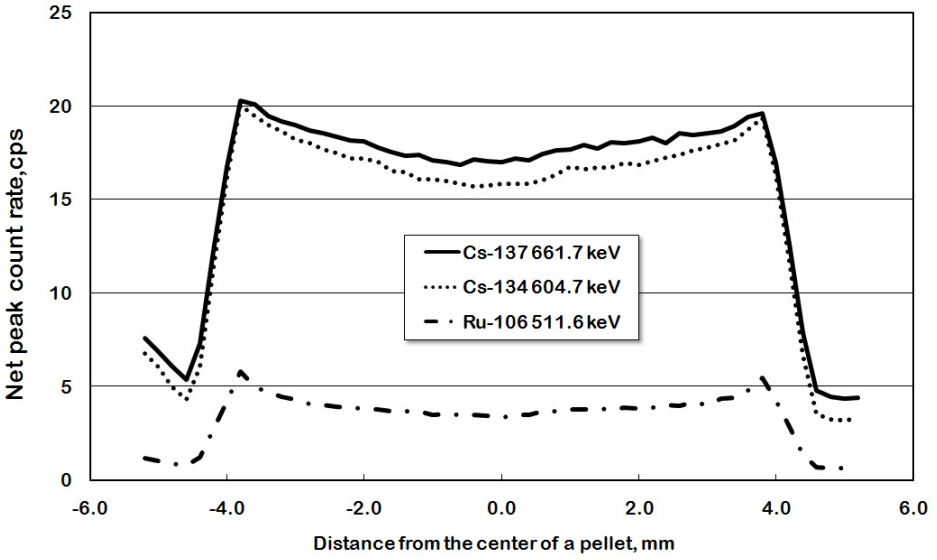

(b) Sample B

Figure 1. Nuclide distributions cross the radial direction of fuel samples

MCNP analysis

MCNP [5] analyses were performed to estimate the effect of gamma ray self-absorption in the source material. Mono-directional source and same intensity of each gamma ray lines were assumed to calculate the cumulative correction factor of the relative efficiency of two gamma rays; 605 keV for Cs-134 and 662 keV for Cs-137. As the result, the self-absorption correction factor ratio of 662 keV per 605 keV was 1.075 in the 3.0 mm disk-shaped source.

CONCLUSIONS

To measure the radial distributions of Cs-137 and Cs-134, a radial gamma scanning was performed on high burnup PWR fuel samples. And a Monte Carlo transport analysis was carried out in order to determine the cumulative correction factor of a radial gamma scanning as a preceding work of correcting the axial burnup estimation for radial Cs distribution.

REFERENCES

[1] Akihiro Sasahara et al., "Neutron and Gamma Ray Source Evaluation of LWR High Burn-up UO2 and MOX Spent Fuels", Journal of Nuclear Science and Technology, 41, 448-456 (2004)
[2] C.T. Walker et al., "Observations on the Release of Cesium from UO2 Fuel", Journal of Nuclear Materials, 240, 32-42 (1996)
[3] Ayman Ibrahim Hawari et al., "High-accuracy Determination of the Relative Full Energy Peak Efficiency Curve of a Coaxial HPGe Detector in the Energy Range 700-1300 keV", Nuclear Instruments and Methods in Physics Research A, 398, 276-286 (1997)
[4] Zbigniew Guzik et al., "TUKAN – An 8K Pulse Height Analyzer and Multi-Channel Scaler With a PCI or a USB Interface", IEEE Transactions on Nuclear Science, 53, 231-235 (2006)
[5] Judith F. Briesmeister, MCNP – A General Monte Carlo N-Particle Transport Code Version 4C (LA-13709-M), Apr. 10, 2000, Oak Ridge National Laboratory

5.16 MODIFIED LASER FLASH THERMAL DIFFUSIVITY MEASUREMENT SYSTEM FOR SHIELDED GLOVE BOX

Daegyu Park, Heemoon Kim, Sangbok Ahn and Wooseok Ryu

PIE & Radwaste Divison
Korea Atomin Energy Research Institute, 150 Dukjin-dong Yusong Daejon Korea
dgpark1@kaeri.re.kr

PIE & Radwaste (Post-Irradiation Examination & Radio-active Waste) division at KAERI(Korea Atomic Energy Research Institute) has carried out post irradiation examinations (PIEs) of the nuclear materials and fuels for the Hanaro reactor, CANDU, PWR and newly developed nuclear fuels. IMEF(Irradiated Material Examination Facility) in PIE & Radwaste division has been developing many kinds of PIE technologies. The thermal conductivity is considered to be one of the most important thermo-physical properties for nuclear fuels and materials. The determination of the thermal conductivity of a nuclear material is accomplished by a measurement of the thermal diffusivity and the use of a defining relation for the diffusivity, specific heat capacity and density. The most widely employed technique is the pulse heating flash. In spite of the many merits in using the pulse heating flash technique, the complexity of the laser flash thermal diffusivity measuring system restricts its use a radioactive environment. Due to a sample's characteristics, the measuring system should be installed in a hot cell or a shielded glove box. Therefore, it is necessary to review, investigate and analyze the related requirement so as to install the measuring system in a hot cell or a shielded glove box. Selected requirement is reflected in the specification of a measuring system and realized requirement is used to solve the related problems.

1

Modified Laser Flash Thermal Diffusivity Measurement System for Shielded Glove Box

2008. 11. 5

Daegyu Park, Heemoon Kim,
Sangbok Ahn, Wooseok Ryu

Contents

2

- Objectives
- Basic Ideas
- Characteristics & System of Laser Flash Method
- Structure & External View of Measuring Parts
- General Requirements of a Apparatus for a Shielded Glove Box & Solutions
- Technical Requirements & Solutions of a Apparatus for a Shielded Glove Box
- Modified Furnace Design
- Modified Sample Holder & Loading Tool
- Modification for Remote control
- Other Modified Items
- Conclusions and Future Plan

2008 KAERI-JAEA Joint Seminar, Nov. 5-7, 2008

Objectives

3

- Final Goals
  - Establishment of thermal diffusivity measurement system for nuclear materials and fuels
    - Modified laser flash thermal diffusivity measurement system for shielded glove box
    - Optimum glove box design and fabrication
    - Movable shielding structure for glove box
    - Specimen cask and adopter
- Interim Goal
  - Modify laser flash thermal diffusivity measurement system for shielded glove box

IMEF KAERI

2008 KAERI-JAEA Joint Seminar, Nov. 5-7, 2008

Basic Ideas

4

- Applying concept for measuring system
  - Measurable for a small specimen owing to the limitation of radio-activities
  - Separable shielding structure from glove box (maintainability, flexibility, low fabrication cost)
  - As small occupation as possible in order to enhance space efficiency
  - High degree of reproducibility and accuracy

IMEF KAERI

2008 KAERI-JAEA Joint Seminar, Nov. 5-7, 2008

Characteristics & System of Laser Flash Method

5

Characteristics

- High degree of reproducibility and accuracy
- Basic simplicity of the method
- The small sample size required
- The rapidity of the measurements
- The ability to use the technique from cryogenic to very high temperature

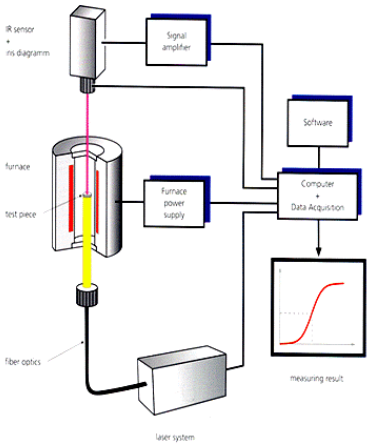

Typical Laser Flash Method Measuring System

Structure & External View of Measuring Parts

6

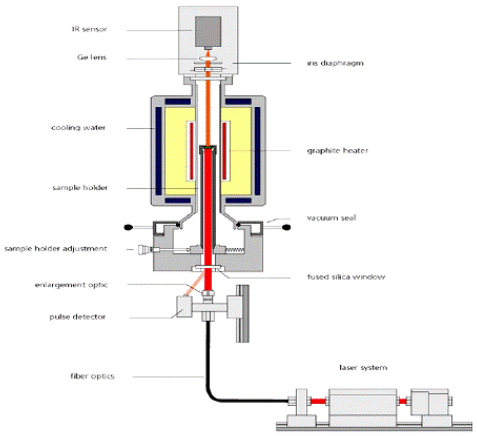

Measuring Parts for Laser Flash Method

External View of Measuring Parts

General Requirements & Solutions of a Apparatus for a Shielded Glove Box

7

Requirement	Practical Solutions
▪ Remote Controllable	▪ Grip, Knob , Manipulator
▪ Good Accessibility and Maintainability	▪ Simple structure design, installation in glove box rather than hot-cell
▪ Durability for Radio-active Radiation	▪ Shielding by lead, selection of proper material
▪ Easy for Decontamination	▪ Proper material, surface treatment
▪ Easy Installation in Hot Cell or Shielded Glove Box	▪ Vertical type design to minimize volume
▪ For Electronic Component to Prevent from Radiation Damage	▪ Shielding by lead, modular type design

Technical Requirements & Solutions of a Apparatus for a Shielded Glove Box (1)

8

- Prevention from a contamination by a exhausted gas :
  Ceramic filter is add
- Sample holder and jig of a small and irregular shape :
  Sample holder and handling tool design
- Available for a vacuum or protective gas use :
  Adopted to furnace design
- Closed cooling water circulation system for furnace :
  Adopted to furnace design
- Non-reaction between a structure material in the furnace and a uranium pellet :
  Use of alumina carrier tube and sample holder

Technical Requirements & Solutions of a Apparatus for a Shielded Glove Box (2)

9

- Tweezers or equivalent measures to handle a small sample :
  Use of existing and air tweezers
- Tool for furnishing LN-2 of the infra-red detector :
  Adoption of LN-2 feeding line
- Convenience of operation and sufficient operation area (e.g. specimen loading, fulfilling LN-2) :
  Applied to glove box design
- Filter selection by considering the period of a replacement, price and capability for filtering a volatile gas (e.g. Cs-137) :
  Ceramic filter

Modified Furnace Design

10

- Available for a vacuum or protective gas use
- Closed cooling water circulation system

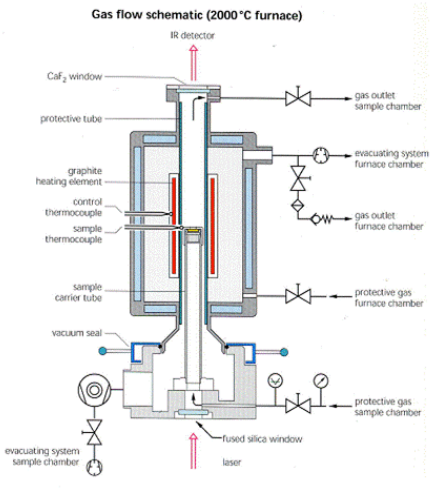

Modified Sample Holder & Loading Tool

11

Size: 12.5mm 9 mm 6 mm

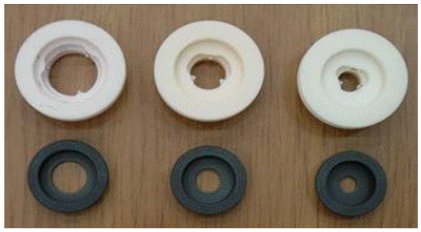

Alumina sample holder

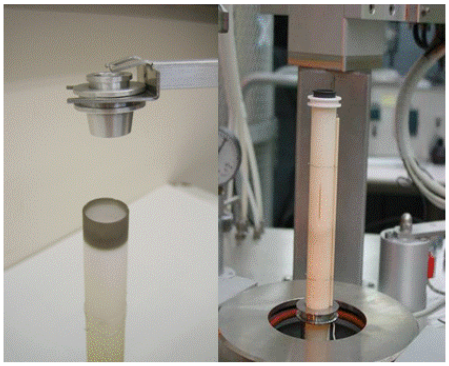

Sample loading tool

IMEF KAERI

2008 KAERI-JAEA Joint Seminar, Nov. 5-7, 2008

Modification for Remote control

12

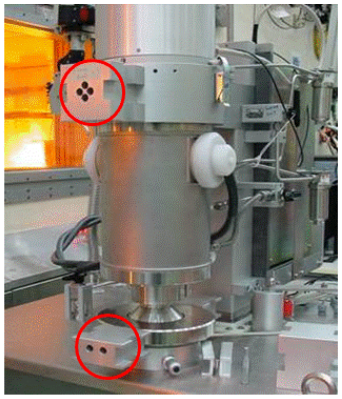

Knob & grip for manipulator

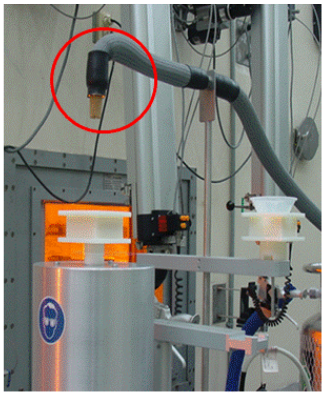

LN-2 furnishing Tool

IMEF KAERI

2008 KAERI-JAEA Joint Seminar, Nov. 5-7, 2008

Other Modified Items

13

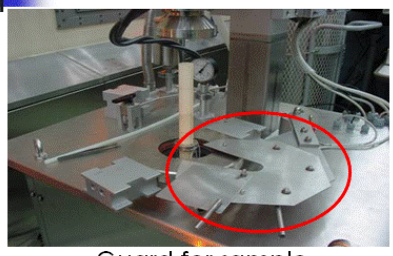

Guard for sample

Lead shielding for I-R detector

Vertical type design

IMEF KAERI

2008 KAERI-JAEA Joint Seminar, Nov. 5-7, 2008

Conclusions and Future Plan

14

- The basic concepts, general and technical requirements of a laser flash thermal diffusivity measuring system are reviewed and analyzed
- Selected requirements are reflected in the specification of measuring system
- Realized requirements are used to solve the related problems
- The measuring part except for data acquisition, laser generating part and control unit of the system will be installed in a shielded glove box in the near future

IMEF KAERI

2008 KAERI-JAEA Joint Seminar, Nov. 5-7, 2008

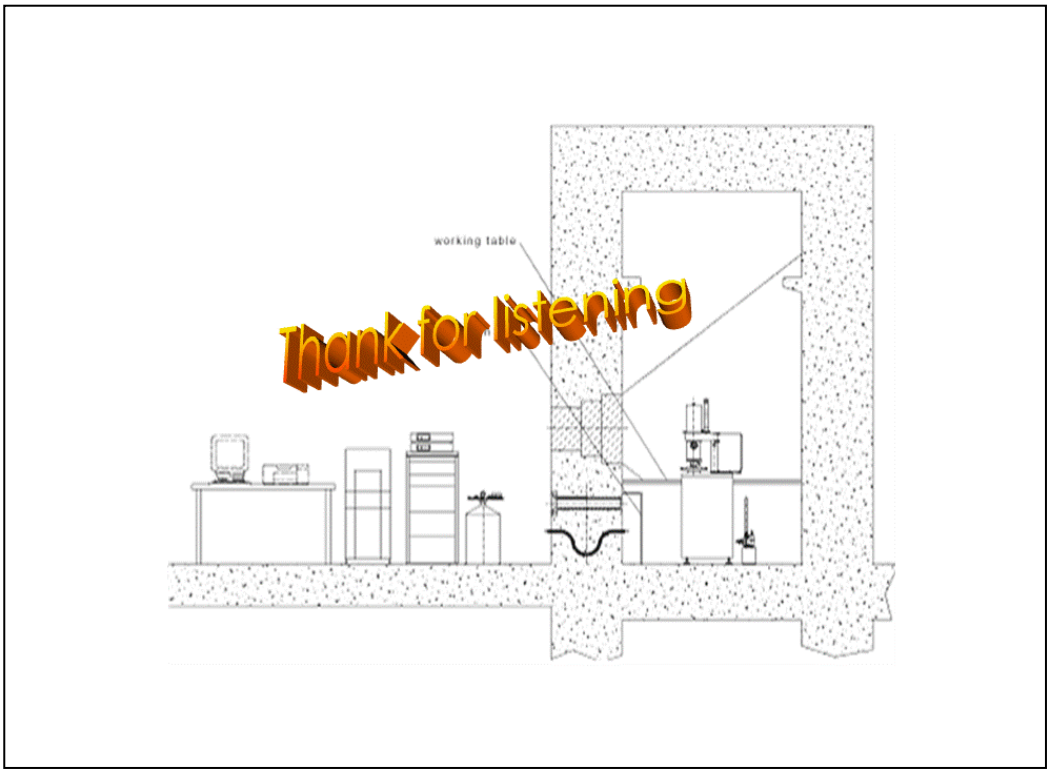
working table
thank for listening

5.17 DEVELOPMENT OF MECHANICAL TEST TECHNIQUES ON THE IRRADIATED GRID ELEMENTS IN PWR FUEL ASSEMBLY

Sangbok Ahn[a], Dosik Kim[a], Seungjai Baik[a], Yongsun Choo[a], Sangyoul Baek[a], Woo-seok Ryu[a]
Dongkeun Ha[b] and Jeongmin Seo[b]

[a]*PIE & Radwaste Division, Korea Atomic Energy Research Institute*
1045 Daedokdaero, Yuseong-gu, Daejon 305-353, Korea
[b]*Nuclear Fuel Development Group, Korea Nuclear Fuel Company*
1047 Daedokdaero, Yuseong-gu, Daejon 305-353, Korea
sbahn@kaeri.re.kr

The mechanical properties of the parts of a nuclear fuel assembly are degraded during the operation of the reactor, through the mechanism of irradiation damage. The properties changes of the parts of the fuel assembly should be quantitatively estimated to ensure the safety of the fuel assembly & rod during the operation. The test techniques developed in this paper are used to produce the irradiation data of the grid 1x1 cell springs, the grid 1x1 cell, the spring on one face of the 1x1 cell, the inner/outer strip of the grid and the welded part. The specimens were irradiated in the CT test hole of HANARO of a 30 MW thermal output at 300℃. From the spring tests of mid grid 1x1 cell and grid plate, the irradiation effects can be examined. The irradiation effects on the irradiation growth also were occurred. The buckling load of mid grid 1x1 cell does not change with a neutron irradiation. From the tensile tests, the strengths increased but the elongations decreased due to an irradiation. The tensile test and microstructure examination of the spot and fillet welded parts are performed for the evaluation of an irradiation effects. Through these tests of components, the essential data on the fuel assembly design could be obtained. These results will be used to update the irradiation behavior databases, to improve the performance of fuel assembly, and to predict the service life of the fuel assembly in a reactor.

Development of Mechanical Test Techniques on Irradiated Grid Elements in a PWR Fuel Assembly

November 6, 2008

Sangbok Ahn, Dosik Kim, Seungjai Baik, Yongsun Choo, Sangyeol Baek and Woo-seok Ryu
Korea Atomic Energy Research Institute

Donggeun Ha, Jeongmin Seo
Korea Nuclear Fuel Company

Korea Atomic Energy Research Institute

2008 KAERI-JAEA Joint Seminar on Advanced Irradiation and PIE Technologies

Contents

I. Introduction

II. Detail Developed Technique List

III. Development Status and Application Results
- Development of Grid 1x1 Cell Spring Test Technique
- Development of Grid 1x1 Cell Buckling Test Technique
- Development of Grid Strip Spring Test Technique
- Development of Tensile Test Technique for Grid Strip Material
- Development of Irradiation Growth Measurement Technique
- Development of Welding Strength Measurement Technique

IV. Concluding Remarks

Korea Atomic Energy Research Institute

I. Introduction

❑ Development trend of PWR nuclear fuel in Korea

Fuel Model	Characteristics	PIE Data Product
WH type, KWU Type		WH, KWU
PLUS-7	- OPR 1000 type reactor - 2002: Complete to develop - 2007: Supply in the commercial reactor	Foreign/Korea
ACE-7	- WH type reactor - 2004: Complete to develop - 2008: Plan to supply in the reactor	Foreign/Korea
Advanced fuel	- Export to the foreign reactors - 2005: Start to develop - 2015: Complete and export	Korea

❑ R&D on the improvement of the PWR fuel reliability in a reactor

- Integrated management system development of fuel reliability
- Development of fuel performance examination technology
- Development of irradiation performance inspection techniques for structural parts

Test techniques are developed to provide PIE data for the newly developing grids and the operated grids in the commercial reactors

Korea Atomic Energy Research Institute

2008 KAERI-JAEA Joint Seminar on Advanced Irradiation and PIE Technologies

❑ Grid View in a PWR Fuel Assembly

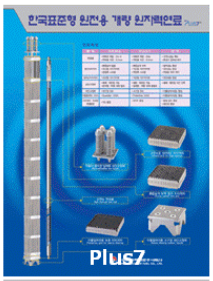

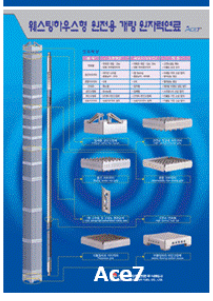

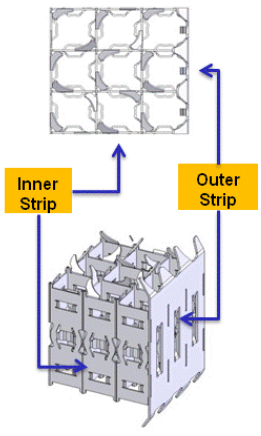

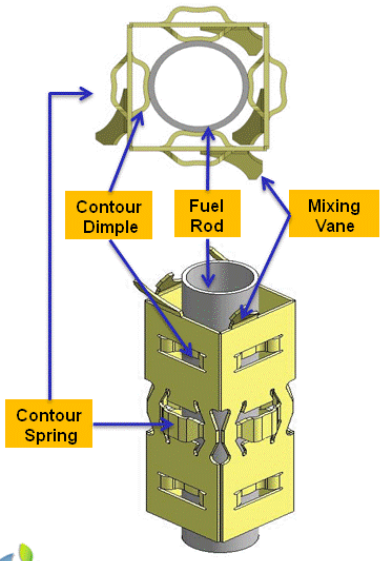

Korea Atomic Energy Research Institute

II. Detail Developed Technique

❑ **Technique characteristics to be developed**

Test Item	Part	PIE Data Product	Remarks
Buckling Test	1x1 Grid Cell	- Buckling load-displacement curve - Buckling load	
Spring Test	1x1 Grid Cell Grid Strip	- Force-Deflection Curve - Plastic deformation amount - Spring Constant(k)	
Tensile Test	Grid Strip	- Load-displacement curve - Strength - Elongation	
Irradiation Growth Measurement	Grid Strip Inconel Material	- Dimension before and after irradiation	
Welding Strength Measurement	Spot Welded Part Butt Welded Part	- Tensile load-displacement curve - Welding strength, elongation	

III. Development and Application of Techniques

❑ **Development of Grid 1x1 Cell Spring Test Technique**

● Shape of grid 1x1 cell

Specimen Shape	Type Dimension
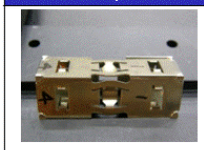	PLUS-7
	Candidate-1
	Candidate-2

● Grip device development

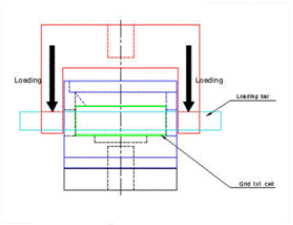

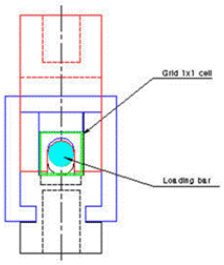

● Application of developed test techniques in a hot cell

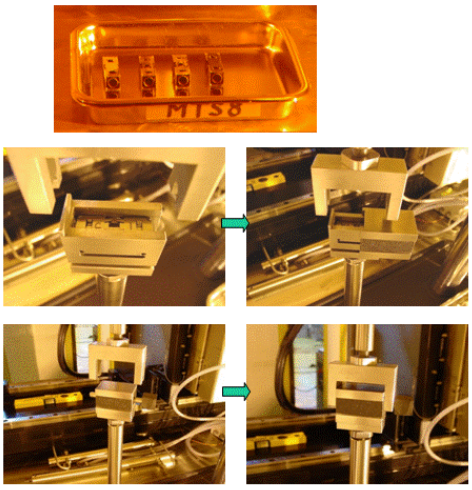

● Example of test results

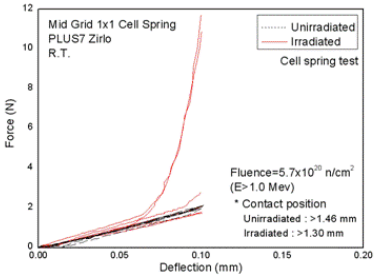

Korea Atomic Energy Research Institute

❑ Development of Grid 1x1 Cell Buckling Test Technique

● Shape of grid 1x1 cell

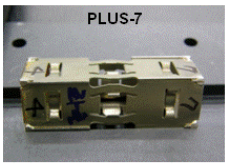

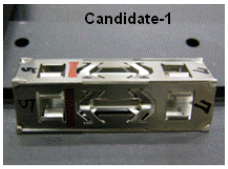

● Development of Fixtures

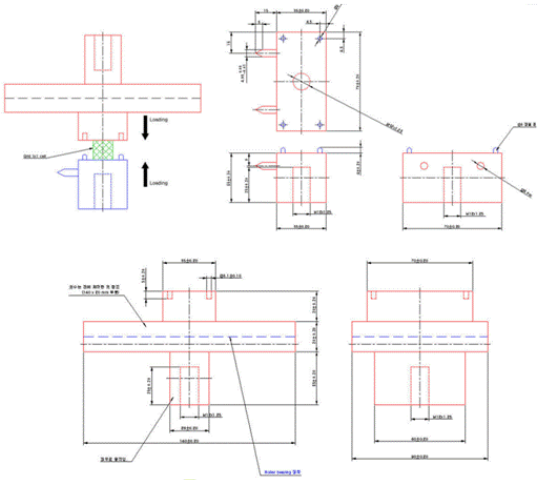

Korea Atomic Energy Research Institute

● Application of developed test technique in a hot cell

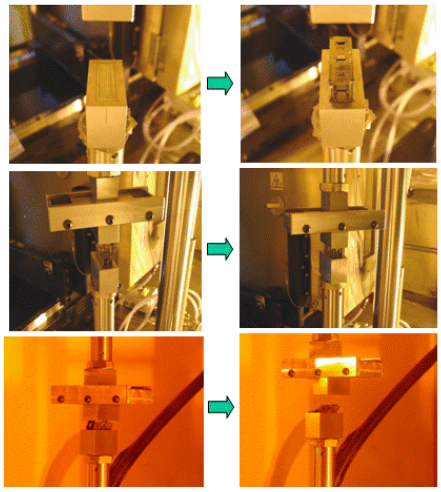

● Example of test results

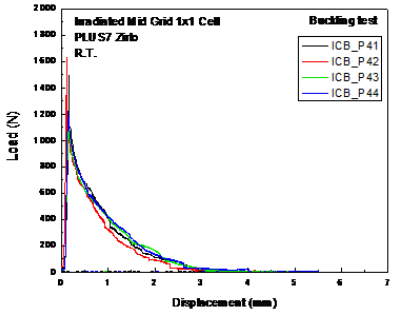

Korea Atomic Energy Research Institute

❑ Development of Grid Strip Spring Test Technique

● Shape of grid strip

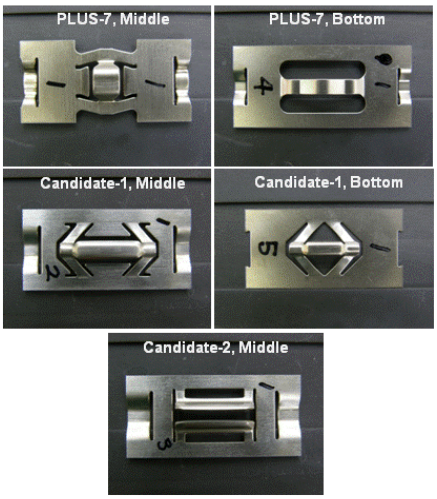

● Development of Fixtures

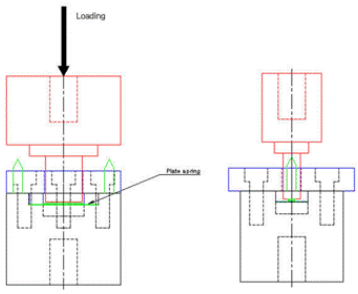

Korea Atomic Energy Research Institute

● Application of developed test technique in a hot cell

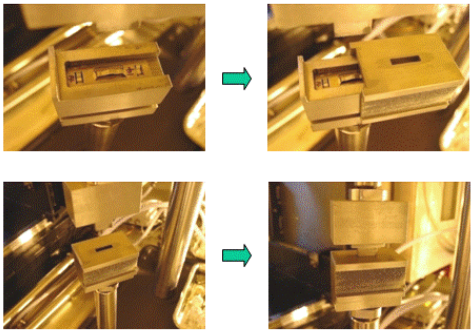

● Example of test results

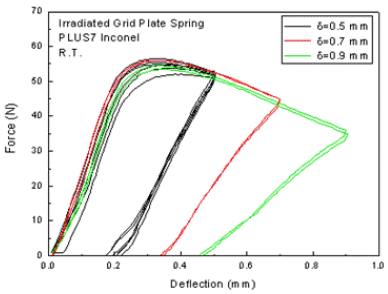

Korea Atomic Energy Research Institute

❑ Development of Tensile Test Technique for Grid Strip Material

● Specification of small specimen

- Longitudinal & transverse small tensile type
- Gage length 9mm, width 5 mm
- Thickness 0.46 mm, 0.66 mm
- Total length 26 mm, grip width 5 mm
- Hole diameter 4 mm

● Development of grip and test procedure

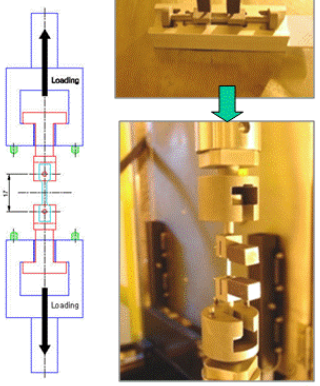

● Example of test results

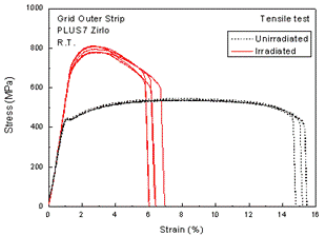

Korea Atomic Energy Research Institute

2008 KAERI-JAEA Joint Seminar on Advanced Irradiation and PIE Technologies

- 13/15 -

❑ Development of Irradiation Growth Measurement Technique

● Specimen specification

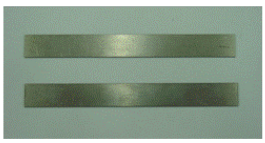

- Inconel mterial and Zr-base material
- Specimen size
  : 8 x 77 x 0.46 [mm] for inner strip
  : 8 x 77 x 0.66 [mm] for inner & outer strip
  : 8 x 77 x 0.81 [mm] for outer strip
  : 6.77 x 77 x 0.38 [mm] for Inconel

● Introduce simple micrometer system (1/1,000 mm)

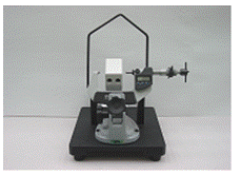

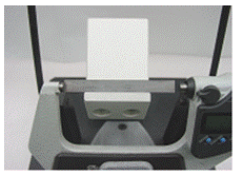

● Measurement results for the irradiated specimens

Material	ID	Unirradiated (mm)	Irradiated (mm)	Irradiation Growth (mm)	Average Irradiation Growth (mm)	Average Growth Rate (%)
XXX-4	101	76.960	77.339	0.379	0.370	0.48
	102	76.955	77.328	0.373		
	104	76.973	77.338	0.365		
	105	76.951	77.321	0.370		
	106	76.970	77.337	0.368		
	107	76.963	77.329	0.366		
	108	76.954	77.328	0.374		
	109	76.966	77.329	0.363		
	110	76.958	77.334	0.375		

Korea Atomic Energy Research Institute

2008 KAERI-JAEA Joint Seminar on Advanced Irradiation and PIE Technologies

- 14/15 -

❑ Development of Welding Strength Measurement Technique (under developing)

● Spot weld specimen

- Specimen size
  : 6.77 x 30 x 1.5 [mm]
  : 6.77 x 25 x 1.5 [mm]

● Butt weld specimen

- Specimen size
  : 6.77 x 30 x 1.5 [mm]
  : 6.77 x 25 x 1.5 [mm]

● Introduction of pneumatic grip device

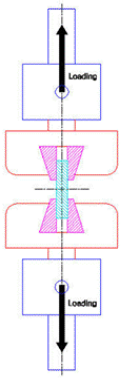

Korea Atomic Energy Research Institute

IV. Concluding Remarks

1. Various mechanical test techniques for the irradiated grid components were successfully developed, and applied to evaluate the irradiation effects on the newly developed grids.

2. The present developed techniques will be continuously improved to evaluate the safety for the operated grid components in the commercial PWR reactors.

This is a blank page.

6. Closing Addresses

This is a blank page.

6.1 **Closing Address**

Hiroshi Hiroi
Director General of Oarai Research and Development center
Japan Atomic Energy Agency

At the end of this seminar, I would like to make a closing address. In this 2008 KAERI/JAEA Joint Seminar, I think that the active and valuable information exchanges were done successfully with a total of 46 presentations in three research fields, which are the newly added research reactor management, advanced irradiation technology and post irradiation technology.

I think also that such information exchanges are supported by the great contribution with chairpersons, members of steering committee, secretaries and other concerning persons in KAERI as well as in JAEA. Here, I express my sincere gratitude to all the participants for making active discussion, and also my sincere gratitude to all contributed persons for their assistance of this seminar.

As mentioned in the opening address, this seminar was held in accordance with the newly concluded cooperation arrangement in the field of peaceful uses of nuclear energy, and I will expect that this seminar will contribute the close research cooperation between both organizations in future.

Now, the Japan Materials Testing Reactor (JMTR) is under refurbishment as introduced in the former presentations, and we are proceeding with refurbishment projects such as renewal of reactor facilities, installation of irradiation facilities by user's requests, renewal of post irradiation facilities etc. Just three years later in 2011, the refurbished JMTR will be re-operated, and at the same time we are also planning to hold the next seminar. Therefore, it is our pleasure to hold the next joint seminar at Oarai Research and Development Center in JAEA at this memorable JMTR year.

Finally, I wish everyone's good health, and expect your success in research and development activities. Moreover, three years later we would like to meet again in the joint seminar, and we will make also useful discussions at Oarai, Japan.

6.2 Closing Address

Woo-Seog Ryu
Co-Chair of the 2008 KAERI-JAEA Joint Seminar
Director of PIE & Radwaste Division
Korea Atomic Energy Research Institute

It is time to bring this joint seminar to a close. In this 2008 KAERI-JAEA seminar on advanced irradiation technology and post-irradiation examination, 13 papers in the track of research reactor management, 10 papers in irradiation technology, 17 papers in post-irradiation examination and 6 papers in plenary session were presented. With that, I would really thank the excellent speakers for well-thought-out and well-presented talks. Those contributions will be a firm basis improving the technologies for neutron irradiation uses of research reactors in Japan and Korea.

This seminar was prepared to give a pleasant place of exchanging fruitful information as well as confirming an old friendship. I am expecting all the participants have enjoyed both the technical discussions and the delighted chatting. In addition, it was a great pleasure to join the field of research reactor management in this seminar, resulting in covering whole areas of neutron irradiation uses. I believe the successful achievements of this joint seminar will contribute to expand the utilization region of research reactors and will spread the understanding of advanced technologies to users of research reactors in fuels and materials R&D.

On behalf of the Organizing Committee of the 2008 KAERI-JAEA Joint Seminar, I would like to thank all the audience for taking the time and giving an intellectual and informative discussion. I would also express my special thanks to the members of organizing committee both of Japan and Korea for their wonderful jobs. It is very proud that this joint seminar continued for 16 years have made a great footprint in the field of neutron irradiation.

We have come to the end of our program. It was a great pleasure to have time with all of you together in this 2008 KAERI-JAEA joint seminar on advanced irradiation technology and post-irradiation examination. The next seminar in Japan, I am sure, will be a successful and pleasant place again. All the Japanese participants are hoped to have a joyful time in Korea even short time left, and back home with warm friendship.

Appendix I

Organization, Number of presentation and participants

This is a blank page.

Organization

Honorary Chair

Kwang-Yong Jee (Vice President, KAERI)

Joint Seminar Co-Chair

Woo-Seog Ryu (Director, KAERI)
Masahiro Ishihara (Deputy Director, JAEA)

Steering Committee

Woo-Seog Ryu (KAERI)	**Hiroshi Kawamura (JAEA)**
Keehong Lee (KAERI)	**Motoji Niimi (JAEA)**
In-Cheol Lim (KAERI)	**Etsuo Ishitsuka (JAEA)**
Youngkee Kim (KAERI)	**Tetsuya Nakagawa (JAEA)**

Secretary

Sangbok Ahn (KAERI) **Kunihiko Tsuchiya (JAEA)**

Track Leader

Post Irradiation Examination	**Sangbok Ahn (KAERI)**	**Akira Shibata (JAEA)**
Irradiatrion Technology	**Bonggoo Kim (KAERI)**	**Kunihiko Tsuchiya (JAEA)**
Research Reactor Management	**Gukhoon Ahn (KAERI)**	**Naohiko Hori (JAEA)**

Technical Committee

Kwonpyo Hong (KAERI)
Choongseong Lee (KAERI)
Kinam Choo (KAERI)
Yongbum Chun (KAERI)

Number of presentations for 2008 KAERI-JAEA Joint Seminar
on Advanced Irradiation and PIE Technologies

Nation	Organization	Number of presentations	
Korea	Korea Atomic Energy Research Institute (KAERI)	25	28
	Korea Nuclear Fuel Company (KNF)	2	
	Kyung Hee University	1	
Japan	Japan Atomic Energy Agency (JAEA)	15	18
	Tohoku University	2	
	Nippon Nuclear Fuel Development Co. Ltd. (NFD)	0	
	Nuclear Development Corporation (NDC)	1	
Total			46

Number of participants for 2008 KAERI-JAEA Joint Seminar
on Advanced Irradiation and PIE Technologies

Nation	Organization	Number of participants	
Korea	Korea Atomic Energy Research Institute (KAERI)	89	93
	Korea Nuclear Fuel Company (KNF)	3	
	Kyung Hee University	1	
Japan	Japan Atomic Energy Agency (JAEA)	13	20
	Tohoku University	5	
	Nippon Nuclear Fuel Development Co. Ltd. (NFD)	1	
	Nuclear Development Corporation (NDC)	1	
Total			113

Appendix II

Brief History of KAERI-JAEA Joint Seminar

This is a blank page.

Brief History of KAERI-JAEA Joint Seminar

1) 1st JAERI-KAERI Joint Seminar on Post Irradiation Examination Technology
   - Opened during Nov. 9 ~ 10, 1992. Oarai, Japan
   - Presented 28 papers (Japan 18, Korea 9, China 1)

2) 2nd KAERI-JAERI Joint Seminar on Post Irradiation Examination Technology
   - Opened during Sep. 20 ~ 22, 1995. Daejeon, Korea
   - Presented 31 papers (Korea 17, Japan 13, China 1)

3) 3rd JAERI-KAERI Joint Seminar on Post Irradiation Examination Technology
   - Opened during Mar. 25 ~ 26, 1999. Oarai, Japan
   - Presented 33 papers (Japan 20, Korea 13)

4) 4th KAERI-JAERI Joint Seminar on Post Irradiation Examination Technology
   - Opened during Oct. 16 ~ 18, 2002. Daejeon, Korea
   - Presented 31 papers (Korea 19, Japan 12)

5) 2002 KAERI-JAERI Joint Seminar on Irradiation Technology
   - Opened during Oct. 31 ~ Nov. 2, 2002. Daejeon, Korea
   - Presented 11 papers (Korea 5, Japan 6)

6) 2005 JAEA-KAERI Joint Seminar on Advanced Irradiation and PIE Technology
   - Opened during Nov. 16 ~ 17, 2005. Oarai, Japan
   - Presented 35 papers (Japan 19, Korea 16)

7) 2008 KAERI-JAEA Joint Seminar on Advanced Irradiation and PIE Technology
   - Opened during Nov. 5 ~ 7, 2008. Daejeon, Korea
   - Presented 46 papers (Korea 28, Japan 18)

This is a blank page.

Appendix III
Schedule and Program Overview

This is a blank page.

Program Overview

	Nov. 5 (Wed)	Nov. 6 (Thu)	Nov. 7 (Fri)
Morning	09:00-09:30 Registration 09:30-10:00 Opening Session 10:00-12:00 Plenary Session (6 presentations)	09:30-12:00 Session B Irradiation Technology (10 presentations)	09:30-11:15 Session C-2 PIE Technology (6 presentations) 11:30-12:00 Closing Session
	12:00-13:30 Lunch	12:00-13:30 Lunch	12:00-13:30 Lunch
Afternoon	13:30-17:30 Session A Research Reactor Management (13 presentations)	13:30-17:00 Session C-1 PIE Technology (11 presentations)	13:30-16:00 Technical Tour Hanaro, IMEF, KNF

2008 KAERI - JAEA joint Seminar on Advanced Irradiation and PIE Technology
(November 5-7, 2008, Daejeon, Korea)

Seminar Program

Nov. 5 (Wed), 2008 — Place : INTEC building (Woonam Hall)

9:00 - 9:30 ***Registration***

9:30 - 10:00 ***Opening Session*** — Chair: Woo-Seog Ryu(KAERI), M. Ishihara (JAEA)

Opening Address
- KAERI — Kwang-Yong Jee
- JAEA — I. Nakajima (M. Niimi)

Taking photos

10:00 - 12:00 ***Plenary Session*** — Chair: Woo-Seog Ryu(KAERI), M. Ishihara (JAEA)

P-1 Present Status and Future Plan of JMTR Project
M.Ishihara (JAEA)

P-2 Record of System Upgrade and Ageing Management of HANARO
Incheol Lim (KAERI)

P-3 Status of Irradiation Technology Development in JMTR
E.Ishitsuka (JAEA)

P-4 Nuclear Fuels and Materials Irradiation Technology Development in HANARO
Bong Goo KIM (KAERI)

P-5 Present Activities of Post Irradiation Examinations in the JMTR Hot Laboratory
A.Shibata (JAEA)

P-6 Current Activities of Post Irradiation Examination at KAERI
Yong-Bum Chun (KAERI)

12:00 - 13:30 ***Luncheon***

13:30 - 17:30 ***Session A (Reactor Management)*** — Chair : In-Cheol Lim(KAERI), M. Niimi (JAEA)

A-1 Utilization of the Irradiation Holes in the Core at HANARO
Choongsung Lee (KAERI)

A-2 Installation of the Sag Compensator for HANARO
Hyungkyoo Kim (KAERI)

A-3 Refurbishment Status on Reactor Facilities of JMTR
M.Niimi (JAEA)

A-4 Implementation of the Safety Culture for HANARO Safety Management
Jongsup Wu (KAERI)

Coffee Break

A-5 The Operation Status and Prospect of Radioisotope Production Facility in HANARO
Minjin Kim (KAERI)

A-6 RI-Production Plan Using JMTR
N.Hori (JAEA)

A-7 Status of the Reactor Trip in HANARO
Mun Lee (KAERI)

Chair : Choongsung Lee(KAERI), N. Hori (JAEA)

A-8 Quantitative Analysis of Gamma-Ray Emitting Radionuclide in Reactor Pool Water of HANARO
Myong-Seop Kim (KAERI)

A-9 Current Status of Irradiation Facilities in JRR-3, JRR-4 and NSRR
T.Kishi (JAEA)

Coffee Break

A-10 The Results of an Ultrasonic Examination for the Flywheel Attached to a Primary Cooling Pump Motor in HANARO
Yong-Chul Park (KAERI)

A-11 Utilization of Reactors Overseas for Study of Radiation Effects in Materials
M.Yamazaki (Tohoku Univ.)

A-12 In-service Inspection of Zirconium Components of HANARO
Yeonggarp Cho (KAERI)

A-13 Introduction to the Cold Neutron Source at HANARO
Sang-ik Wu (KAERI)

Nov. 6 (Thu), 2008 Place : NTC building (Room 23-106)

9:30 - 12:00 ***Session B (Irradiation Technology)*** Chair : Young-Ki Kim (KAERI), T. Shikama (Tohoku Unv.

B-1 Joining Techniques Development for Neutron Irradiation Tests and Post Irradiation Examinations in JMTR-HL
K.Tsuchiya (JAEA)

B-2 Development of Fuel Test Loop in HANARO
Sungho Ahn (KAERI)

B-3 Safety Research Program of LWR Fuels and Materials Using the Japan Materials Testing Reactor
S.Hanawa (JAEA)

B-4 A Basic Design of a Double Cladding Fuel Rod to Control the Irradiation Temperature of Nuclear Fuels
Jae Min Sohn (KAERI)

B-5 Design and Fabrication of a Capsule for a Material Irradiation in an OR Hole of HANARO
Man-Soon CHO (KAERI)

Coffee Break

B-6 Advances in Material Capsule Technology in HANARO
Kee-Nam CHOO (KAERI)

B-7 Development of a Capsule Assembly Machine for the Re-irradiation Tests in HANARO
Young-Hwan Kang (KAERI)

B-8 Development and Design for Mo-Production Facility in JMTR
H.Izumo (JAEA)

B-9 Development on ^{99}Mo Production Technology by Molybdenum Solutior Irradiation Method
E.Ishitsuka (JAEA)

B-10 Practice of Adding Value to Materials by a Neutron Irradiation in Research Reactors
Soo-Youl Oh (KAERI)

12:00 - 13:30 ***Luncheon***

13:30 - 17:00 ***Session C-1 (PIE Technology)*** Chair : Jaeik Kim (KNF), K. Tsuchiya (JAEA)

C-1 Irradiated Fuel Examination Program for Advanced PWR Fuels in Korea
Jaeik Kim (KNF)

C-2 Microstructure and Elemental Distribution of Americium-Containing MOX Fuel under the Short-Term Irradiation Tests
K. Tanaka (JAEA)

C-3 Measurements of Xe Diffusion Coefficient of UN
Kwangheon Park (Kyunghee Univ.)

C-4 Research Infrastructure for Actinide Science at IMR
M. Watanabe (Tohoku Univ.)

Coffee Break

C-5 PIE Techniques for Hydride Reorientation Test at NDC
T. Tsuda (NDC)

C-6 Improved Technique for Hydrogen Concentration Measurement in Fuel Claddings by Backscattered Electron Image Analysis (II)
A. Onozawa (JAEA)

Chair : Yong-Bum Chun(KAERI), E. Ishitsuka (JAEA)

C-7 Hoop Strength and Ductility Evaluation of Irradiated Fuel Cladding
Sunky Kim (KAERI)

C-8 Preliminary Irradiation Test for New Material Selection on Lifetime Extension of Beryllium Reflector
K. Tsuchiya (JAEA)

Coffee Break

C-9 Multiscale Modeling Simulations of Point Defect Production in Neutron-Irradiated Iron
Junhyun Kwon (KAERI)

C-10 Measurement of Deformation of FBR Fuel Assembly Wrapper Tube by an Innovative Technique
Shinji Sasaki (JAEA)

C-11 Transient Burst Techniques and Results of the Examination for Irradiated PNC316 Steel
T.Inoue (JAEA)

Nov. 7 (Fri), 2008 Place : NTC building (Room 23-106)

9:30 - 11:15 ***Session C-2 (PIE Technology)*** Chair : Sang-Bok Ahn(KAERI), A.Shibata (JAEA)

C-12 In-Reactor Fuel Performance Examination Technology in Korea
Jungcheol Shin (KNF)

C-13 Performance Evaluation of Large U-Mo Particle Dispersed Fuel Irradiated in HANARO
Ho Jin Ryu (KAERI)

C-14 Burnup Determination of High Burnup PWR Fuel by Neodymium and Cesium Isotope Monitor Methods Based on Isotope Dilution Mass Spectrometric Measurement
Jungsuk Kim (KAERI)

Coffee Break

C-15 Micro Gamma Scanning on the High Burnup PWR Fuel Samples
Hyoung-Mun Kwon (KAERI)

C-16 Modified Laser Flash Thermal Diffusivity Measurement System for Shielded Glove Box
Daegyu Park (KAERI)

C-17 Development of Mechanical Test Techniques on the Irradiated Grid Elements in PWR Fuel Assembly
Sang-Bok Ahn (KAERI)

11:30 - 12:00 ***Closing Session*** Chair: Woo-Seog RYU (KAERI), M. Ishihara (JAEA)

Closing address
- JAEA H. Hiroi (M. Ishihara)
- KAERI Woo-Seog Ryu

12:00 - 13:30 ***Luncheon***

13:30 - 16:00 ***Technical Tour***

- Hanaro, IMEF, KNF

This is a blank page.

国際単位系（SI）

表１．SI 基本単位

基本量	SI 基本単位	
	名称	記号
長さ	メートル	m
質量	キログラム	kg
時間	秒	s
電流	アンペア	A
熱力学温度	ケルビン	K
物質量	モル	mol
光度	カンデラ	cd

表２．基本単位を用いて表されるSI組立単位の例

組立量	SI 基本単位	
	名称	記号
面積	平方メートル	m^2
体積	立法メートル	m^3
速さ，速度	メートル毎秒	m/s
加速度	メートル毎秒毎秒	m/s^2
波数	毎メートル	m^{-1}
密度（質量密度）	キログラム毎立法メートル	kg/m^3
質量体積（比体積）	立法メートル毎キログラム	m^3/kg
電流密度	アンペア毎平方メートル	A/m^2
磁界の強さ	アンペア毎メートル	A/m
（物質量の）濃度	モル毎立方メートル	mol/m^3
輝度	カンデラ毎平方メートル	cd/m^2
屈折率	（数の） 1	1

表５．SI 接頭語

乗数	接頭語	記号	乗数	接頭語	記号
10^{24}	ヨタ	Y	10^{-1}	デシ	d
10^{21}	ゼタ	Z	10^{-2}	センチ	c
10^{18}	エクサ	E	10^{-3}	ミリ	m
10^{15}	ペタ	P	10^{-6}	マイクロ	μ
10^{12}	テラ	T	10^{-9}	ナノ	n
10^{9}	ギガ	G	10^{-12}	ピコ	p
10^{6}	メガ	M	10^{-15}	フェムト	f
10^{3}	キロ	k	10^{-18}	アト	a
10^{2}	ヘクト	h	10^{-21}	ゼプト	z
10^{1}	デカ	da	10^{-24}	ヨクト	y

表３．固有の名称とその独自の記号で表されるSI組立単位

組立量	SI 組立単位			
	名称	記号	他のSI単位による表し方	SI基本単位による表し方
平面角	ラジアン(a)	rad		$m \cdot m^{-1}=1$(b)
立体角	ステラジアン(a)	sr(c)		$m^2 \cdot m^{-2}=1$(b)
周波数	ヘルツ	Hz		s^{-1}
力	ニュートン	N		$m \cdot kg \cdot s^{-2}$
圧力，応力	パスカル	Pa	N/m^2	$m^{-1} \cdot kg \cdot s^{-2}$
エネルギー，仕事，熱量	ジュール	J	N・m	$m^2 \cdot kg \cdot s^{-2}$
工率，放射束	ワット	W	J/s	$m^2 \cdot kg \cdot s^{-3}$
電荷，電気量	クーロン	C		s・A
電位差（電圧），起電力	ボルト	V	W/A	$m^2 \cdot kg \cdot s^{-3} \cdot A^{-1}$
静電容量	ファラド	F	C/V	$m^{-2} \cdot kg^{-1} \cdot s^4 \cdot A^2$
電気抵抗	オーム	Ω	V/A	$m^2 \cdot kg \cdot s^{-3} \cdot A^{-2}$
コンダクタンス	ジーメンス	S	A/V	$m^{-2} \cdot kg^{-1} \cdot s^3 \cdot A^2$
磁束	ウエーバ	Wb	V・s	$m^2 \cdot kg \cdot s^{-2} \cdot A^{-1}$
磁束密度	テスラ	T	Wb/m^2	$kg \cdot s^{-2} \cdot A^{-1}$
インダクタンス	ヘンリー	H	Wb/A	$m^2 \cdot kg \cdot s^{-2} \cdot A^{-2}$
セルシウス温度	セルシウス度(d)	℃		K
光束	ルーメン	lm	cd・sr(c)	$m^2 \cdot m^{-2} \cdot cd=cd$
照度	ルクス	lx	lm/m^2	$m^2 \cdot m^{-4} \cdot cd=m^{-2} \cdot cd$
（放射性核種の）放射能	ベクレル	Bq		s^{-1}
吸収線量，質量エネルギー分与，カーマ	グレイ	Gy	J/kg	$m^2 \cdot s^{-2}$
線量当量，周辺線量当量，方向性線量当量，個人線量当量，組織線量当	シーベルト	Sv	J/kg	$m^2 \cdot s^{-2}$

(a)ラジアン及びステラジアンの使用は、同じ次元であっても異なった性質をもった量を区別するときの組立単位の表し方として利点がある。組立単位を形作るときのいくつかの用例は表４に示されている。
(b)実際には、使用する時には記号rad及びsrが用いられるが、習慣として組立単位としての記号“１”は明示されない。
(c)測光学では、ステラジアンの名称と記号srを単位の表し方の中にそのまま維持している。
(d)この単位は、例としてミリセルシウス度m℃のようにSI接頭語を伴って用いても良い。

表４．単位の中に固有の名称とその独自の記号を含むSI組立単位の例

組立量	SI 組立単位		
	名称	記号	SI 基本単位による表し方
粘度	パスカル秒	Pa・s	$m^{-1} \cdot kg \cdot s^{-1}$
力のモーメント	ニュートンメートル	N・m	$m^2 \cdot kg \cdot s^{-2}$
表面張力	ニュートン毎メートル	N/m	$kg \cdot s^{-2}$
角速度	ラジアン毎秒	rad/s	$m \cdot m^{-1} \cdot s^{-1}=s^{-1}$
角加速度	ラジアン毎平方秒	rad/s^2	$m \cdot m^{-1} \cdot s^{-2}=s^{-2}$
熱流密度，放射照度	ワット毎平方メートル	W/m^2	$kg \cdot s^{-3}$
熱容量，エントロピー	ジュール毎ケルビン	J/K	$m^2 \cdot kg \cdot s^{-2} \cdot K^{-1}$
質量熱容量（比熱容量），質量エントロピー	ジュール毎キログラム毎ケルビン	J/(kg・K)	$m^2 \cdot s^{-2} \cdot K^{-1}$
質量エネルギー（比エネルギー）	ジュール毎キログラム	J/kg	$m^2 \cdot s^{-2} \cdot K^{-1}$
熱伝導率	ワット毎メートル毎ケルビン	W/(m・K)	$m \cdot kg \cdot s^{-3} \cdot K^{-1}$
体積エネルギー	ジュール毎立方メートル	J/m^3	$m^{-1} \cdot kg \cdot s^{-2}$
電界の強さ	ボルト毎メートル	V/m	$m \cdot kg \cdot s^{-3} \cdot A^{-1}$
体積電荷	クーロン毎立方メートル	C/m^3	$m^{-3} \cdot s \cdot A$
電気変位	クーロン毎平方メートル	C/m^2	$m^{-2} \cdot s \cdot A$
誘電率	ファラド毎メートル	F/m	$m^{-3} \cdot kg^{-1} \cdot s^4 \cdot A^2$
透磁率	ヘンリー毎メートル	H/m	$m \cdot kg \cdot s^{-2} \cdot A^{-2}$
モルエネルギー	ジュール毎モル	J/mol	$m^2 \cdot kg \cdot s^{-2} \cdot mol^{-1}$
モルエントロピー，モル熱容量	ジュール毎モル毎ケルビン	J/(mol・K)	$m^2 \cdot kg \cdot s^{-2} \cdot K^{-1} \cdot mol^{-1}$
照射線量（X線及びγ線）	クーロン毎キログラム	C/kg	$kg^{-1} \cdot s \cdot A$
吸収線量率	グレイ毎秒	Gy/s	$m^2 \cdot s^{-3}$
放射強度	ワット毎ステラジアン	W/sr	$m^4 \cdot m^{-2} \cdot kg \cdot s^{-3}=m^2 \cdot kg \cdot s^{-3}$
放射輝度	ワット毎平方メートル毎ステラジアン	$W/(m^2 \cdot sr)$	$m^2 \cdot m^{-2} \cdot kg \cdot s^{-3}=kg \cdot s^{-3}$

表６．国際単位系と併用されるが国際単位系に属さない単位

名称	記号	SI 単位による値
分	min	1 min=60s
時	h	1h =60 min=3600 s
日	d	1 d=24 h=86400 s
度	°	1° =(π/180) rad
分	’	1’ =(1/60)° =(π/10800) rad
秒	”	1” =(1/60)’ =(π/648000) rad
リットル	l、L	1l=1 $dm^3=10^{-3}m^3$
トン	t	1t=10^3 kg
ネーパ	Np	1Np=1
ベル	B	1B=(1/2)ln10(Np)

表７．国際単位系と併用されこれに属さない単位でSI単位で表される数値が実験的に得られるもの

名称	記号	SI 単位であらわされる数値
電子ボルト	eV	1eV=1.60217733(49)×10^{-19}J
統一原子質量単位	u	1u=1.6605402(10)×10^{-27}kg
天文単位	ua	1ua=1.49597870691(30)×10^{11}m

表８．国際単位系に属さないが国際単位系と併用されるその他の単位

名称	記号	SI 単位であらわされる数値
海里		1海里=1852m
ノット		1ノット=1海里毎時=(1852/3600)m/s
アール	a	1 a=1 $dam^2=10^2m^2$
ヘクタール	ha	1 ha=1 $hm^2=10^4m^2$
バール	bar	1 bar=0.1MPa=100kPa=1000hPa=10^5Pa
オングストローム	Å	1 Å=0.1nm=10^{-10}m
バーン	b	1 b=100$fm^2=10^{-28}m^2$

表９．固有の名称を含むCGS組立単位

名称	記号	SI 単位であらわされる数値
エルグ	erg	1 erg=10^{-7} J
ダイン	dyn	1 dyn=10^{-5}N
ポアズ	P	1 P=1 dyn・s/cm^2=0.1Pa・s
ストークス	St	1 St =1$cm^2/s=10^{-4}m^2/s$
ガウス	G	1 G ≙10^{-4}T
エルステッド	Oe	1 Oe ≙(1000/4π)A/m
マクスウェル	Mx	1 Mx ≙10^{-8}Wb
スチルブ	sb	1 sb =1$cd/cm^2=10^4cd/m^2$
ホト	ph	1 ph=10^4lx
ガル	Gal	1 Gal =1$cm/s^2=10^{-2}m/s^2$

表10．国際単位に属さないその他の単位の例

名称	記号	SI 単位であらわされる数値
キュリー	Ci	1 Ci=3.7×10^{10}Bq
レントゲン	R	1 R = 2.58×10^{-4}C/kg
ラド	rad	1 rad=1cGy=10^{-2}Gy
レム	rem	1 rem=1 cSv=10^{-2}Sv
X線単位		1X unit=1.002×10^{-4}nm
ガンマ	γ	1γ=1 nT=10^{-9}T
ジャンスキー	Jy	1 Jy=10^{-26}W・m^{-2}・Hz^{-1}
フェルミ		1 fermi=1 fm=10^{-15}m
メートル系カラット		1 metric carat = 200 mg = 2×10^{-4}kg
トル	Torr	1 Torr = (101 325/760) Pa
標準大気圧	atm	1 atm = 101 325 Pa
カロリー	cal	
ミクロン	μ	1 μ =1μm=10^{-6}m

（第７版，1998年改訂）

Japan Atomic Energy Agency

Korea Atomic Energy Research Institute